Leveraging Copper Chelators as Targeted Therapy for *BRAF*^{V600E} Mutant Thyroid Cancer

by

MengMeng Xu

Department of Pharmacology and Cancer Biology
Duke University

Date:_____

Approved:

_____
Christopher Counter, Supervisor

_____
Gerard Blobe

_____
David Kirsch

_____
Christopher Kontos

_____
Ann Marie Pendergast, Chair

Dissertation submitted in partial fulfillment of
the requirements for the degree of Doctor
of Philosophy in the Department of
Pharmacology and Cancer Biology in the Graduate School of
Duke University

2018

ABSTRACT

Leveraging Copper Chelators as Targeted Therapy for *BRAF*^{V600E} Mutant Thyroid Cancer

by

MengMeng Xu

Department of Pharmacology and Cancer Biology
Duke University

Date:_____

Approved:

_____
Christopher Counter, Supervisor

_____
Gerard Blobe

_____
David Kirsch

_____
Christopher Kontos

_____
Ann Marie Pendergast, Chair

An abstract of a dissertation submitted in partial
fulfillment of the requirements for the degree
of Doctor of Philosophy in the Department of
Pharmacology and Cancer Biology in the Graduate School of
Duke University

2018

Abstract

The incidence of thyroid cancer, and in particular papillary thyroid cancer (PTC), is rising faster than that of any other malignancy in the United States. Thyroid cancer is now the most common endocrine cancer and the fifth most common cancer in women. While most thyroid cancers are treated effectively with surgical resection and radioiodine therapy, survival drops precipitously in metastatic or radioiodine-resistant disease. 60% of papillary thyroid cancers (PTC) have an oncogenic V600E mutation in the kinase BRAF, which leads to a constitutively active and oncogenic kinase. This mutation has been associated with as well as a 2.14-fold increase in recurrent/persistent disease. Excitingly, inhibitors against this mutant kinase or its substrates, the MEK1/2 kinases, can prolong progression free survival or stabilize disease in radioiodine-refractory thyroid cancer patients. However, the indolent nature of PTC may be a challenge to the clinical adaption of these inhibitors, as the financial and physical toxicities of these treatments may be amplified over the prolonged time-course typical of PTC. MEK1/2 require copper (Cu) for kinase activity and can be inhibited with the well-tolerated and economical Cu chelator tetrathiomolybdate (TM). Cu chelators have been in use for decades in patients with Wilson's Disease, a disease of Cu accumulation. Unlike current BRAF and MEK inhibitors, Cu chelators can be well tolerated for decades with few side effects, and thus may find use in long-term inhibition of $BRAF^{V600E}$ signaling in PTC.

Here I test the ability of Cu chelator TM to inhibit tumor growth in *$BRAF^{V600E}$*-mutant PTC. TM inhibited MEK1/2 kinase activity and transformed growth of human

BRAF^{V600E}-mutant PTC cells as well as or more potently than standard-of-care drugs. Consistent with TM deriving its antineoplastic activity by inhibiting MEK1/2, expression of activated ERK2, a substrate of MEK1/2, overcame the ability of TM to suppress growth of *BRAF*^{V600E}-mutant PTC cells. TM was also effective in a genetically engineered mouse model of *Braf*^{V600E}-mutant PTC; oral TM reduced tumor burden as well as a clinical BRAF inhibitor. This *in vivo* effect was attributed to a reduction of phospho-Erk1/2 signaling in the tumors. Additionally, long-term maintenance therapy using TM after cessation of a clinical BRAF inhibitor reduced tumor volume in the same mouse model. Genetic reduction of the Cu transporter CTR1 in developing tumors also trended towards a survival advantage in mice with *Braf*^{V600E}-mutant PTC. Finally, TM also enhanced the antineoplastic activity of standard of care clinical BBRAF inhibitor drugs. These results support the clinical evaluation of Cu chelation as targeted therapy for *Braf*^{V600E}-mutant PTC and suggests three possible avenues for clinical exploration: *i*) as a less toxic monotherapy for *Braf*^{V600E}-mutant PTC, *ii*) as long-term maintenance therapy after initial treatment, and *iii*) as a combination-therapy amplifying the antineoplastic effects of other treatment modalities.

Dedication

To my partner, family, friends, mentors, and advisors—everything I do is a reflection of your constant love and support.

Contents

List of Tables

List of Figures

1. Introduction

1.1 Natural history of thyroid cancer

1.1.1 Introduction to thyroid cancer

The thyroid is a butterfly shaped endocrine organ located just below the larynx with one lobe positioned on each side of the anterior trachea connected by an isthmus. This encapsulated gland is mainly responsible for producing thyroid hormones important for metabolism regulation. The thyroid consists of many follicles containing a colloid of thyroglobulin and iodide/iodine that the surrounding thyrocytes (also known as follicular cells, thyroid epithelial cells, or T thyrocytes) use to produce the thyroid hormones: thyroxine (T4) and triiodothyronine (T3). The follicles are interspersed with neuroendocrine parafollicular cells (also known as C cells or C thyrocytes), which produce calcitonin, a hormone that promotes the absorption of calcium. The final cell type found in the thyroid are endothelial cells forming the capillary system responsible for transporting thyroid stimulating hormone (TSH) from the pituitary to the thyroid (Figure 1) (Kumar, Abbas et al. 2010). The follicular and parafollicular cell types give rise to all four types of thyroid cancer: papillary thyroid cancer (PTC), follicular thyroid cancer (FTC), anaplastic thyroid cancer (ATC), and medullary thyroid cancer (MTC) (Kumar, Abbas et al. 2010).

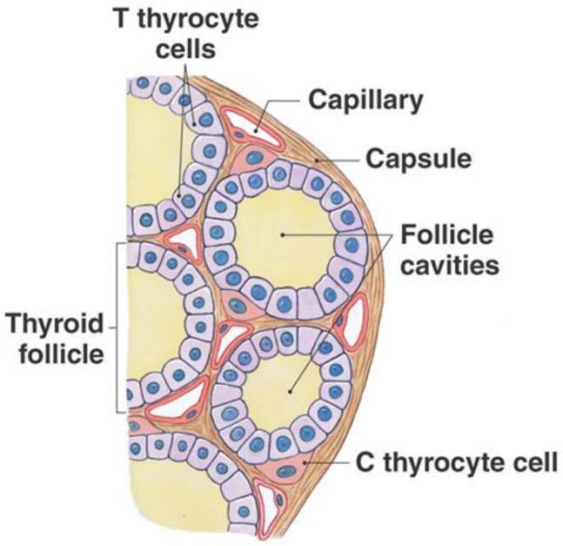

Figure 1: Diagram of the normal thyroid gland structure.
Image from lecture prepared by Jason LaPres, copyright 2009 Pearson Education, Inc.

While thyroid nodules are found by ultrasound in 19-68% of adults (Haugen, Alexander et al. 2016), thyroid cancer is a relatively rare disease, accounting for about 1.5% of all cancers (Howlader N 2017). However, the incidence of thyroid cancer is rising faster than that of any other malignancy in the United States. New cases have more than tripled over the past four decades (Howlader N 2017). Thyroid is now the most common endocrine cancer and the most commonly diagnosed cancer in women under 35 years of age (Howlader N 2017). Thyroid cancer is projected to become the third most common cancer in women by 2019 (Aschebrook-Kilfoy, Schechter et al. 2013). Although some of this increased incidence is accounted for by increasing use and quality of ultrasound technology, the concurrent increase in diagnosis of larger and later stage tumors implies a true rise in disease incidence (Enewold, Zhu et al. 2009, Lim, Devesa et

al. 2017), which is further supported by an increasing rate of thyroid cancer associated mortality (Howlader N 2017).

Thyroid cancer is a disease predominantly diagnosed in women during the early and middle adult years. More even gender distribution is found in patients who are diagnosed in childhood or late life (Kumar, Abbas et al. 2010). There are multiple categorizations for thyroid cancer. Medullary thyroid cancer (MTC) is the only malignancy to arise from parafollicular C cells, while follicular (FTC), papillary (PTC), and anaplastic (ATC) thyroid cancers arise from follicular thyrocytes. Follicular and papillary thyroid cancers are also referred to as differentiated thyroid cancer (DTC) while anaplastic thyroid cancer is considered de-differentiated thyroid cancer (DeTC). >85% of thyroid cancer cases are attributed to PTC, 5-15% are attributed to FTC, <5% are attributed to ATC, and <5% are attributed to MTC (Kumar, Abbas et al. 2010) (Table 1).

Table 1: Subtypes of thyroid cancer.
Table created using frequencies, cell of origin, and subtype information reported in Robbins and Cotran Pathologic Basis of Disease, 8th edition. *N/A:* not applicable.

Cancer Type	Frequency	Cell of Origin	Subtype
Papillary Thyroid Cancer (PTC)	>85%	Follicular Cells	DTC
Follicular Thyroid Cancer (FTC)	5-15%	Follicular Cells	DTC
Anaplastic Thyroid Cancer (ATC)	<5%	Follicular Cells	DeTC
Medullary Thyroid Cancer (MTC)	<5%	Parafollicular Cells	N/A

N/A: not applicable

1.1.2 Types of thyroid cancer

As previously mentioned, there are four main types of thyroid cancer that can arise from the thyroid follicular and parafollicular cells: papillary thyroid cancer (PTC), follicular thyroid cancer (FTC), anaplastic thyroid cancer (ATC), and medullary thyroid cancer (MTC). The pathology of each cancer type is summarized in this section.

1.1.2.1 Papillary thyroid cancer (PTC)

PTC is the thyroid cancer subtype responsible for the increasing incidence of thyroid cancer over the past four decades (Figure 2) (Davies and Welch 2014). This steady increase in incidence has led to PTC becoming the dominant thyroid cancer subtype, now accounting for ~90% of all thyroid cancers in the United States (Davies and Welch 2014) (Table 1). While the majority of this increased incidence is in small tumors (<1 cm), there has also been a 40% increase in diagnosis of large, symptomatic tumors (>4 cm). This increase in incidence of tumors of all sizes (Enewold, Zhu et al. 2009, Lim, Devesa et al. 2017) and increased mortality (Howlader N 2017) due to thyroid cancer supports a true rise in incidence beyond that explained by the increasing use and quality of ultrasound technology. While the canonical risk factor for PTC is exposure to ionizing radiation during the first two decades (Kumar, Abbas et al. 2010), recent environmental research has associated exposure to flame retardant chemicals, decabromodiphenyl ether (BDE-209) and tris(2-chloroethyl) phosphate, with PTC occurrence (Hoffman, Lorenzo et al. 2017).

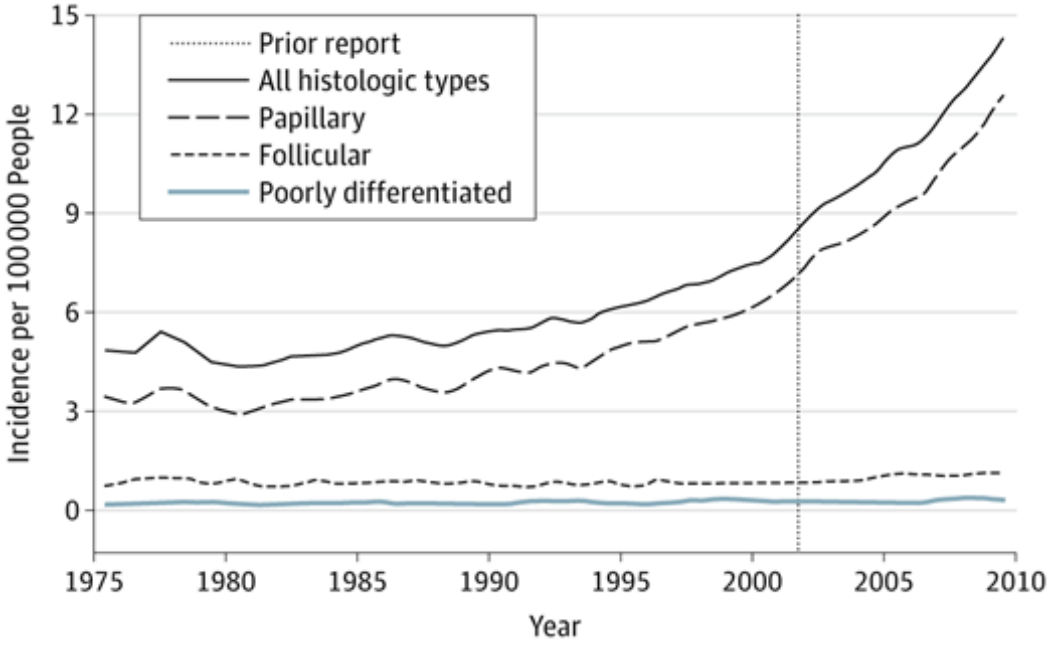

Figure 2: Thyroid cancer incidence and mortality, 1975 to 2009.
Trends for thyroid cancer of all histologic types are shown. Incidence data are from Surveillance, Epidemiology, and End Results (SEER) 9, 1975 to 2009, maintained by the National Cancer Institute, National Institutes of Health, released April 2012, based on the November 2011 submission. Figure used with permission from Davies and Welch. *JAMA*. 2014.

Papillary thyroid cancer can occur as a single lesion or multifocal disease. These lesions can be well circumscribed or ill-defined and can contain calcifications, fibrotic areas, and cysts. One macroscopic hallmark of PTC is concentrically calcified structures called psammoma bodies that can be found within the core of PTC papillae but are extremely rare in follicular and medullary carcinomas. While the macroscopic structure of these tumors can contain its name sake papillary structure (fibrovascular stock covered by single or multiple layers of cuboidal epithelial cells), the tumors are

diagnosed histologically. Dispersed chromatin resulting in "Orphan Annie Eye" nuclear clearing and nuclear groves resembling intranuclear inclusions are the diagnostic hallmarks of PTC (Kumar, Abbas et al. 2010). While involvement of blood vessels is rare, focal lymphatic invasion is common, with 37-64% of PTC cases showing metastases to regional cervical lymph nodes at time of diagnosis (Randolph, Duh et al. 2012). Distant metastases to the lung and bone can be found 2-10% of patients at time of diagnosis (Howlader N 2017).

The invasive potential of PTC can vary depending on the subtype of tumor involved. The follicular variant of PTC contains PTC-like nuclei clearing and grooving, but follicular architecture (Yu, Schneider et al. 2013). These follicular variant PTC were more likely to contain RAS mutations (see section 1.2.3) and were correlated with low rates of lymph node metastases (Adeniran, Zhu et al. 2006). Conversely, the tall-cell variant of PTC has a higher rate of extrathyroidal extension and lymph node metastasis, and are more likely to present at an advanced stage (Johnson, Lloyd et al. 1988). BRAF mutations (see section 1.2.2) or RET/PTC translocations (see section 1.2.4) are the most common mutations (55-100%) occurring in tall cell variant PTC (Ghossein and Livolsi 2008, Kumar, Abbas et al. 2010). Lastly, the diffuse sclerosing variant of PTC is most commonly found in younger patients. Like the tall-cell variant, lymphocytic invasion is common in diffuse sclerosing PTC, in which lymph node metastases are found in almost all cases (Adeniran, Zhu et al. 2006, Kumar, Abbas et al. 2010).

1.1.2.2 Follicular thyroid cancer (FTC)

FTC is the second most common thyroid cancer, accounting for 5-15% of all thyroid cancer cases in the United States (Table 1). FTC has a 3:1 female to male distribution and tends to be diagnosed later in life than PTC (Kumar, Abbas et al. 2010). Iodine deficiency maybe a risk factor for FTC. For instance, in East India where only ~3% of household salt was sufficiently iodinated (Chandra, Singh et al. 2006), FTC accounted for ~24% of all thyroid cancers (Shah, Jain et al. 2018). FTC generally present as a well circumscribed single nodule or a large infiltrative lesion that has already penetrated the thyroid capsule and extended into the surrounding anatomy. FTC tumors are grossly flesh-like with small foci of hemorrhage, but few cysts or calcifications (Kumar, Abbas et al. 2010). Microscopically, FTC contain solid sheets of cells interspersed with colloid filled follicles similar to normal thyroid follicles. Histologically, FTC is distinguished from PTC by the lack of nuclear clearing and grooves (Sobrinho-Simões, Eloy et al. 2011).

Unlike PTC, which spreads through the lymphatic system, FTC spreads via the vascular system (Kumar, Abbas et al. 2010, Sobrinho-Simões, Eloy et al. 2011). Patients diagnosed with FTC at an advanced stage often have disseminated disease metastasizing to the lung, bone, and liver. Due to this inclination for wide-spread metastases, prognosis for FTC patients is highly dependent on the level of invasion (Sobrinho-Simões, Eloy et al. 2011). Patients with local disease can have a greater than

90% 10-year survival, while patients with metastatic disease have a 50% 10-year survival rate (Kumar, Abbas et al. 2010).

1.1.2.3 Anaplastic thyroid cancer (ATC)

ATC are dedifferentiated tumors that arise from follicular thyrocytes (Kumar, Abbas et al. 2010). ATC accounts for less than 5% of all thyroid cancers in the United States (Table 1), but is the most aggressive of all subtypes with mortality rates approaching 100% (Are and Shaha 2006). ATC generally presents as a rapidly growing neck mass that has already spread to the adjacent anatomy or metastasized to the lung by the time of diagnosis (Keutgen, Sadowski et al. 2015). There are no effective treatments for the disease, and almost all patients succumb within a year of diagnosis due to disruption or invasion of vital structures in the neck (Are and Shaha 2006, Kumar, Abbas et al. 2010, Keutgen, Sadowski et al. 2015).

As its name implies, ATC is comprised of highly anaplastic cells ranging in morphology from pleomorphic giant cells to sarcomatous spindle cells or a mix of the two cell types. 25% of ATC patients have had a pervious medical history of a differentiated thyroid cancer (DTC) and another 25% found to have an additional DTC at autopsy (Kumar, Abbas et al. 2010). Studies have found that ATC could arise from DTC (Quiros, Ding et al. 2005). Inactivation of p53 leading to the development of ATC in a BRAF mutant PTC genetically engineered mouse model further supports these clinical findings (McFadden, Vernon et al. 2014).

1.1.2.4 Medullary thyroid cancer

Medullary thyroid cancer (MTC), the rarest of the thyroid cancers (Table 1), accounts for only 1-2% of thyroid cancers in the United States (Wells, Asa et al. 2015). MTC is the only cancer to arise from the parafollicular calcitonin-producing C cells, and thus the only neuroendocrine tumor to arise from the thyroid gland (Ghofrani and Ocal 2015). While most MTC arises from sporadic mutations in the patient's 40s or 50s, about 25% of MTC arise in younger patients as part of the familial multiple endocrine neoplasia type 2 (MEN2) syndrome (Roy, Chen et al. 2013). Activating point mutations in the RET proto-oncogene is important for the development of both the sporadic and the familial forms of MTC (Roy, Chen et al. 2013). MTC usually presents as solidary nodules in sporadic cases and bilateral, multi-focal modules in MEN2 MTC (Ghofrani and Ocal 2015). In both forms, the resultant tumor is firm, pale, and infiltrative, with focal hemorrhage and necrosis. Histologically, MTC consists of polygonal or spindle-shaped cells forming nests, trabeculae, and follicles within the tumor (Ghofrani and Ocal 2015). In some cases, amyloid deposits consisting of altered calcitonin polypeptides can be found in the stroma adjacent to MTC tumors. Like the other types of thyroid cancer, MTC typically presents as a mass in neck. However, because of its neuroendocrine nature, patients with MTC can also present with paraneoplastic syndrome caused by the over secretion of calcitonin (Ghofrani and Ocal 2015).

1.1.3 Current treatment for PTC

Focusing specifically on treatment for PTC, once a thyroid nodule has been confirmed to be PTC by fine needle aspiration, the treatment course begins with surgery. Unless vital local anatomy is involved, the primary tumor and any involved lateral neck lymph nodes are surgically removed. Depending on the size and number of primary tumors and involvement of lateral lymph nodes, this initial surgery could involve a lumpectomy, unilateral lobectomy, or total thyroidectomy. Following surgery, patients receive T4 levothyroxine (thyroid hormone) therapy to replace normal hormone production and suppress tumor growth. Thyroid stimulating hormone (TSH) is then measured four or six weeks after surgery to ensure that thyroid hormone supplementation is suppressing the production of TSH, which can augment PTC growth. This treatment progression is outlined in the 2015 American Thyroid Association (ATA) guideline (Haugen, Alexander et al. 2016).

At this initial treatment, the ATA system is used to estimate risk of recurrence based on the tumor, node, metastasis system (TNM) (Table 2) (Haugen, Alexander et al. 2016). Low risk PTC patients with disease confined to thyroid receive thyroglobulin (Tg) and TSH monitoring until a follow-up visit leads to reassignment into a higher risk category. Patients with residual disease, microscopic invasion of surrounding tissue, or metastases then receive radioactive iodine-131 (RAI) therapy (Tuttle, Ross et al. 2018). Patients are monitored every three to six months after initial treatment, with a neck

ultrasound performed every six or twelve months. High risk patients with elevated Tg will also receive magnetic resonance imaging (MRI) and computed tomography (CT) scans and fluorodeoxyglucose (FDG)-PET imagining. Follow-up after the first one or two years post-surgery is dependent on each patient's risk as defined by the ATA guideline risk stratification system (Table 2). Although most recurrences occur within five years of initial diagnosis, recurrence can occur decades later (Xing 2010). Thus, serum TSH in PTC patients is measured annually or six to eight weeks after each dose adjustment of T4. If a patient is found to have local recurrent disease or an isolated metastasis, removal through surgical resection or external beam radiation can be attempted. Extensive or scattered metastases may be treated with RAI if scans show iodine uptake (Tuttle, Ross et al. 2018). Unfortunately, recurrent tumors often do not uptake RAI avidly (Vassilopoulou-Sellin, Schultz et al. 1996). For these tumors and all non-RAI responsive PTC, systemic therapy may be necessary.

Table 2: ATA risk stratification system for persistent/recurrent PTC.
Table created using data from Haugen *et al.* 2015 ATA Guidelines for Adult Patients with Thyroid Nodules and Differentiated Thyroid Cancer.

Risk Category	Criteria	TNM stage
Low Risk	• All macroscopic tumor resected • No local invasion • No local or distant metastases • Non-aggressive histology • No RAI avidity outside of thyroid	N0 (no lymphatic metastases) Or ≤ 5 lymph node micrometastases (<0.2 cm in diameter)
Intermediate Risk	• Microscopic invasion into the perithyroidal soft tissues • RAI avid metastatic foci in the neck only post-treatment • Vascular invasion present • Aggressive • 1-4 cm primary tumor with positive $BRAF^{V600E}$ mutation • Multifocal PTC with extrathyroidal extension and positive $BRAF^{V600E}$ mutation	N1 or > 5 lymph node micrometastases (<0.2 cm in diameter)
High Risk	• Macroscopic invasion of tumor into perithyroidal soft tissues • Incomplete tumor resection • Distant metastases • High post-operative serum thyroglobulin	N1 with node >3cm in largest dimension

Tyrosine kinase inhibitors (TKI) have taken precedence over cytotoxic chemotherapy as the therapy of choice for aggressive RAI-resistant PTC. Patients with >1 cm tumors growing at a rate > 20% per year are initially treated with the current first-line standard-of-care TKI, lenvatinib, which mainly targets PDGFRβ, RET, and VEGFR-1 (Stjepanovic and Capdevila 2014). This drug has been shown to increase median progression-free survival (PFS) from 3.6 months in the placebo group to 18.3 months (Schlumberger, Tahara et al. 2015). Disease non-responsive to lenvatinib may then be

treated with sorafenib. Sorafenib is a second-line TKI which mainly targets VEGFR-2, c-KIT, PDGFRβ, RET, VEGFR-1, BRAF, and VEGFR-3 (Stjepanovic and Capdevila 2014). This drug was shown to improve PFS from 5.8 months in the placebo group to 10.8 months (Brose, Nutting et al. 2014). VEGFR inhibitors pazopanib, sunitinib, and vandetanib may also be administered off-label for their anti-angiogenic properties (Sherman, Ross et al. 2016). Unfortunately, both these FDA-approved treatments — lenvatinib and sorafenib — have significant side-effects of treatment. 14.2% and 16% of patients discontinued treatment due to intolerable toxicities to lenvatinib and sorafenib, respectively (Brose, Nutting et al. 2014, Schlumberger, Tahara et al. 2015). Thus, more effective, less toxic methods of treatment for aggressive PTC remain necessary.

1.1.4 Prognosis for PTC

Prognosis for PTC is determined at time of diagnosis then adjusted dynamically during and after initial treatment. Initial staging using the TNM classification system can be used to stratify risk of recurrence following ATA guidelines (Table 2) (Haugen, Alexander et al. 2016). A 2010 retrospective review showed that this system effectively predicted risk of recurrence or persistent disease as 3%, 21%, and 68% of patients with low-, intermediate-, and high-risk disease, respectively (Tuttle, Tala et al. 2010). Other prognostic features not evaluated by the ATA TNM system include age at diagnosis (Bischoff, Curry et al. 2013), tumor size (Ito, Kudo et al. 2012), soft-tissue invasion, site of

distant metastases (Casara, Rubello et al. 1993, Chiu, Delpassand et al. 1997), FDG uptake (Robbins, Wan et al. 2006), histological subtype (Ghossein, Leboeuf et al. 2007), and molecular characteristics (Klein, Vignaud et al. 2001, Elisei, Viola et al. 2012, Melo, da Rocha et al. 2014) (Table 3).

Table 3: Clinical and pathologic prognostic factors for aggressive PTC.
Table created using prognostic factors consolidated from various sources. [1]As described in Bischoff *et al. Endocr Pract* 2013. [2]As described in Ito *et al. Endocr J* 2012. [3]As described in Casara *et al. J Nucl Med.* 1993. and Chiu *et al. J Clin Endocrinol Metab.* 1997. [4]As described in Robbins *et al. J Clin Endocrinol Metab.* 2006. [5]As described in Ghossein *et al. Thyroid*. 2007. [6]As described in Elisei *et al. J Clin Endocrinol Metab.* 2012. [7]As described in Melo *et al. J Clin Endocrinol Metab.* 2014. [8]As described in Klein *et al. J Clin Endocrinol Metab.* 2001.

Prognostic Factor	Effect
Age[1]	Continuum of increasing disease-specific mortality with increasing age
Tumor size[2]	tumors >2cm is an independent prognostic factor
Soft-tissue invasion[3]	Involvement of local anatomy (trachea, esophagus, recurrent laryngeal nerves, or spinal cord) increases risk of death five-fold
FDG uptake[4]	High FDG uptake had < 50% three-year, disease-specific survival
Histological variant[5]	Tall cells variant of PTC has a worse prognosis than classic PTC
Mutational Status	BRAF V600E[6], TERT mutation[7], VEGF expression[8]

Historically, patients diagnosed with early stage PTC that responded well to surgical resection with or without radioactive iodine (RAI) therapy have an excellent survival rate. In fact, the 10-year survival rate for Stage I and II disease in the United States are 99.1% and 85.3%, respectively. Survival for stage III disease (regional lymph

node involvement) is expectedly worse at 76.7%, while survival for Stage IV (distant metastasis) disease drops precipitously to 37.0%. Initial disease response to RAI also clearly demarcates a difference in survival. Patients with a complete response have a 10-year survival of 99.8%. Survival drops to 65.4%, 44.4%, and 14.6% for patients with partial response, stable disease, and progressive disease, respectively, on initial RAI treatment (Sciuto, Romano et al. 2009) (Table 4). However, even in patients initially responsive to RAI, there is a 20-30% recurrence rate within 10-15 years of diagnosis (Xing 2010). These findings indicate that although thyroid cancer generally has a good prognosis after standard treatment with surgery, TSH suppression, and RAI ablation, there is still a need for better therapy in patients with advanced stage disease or disease not-responsive to RAI treatment.

Table 4: PTC 10-year survival rate by disease stage and RAI response.
% survival by disease stage and RAI response were adapted from Sciuto et al. *Ann Oncol.* 2009.

Disease Stage	10-year Survival
Stage I	99.1%
Stage II	85.3%
Stage III	76.7%
Stage IV	37.0%

RAI response	10-year Survival
Complete response	99.8%
Partial response	65.4%
Stable disease	44.4%
Progressive disease	14.60%

1.1.5 Financial impact of thyroid cancer

Financial toxicity and its effect on quality of life is an increasingly sentient topic in cancer care (Zafar, McNeil et al. 2015, Zafar 2016). Given the decades long prognosis of patients diagnosed with PTC and the need for continuous monitoring and reevaluation, the financial strain of PTC has a significant impact on patient outcomes (Husson, Haak et al. 2011). In fact, patients with PTC have one of the highest rates of personal bankruptcy due to cancer care amongst all cancer types, (Ramsey, Blough et al. 2013). This financial impact is consistent in all patients diagnosed with thyroid cancer, regardless of stage of disease at time of diagnosis (Gallop, Kerr et al. 2015). Unlike most other cancers, due to good disease survival rate and the need for continuous monitoring in case of recurrence decades after initial diagnosis, most of the cost in PTC treatment is incurred during the continuing treatment phase after initial therapy (Lubitz, Kong et al. 2014). In 2013, there was an aggregate of approximately 670,000 patients receiving treatment for thyroid cancer in the United States. Together these patients consume more than $1.5 billion in health care spending per year (Lubitz, Kong et al. 2014). This sum is projected to reach more than $3.5 billion per year by 2030 (Lubitz, Kong et al. 2014). Despite reputation as a "relatively benign" cancer, the financial impact of thyroid cancer is not only significant to patient quality of life (Ramsey, Blough et al. 2013), but also to the national trend of rising health care costs (Lubitz, Kong et al. 2014).

1.1.6 Challenges facing thyroid cancer treatment

Because PTC is typically diagnosed in patients under 55 years of age but reaches peak disease-specific death in the 70s, thyroid cancer treatment faces a unique, decades-long clinical challenge between balancing appropriate therapy with patient quality of life (Kitahara and Sosa 2016, Lubitz and Sosa 2016). A survey of patient reported quality of life priorities found fatigue, financial anxieties, and fear of cancer progression to be the most sentient issues for patients (Singer, Husson et al. 2016). While fatigue is an unavoidable side-effect of losing endogenous thyroid hormone production and is managed by adjusting thyroxine dosage, financial solvency and fear of disease progression are more nebulous issues.

As previously discussed, the financial strain of thyroid cancer is a significant issue to patients and the United States health care system (Lubitz, Kong et al. 2014). This issue is especially urgent for patients who require TKI therapy for RAI-resistant disease. The FDA-approved TKIs lenvatinib and sorafenib cost ~$6,000 and ~$2,000 per 28-day cycle, respectively (Zhang, Yang et al. 2015). These costs, in combination with necessary scans and follow-up Tg and TSH evaluations, could easily exceed the annual limit on many insurance policies (Zhang, Yang et al. 2015). In fact, a study on the cost effectiveness of sorafenib found that the TKI did not surpass the willingness-to-pay threshold of patients with advanced hepatocellular carcinoma (Zhang, Yang et al. 2015). Given the inability for sorafenib to past the willingness-to-pay threshold in a more

aggressive disease that would likely require a shorter treatment period, thyroid cancer patients likely face an even more difficult decision between financial solvency and sorafenib treatment. This would presumably be an even larger issue for patients who receive the front-line drug lenvatinib, which costs approximately three times more than sorafenib.

The financial toxicities of TKI treatment are not the only barriers towards advanced therapy for aggressive thyroid cancer. Small molecule inhibitors like TKIs also have physical toxicities that patients must endure. In a Phase III trial of lenvatinib in RAI-refractory thyroid cancer, 14.2% of patients treated with lenvatinib had to discontinue treatment due to adverse effects. Adverse events occurred in >40% of patients and included hypertension (67.8%), diarrhea (59.4%), fatigue (59.0%), decreased appetite (50.2%), decreased weight (in 46.4%), and nausea (in 41.0%) (Schlumberger, Tahara et al. 2015). Likewise, a Phase III trial of sorafenib in thyroid cancer required dose modification in 78% and therapy discontinuation in 19% of patient. Adverse events occurred in almost all patients with hand-foot skin reaction (76.3%), diarrhea (68.6%), alopecia (67.1%), and rash (50.2%) being the most common complaints (Brose, Nutting et al. 2014). These robust side-effect profiles are a challenge further complicating the viability of maintaining adequate lenvatinib or sorafenib dosage during ongoing treatment for responsive disease.

1.2 Genetics of PTC

1.2.1 Landscape of mutations

Mutations that activate the mitogen-activated protein kinase (MAPK) pathway are common in papillary thyroid cancer PTC (Figure 3). There are activating point mutations in *BRAF* and *RAS* as well as *RET*/*PTC* translocations, which account for 60%, 13%, and 7.3% of PTC mutations, respectively (Nikiforov and Nikiforova 2011, Xing 2013, TCGA 2014). These mutations appear to be mutually exclusive, as there is no overlap in a single PTC case (Kimura, Nikiforova et al. 2003, Soares, Trovisco et al. 2003). In fact, each of these mutations is strongly associated with distinct disease characteristics. *BRAF*-mutant PTC is a more aggressive cancer than *RAS*-mutant or *RET*/*PTC* translocation-positive PTC (Elisei, Viola et al. 2012, Kakarmath, Heller et al. 2016). It has been suggested that this difference is because *BRAF* mutations occur further downstream in the MAPK pathway than *RAS* mutations and RET/PTC translocations and are thus not constrained by ERK-to-RAF negative feedback (Pratilas, Taylor et al. 2009). This difference in signaling may also account for the mutational-dependent phenotype of PTC. *BRAF*-mutant tumors are generally less differentiated and resistant to RAI, and this is associated with downregulation of genes responsible for iodine uptake and metabolism (Durante, Puxeddu et al. 2007, 2014).

Mutations in the promoter region of the telomerase reverse transcriptase (*TERT*) gene also account for 9% of PTC mutations (Melo, da Rocha et al. 2014, TCGA 2014).

Unlike the association of MAPK pathway, mutations with certain histological variants, *TERT* mutations are found throughout the variants. Although they are not associated with variant-linked characteristics of aggressiveness, TCGA analysis did find *TERT* mutations more common in older patients and patients with a higher risk of recurrence (Melo, da Rocha et al. 2014, TCGA 2014). *TERT* promoter mutations have been identified as an independent prognostic factor (Melo, da Rocha et al. 2014). Recent studies have shown the concomitant existence of a TERT mutation with a $BRAF^{V600E}$ mutation to be highly indicative of very aggressive disease (Xing, Liu et al. 2014, Liu, Bishop et al. 2016).

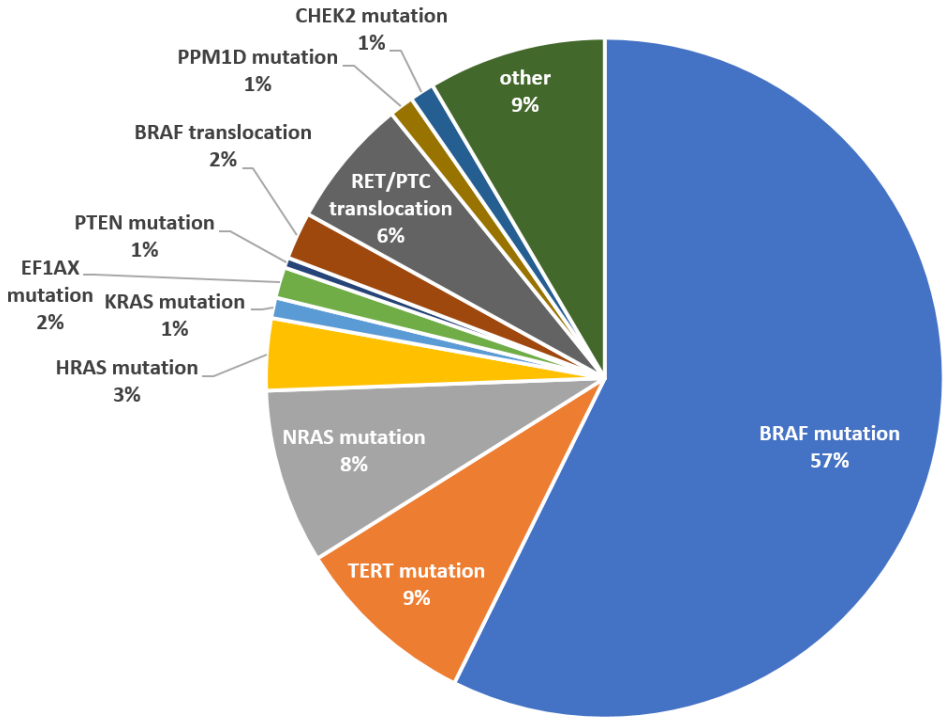

Figure 3: Pie chart of the genetic landscape of PTC.
Figure created using data from 2014 TCGA analysis of papillary thyroid cancer.

Previously unknown mutations in *EIF1AX*, *PPM1D*, and *CHEK2* were identified by The Cancer Genome Atlas (TGCA) (TCGA 2014). The protein product of *EIF1AX* mediates transfer of the initiating Met-tRNA to 40S ribosomal subunits, which form the preinitiation complex for protein translation. *EIF1AX* mutations tend to coincide with the less aggressive, *RAS*-like follicular variants of PTC (Karunamurthy, Panebianco et al. 2016). Mutations in *PPM1D* and *CHEK2* occur concurrently with mutations in the MAPK pathway. Although not much is known about the role of these DNA repair proteins in PTC, they have been associated with pancreatic (Wu, Guo et al. 2016), lung (Yang, Gao et al. 2015), and breast cancers as well (Ruark, Snape et al. 2013).

1.2.2 *BRAF* mutations

BRAF mutations account for approximately 60% of PTC mutations (Nikiforov and Nikiforova 2011, Xing 2013, TCGA 2014). Almost 100% of mutations in *BRAF* are 1799T>A substitutions that results in a valine (V) to glutamic acid (E) point mutation at amino acid 600 (V600E) (Wan, Garnett et al. 2004). The V600E mutations appears to be the most common mutation for two reasons: *i*) this codon appears to be more susceptible to mutation than adjacent sites, as suggested by the presence of rare double mutations in at the V600 codon, and *ii*) the ability of this mutation to introduce a negatively charged residue adjacent to the S599 RAS phosphorylation site, which completely bypasses RAS regulation (unlike mutations at adjacent sites) by mimicking phosphorylation triggered

by activated RAS (Davies, Bignell et al. 2002). This mutation occurs in the kinase domain and results in a constitutively-active monomeric BRAF (Xing 2013). This constitutively active BRAF kinase leads to increased phosphorylation and activation of MEK1/2 kinases, which in turn phosphorylate and activate ERK1/2 kinases. Such activation of the MAPK pathway promotes the expression of an array of cell survival and proliferation genes that drive tumorigenesis (Bos 1989, Schubbert, Shannon et al. 2007) (Figure 4). The *BRAF*^{V600E} mutation is considered a driver mutation in PTC, as it appears early in human PTC (de Biase, Cesari et al. 2014) and causes PTC when recreated in mice (Charles, Iezza et al. 2011).

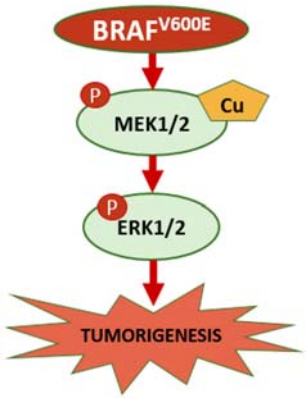

Figure 4: Schematic of Cu in BRAF^{V600E} signaling.

BRAF mutations are associated with the more aggressive forms of PTC (Adeniran, Zhu et al. 2006, Kakarmath, Heller et al. 2016). 97% of tall-cell PTC, the most aggressive PTC variant, are *BRAF* mutant (Ghossein and Livolsi 2008, de Biase, Cesari et al. 2014, TCGA 2014). In addition to its association with the most aggressive PTC

variant, *BRAF*-mutant PTC are also less differentiated than PTC driven by other mutations (Costa, Herrero et al. 2008). A positive *BRAF* mutational status has been identified as an independent prognostic factor for poor outcomes in patients with low-risk PTC (Elisei, Viola et al. 2012). $BRAF^{V600E}$ mutational status has also been shown to further designate patients into a higher risk category, even in the setting of comparable extent of lymph node and distant metastases (Xing, Alzahrani et al. 2013). Recent studies have shown $BRAF^{V600E}$ coexistence with $TERT^{C228T}$ to be a predictor of highly aggressive disease (Xing, Liu et al. 2014, Liu, Bishop et al. 2016).

Additionally, positive *BRAF* multinational status may predict resistance to RAI treatment, as PTC driven by these mutations have a lower expression of genes involved in iodine metabolism (Durante, Puxeddu et al. 2007, TCGA 2014). Suppression of the MAPK pathway in $BRAF^{V600E}$-mutant PTC has been shown to restore expression of genes involved in iodine metabolism (Liu, Hu et al. 2007). This evidence is strong enough that *BRAF*-mutational status may be considered as a guide for determining the use of RAI therapy (Xing 2010, Elisei, Viola et al. 2012). The MEK inhibitor, selumetinib, has also been shown to restore RAI sensitivity in patients with aggressive RAI-resistant PTC (Larson, Osborne et al. 2017).

1.2.3 *RAS* mutations

RAS mutations account for 13% of all PTC mutations (Vasko, Ferrand et al. 2003). A TCGA analysis of *RAS* mutations in PTC revealed a range of mutations in all three RAS genes: *NRAS*, *HRAS*, and *KRAS*. 65% of RAS mutations are found in *NRAS*, all of which are glutamine (Q) to arginine (R) mutations at amino acid 61. 27% of *RAS* mutations are in *HRAS*. While these mutations are at amino acid 61, 78% of them are glutamine (Q) to arginine (R) mutations (Q61R) and 22% glutamine (Q) to lysine (K) mutations (Q61K). *KRAS* mutations make up the remaining <8% of *RAS* mutations, and are also mainly found at amino acids 61 (TCGA 2014). These mutations result in different biochemical perturbations that ultimately all leave the protein in the oncogenic, active (GTP-bound) state.

RAS-mutant PTC are generally less aggressive than *BRAF*-mutant PTC (Adeniran, Zhu et al. 2006, Kakarmath, Heller et al. 2016). Unlike $BRAF^{V600E}$ mutations, *RAS* mutations have been identified in benign thyroid adenomas and have been implicated in the development of FTC (Nikiforov and Nikiforova 2011). Tumors harboring *RAS* point mutations tend to be the follicular variant of PTC, which is known to be less aggressive clinically (Zhu, Gandhi et al. 2003). In fact, the identification of *RAS* mutations on diagnostic fine needle aspirates has been proposed as a marker of less aggressive PTC and an indicator for more conservative clinical management (Howell, Hodak et al. 2013, Xing 2016).

1.2.4 *RET/PTC* translocations

There are many types of *RET*/*PTC* translocation that result in oncogenic PTC rearrangements. *RET* is a proto-oncogene gene which encodes a receptor tyrosine kinase (RTK). *RET*/*PTC* translocations occurs between the 3' tyrosine kinase portion of *RET* and the 5' portion of its partner gene. Although there are more than 10 possible partner genes for the *RET*/*PTC* translocation, the most common partner genes are *H4(D10S170)* (*RET*/*PTC1*) and *ELE1* (*RET*/*PTC3*), which together, account for >90% of all rearrangements (Nikiforov 2002, Prescott and Zeiger 2015). This rearrangement leads to the formation of ligand-independent dimers and recruits signaling adapters to a phosphorylated tyrosine^{1062}, resulting in constitutive activation of the *RET* fusion oncoprotein. This leads to the constitutive activation of both MAPK and PI3K/AKT pathways (Castellone, De Falco et al. 2009, Prescott and Zeiger 2015). Since the PI3K/AKT pathway is the primary pathway for FTC oncogenesis, *RET*/*PTC* translocations are more closely associated with the more benign follicular variant of PTC (Santarpia, Myers et al. 2010, Xing 2010). Because of the presence of *RET*/*PTC* in benign thyroid diseases, findings of *RET* rearrangements on fine needle aspiration is not indicative of PTC, nor does it provide clinical insights into disease prognosis (Prescott and Zeiger 2015).

1.3 MAPK inhibition *in* $BRAF^{V600E}$-mutant cancers

Clinical use of small molecule inhibitors in $BRAF^{V600E}$-mutant disease is a recent development adapted from $BRAF^{V600E}$-mutant melanoma. There have been three generations of RAF inhibitors. Two second-generation RAF inhibitors, vemurafenib and dabrafenib, have now been FDA approved for $BRAF^{V600E}$-mutant melanoma and third-generation RAF inhibitors are showing promise in early clinical trials (Chapman, Hauschild et al. 2011, Hauschild, Grob et al. 2012). Evidence from these single agent clinical trials suggested that more potent inhibition of the MAPK pathway maybe more effective at inhibiting tumor growth (Bollag, Hirth et al. 2010). As such, double inhibition of RAF and MEK were also tested in melanoma, and their increased efficacy over single agent RAF inhibitors has led to FDA approval in melanoma (Long, Stroyakovskiy et al. 2014). Table 5 summarizes the approved TKIs and MAPK inhibitors addressed in Sections 1.3.1-1.3.4.

Table 5: Status of MAPK inhibitors in melanoma and PTC.
The MAPK inhibitors and their survival status in melanoma and PTC consolidated from various sources. [1]As described in Stjepanovic and Capdevila. *Biologics.* 2014. [2]As described in Chapman *et al. N Eng J Med.* 2011. [3]As described in Long *et al. Endocr J.* 2017. [4]As described in Larkin *et al. N Eng J Med.* 2014. [5]As described Schlumberger *et al. N Eng J Med.* 2015. [6]As described in Brose *et al. Lancet.* 2014. [7]As described in Brose *et al. Lancet Oncol.* 2016. [8]As described in Falchook *et al. Thyroid.* 2015. [9]In progress clinical trial number NCT02393690.

Drug	Type/targets	Melanoma	PTC
lenvatinib	TKI against PDGFRβ, RET, and VEGFR-1[1]	--	Approved[5]
sorafenib	1st generation BRAF inhibitor; TKI against VEGFR-2, c-KIT, PDGFRβ, RET, VEGFR-1, BRAF, and VEGFR-3 [1]	--	Approved[6]
vemurafenib	2nd generation BRAF inhibitor	approved[2]	Phase II[7]
dabrafenib	2nd generation BRAF inhibitor	approved as dabrafenib-trametinib combination therapy[3]	Phase I[8]
trametinib	MEK inhibitor	approved as dabrafenib- trametinib combination therapy[3]	--
cobimetinib	MEK inhibitor	approved as vemurafenib-cobimetinib combination therapy[4]	--
selumetinib	MEK inhibitor	--	Phase II for restoring RAI sensitivity[9]

1.3.1 BRAF inhibitor therapy

In normal RAS-RAF signaling, monomeric RAF is a cytosolic protein that remains in its closed inactive formation until it is translocated to the membrane and associated with active, GTP-bound RAS through a RAS-binding domain (RBD) in the N-terminus of RAF. In the process of binding to RAS, the N-terminus of RAF becomes dissociated from its C-terminus. This unfolding the protein in this fashion exposes the

ATP/ADP binding site, magnesium binding (DFG motif) site, and activation segment. The final component to a catalytically active RAF is the change of the N-terminal lobe αC-helix from the OUT to the IN position. RAF activated through these processes can then phosphorylate its substrates MEK 1 and MEK 2, which in-turn phosphorylate its substrates ERK 1 and ERK 2. Phosphorylation of ERK serves as a feedback mediator of MAPK signaling by disrupting the membrane RAS/RAF interaction and releasing RAF from the above described active plasma membrane bound state. The main mechanism through which RAF inhibitors act is by stabilizing the αC-helix in an inactive, OUT conformation and by preventing dimerization of RAF proteins (Wan, Garnett et al. 2004, Karoulia, Wu et al. 2016, Karoulia, Gavathiotis et al. 2017).

Another level of complexity in RAS/RAF signaling is the homo-and hetero-dimerization that can occur between RAF isoforms. As described above, inactive RAF proteins in the cytoplasm are folded in such a way that the N-terminal regulatory domain autoinhibits the C-terminal kinase domain. These RAF proteins often exist in dimers bound by 14-3-3, which stabilize this autoinhibited state by binding the phosphorylation sites at both the N- and C-termini. Following growth factor-induced conversion of GDP-bound RAS to GTP-bound RAS, 14-3-3 is released and the dimeric RAF is activated. Although most dimers are BRAF/CRAF heterodimers, a basal level of BRAF/BRAF dimerization can also be increased by 2-fold with growth-factor induced signaling. However, CRAF does not self-dimerize and growth-factor induced activation

of CRAF is highly dependent upon BRAF. In fact, BRAF proteins with intermediate and impaired kinase activity have been shown to increase MAPK activity by dimerization with CRAF (Freeman, Ritt et al. 2013). BRAF dependent activation of CRAF is especially important in the paradoxical activation of the MAPK pathway by second-generation BRAF inhibitors, in which inhibitor bound BRAF has a greater affinity for binding and activating wildtype CRAF (described below) (Rajakulendran, Sahmi et al. 2009). Dimerization is also the nexus for another mechanism of BRAF inhibitor resistance. Namely, the self-homodimerization of $BRAF^{V600E}$ spice variants (Freeman, Ritt et al. 2013, Lito, Rosen et al. 2013).

The first generation of RAF inhibitors were synthesized before the discovery of BRAF mutations. Of these drugs, sorafenib was the only first-generation inhibitor to receive clinical approval (Escudier, Eisen et al. 2007, Llovet, Ricci et al. 2008, Brose, Nutting et al. 2014). Sorafenib binds and stabilizes the αC-helix in a catalytically active IN conformation (αC-IN), but hinders RAF activation by competing with at the ATP binding site. However, sorafenib likely inhibits tumor growth through its multi-kinase profile as it has equal effect on tumor growth regardless of *BRAF* mutational status. (Karoulia, Gavathiotis et al. 2017).

Second-generation RAF inhibitors stabilize the αC-helix in the inactive, OUT conformation (αC-OUT). Unfortunately, inhibitor bound, αC-OUT RAF can still dimerize with another RAF protomer. This second protomer is stabilized in the active

αC-IN form because of steric interference from the inhibitor bound αC-OUT RAF (Karoulia, Wu et al. 2016). Thus, while αC-OUT inhibitors such as vemurafenib are effective at preventing aberrant signal by the monomeric $BRAF^{V600E}$ protein, they simultaneously stabilize catalytically active αC-OUT/αC-IN dimers and promote paradoxical activation of the MAPK pathway (Rajakulendran, Sahmi et al. 2009). Additionally, both second-generation RAF inhibitors, vemurafenib and dabrafenib, promote a second mechanism of resistance by promoting RAF interaction with RAS-GTP. This is accomplished by displacing the αC-helix R506 residue towards the IN position, which increases the RAF affinity for RAS-GTP (Karoulia, Wu et al. 2016). Both these mechanisms lead to paradoxical activation of the MAPK pathway by second-generation RAF inhibitors, which can lead to the distinct dermal side-effect profile of these drugs (see Section 1.4.1).

Despite the side-effect profiles generated by the above discussed paradoxical MAPK activation, second-generation RAF inhibitors have been approved in $BRAF^{V600E}$-mutant melanoma. Vemurafenib, the first second-generation RAF inhibitor approved, was shown to be effective in almost 50% of patients with metastatic melanoma. Vemurafenib treatment improved overall 6-months survival from 64% in the then standard-of-care dacarbazine-treated group to 84% in the vemurafenib-treated group (Chapman, Hauschild et al. 2011). Dabrafenib was similarly effective in patients with metastatic, resectable $BRAF^{V600E}$-mutant melanoma. The Phase II clinical trial that led to

FDA approval of dabrafenib revealed an improved median PFS from 2.7 months on dacarbazine treatment to 5.1 months on dabrafenib treatment (Hauschild, Grob et al. 2012). While these second-generation RAF inhibitors have been approved for *BRAF*^{V600E} mutant melanoma, they have side-effect profiles severe enough to warrant discontinuation (Chapman, Hauschild et al. 2011, Hauschild, Grob et al. 2012) and a limited treatment duration due to development of drug resistance (Lito, Rosen et al. 2013).

Third-generation RAF inhibitors currently under preclinical and Phase I clinical trials are thought to be able to overcome some of the paradoxical MAPK activation seen in second-generation RAF inhibitors. These third-generation RAF inhibitors prevent dimerization through two possible mechanisms. The first class of inhibitors bind, inhibit, and stabilize the αC helix in an IN position (αC-IN), thereby preventing the formation of active αC-IN/αC-OUT dimers seen in second-generation αC-OUT conformation stabilizing inhibitors. Third-generation inhibitors simultaneously stabilize the DGF domain in an OUT formation to prevent MAPK activation through binding to RAS-GTP. The second class of these inhibitors are 'paradox breaker' αC-OUT inhibitors with sulfonamide and sulfamide substitutions. While these inhibitors still stabilize the αC-OUT conformation and induce αC-OUT/IN dimerization, they do not promote RAF binding of RAS-GTP because they stabilize the R506 residue in the non-RAS-GTP binding OUT conformation (Karoulia, Wu et al. 2016, Karoulia, Gavathiotis et al. 2017).

1.3.2 MEK inhibitor therapy

MEK 1 and 2 (MEK1/2) are the primary substrate of RAF kinase (Xing 2013). As such, MEK1/2 were logical targets for preventing abnormal MAPK signaling. Although many non-ATP-competitive, allosteric MEK inhibitors have been developed in recent years, only trametinib and cobimetinib have been approved by the FDA for $BRAF^{V600E}$-mutant melanoma. Trametinib was shown to be more effective in $BRAF^{V600}$-mutant melanoma than $BRAF^{WT}$-melanoma (Falchook, Lewis et al. 2012). In a Phase III clinical trial of *BRAFV600E*-mutant melanoma, trametinib improved PFS from 1.5 months in patients treated with the then standard-of-care dacarbazine to 4.8 months in patients treated with trametinib (Flaherty, Robert et al. 2012). Other MEK inhibitors, such selumetinib and cobimetinib, are currently in clinical trials with encouraging results (Zhao and Adjei 2014). However, MEK inhibitor as a monotherapy does not appear as effective as RAF inhibitor monotherapy (Falchook, Lewis et al. 2012, Grimaldi, Simeone et al. 2014). Moreover, high potency MAPK inhibition has been correlated with better response (Bollag, Hirth et al. 2010). As such, the investigatory direction of clinical MEK inhibitors has been in the realm of combination therapy with existing RAF inhibitors.

1.3.3 Combination therapy

Initial trials of combined BRAF and MEK inhibitor therapy were tested because of the need for more potent MAPK inhibition and the need to prevent paradoxical

MAPK activation seen in BRAF inhibitor single therapy (Bollag, Hirth et al. 2010). Fortunately, these combination therapies have been effective in both regards. The FDA approved the combination of dabrafenib and trametinib based on interim results from a Phase III trial showing that this double therapy increased PFS to 9.3 months from 8.8 months in the dabrafenib-only group (Long, Stroyakovskiy et al. 2014). The benefits of this therapy persisted for three years, with 22% PFS in combination treated patients and 12% PFS in the dabrafenib treated patients at 3 years (Long, Flaherty et al. 2017). Five-year follow up in the same patients showed that the dabrafenib and trametinib double-therapy could elicit durable PFS of 13% at both four and five years with an overall survival at 30% and 28%, respectively (Long, Eroglu et al. 2017). Combination therapy with the BRAF inhibitor vemurafenib and MEK inhibitor cobimetinib showed similar results, with patients who had previously progressed on vemurafenib single-therapy experiencing an average PFS of 2.8 months and patients naïve to vemurafenib experiencing a PFS of 13.7 months (Ribas, Gonzalez et al. 2014). A Phase III trial comparing combination therapy with vemurafenib and cobimetinib against vemurafenib demonstrated an improvement in overall survival from 17.4 months in vemurafenib-only patients to 22.3 months in combination-treated patients (Ascierto, McArthur et al. 2016). In addition to its superior clinical efficacy over single-therapy, both combination therapies demonstrated a decreased incidence of keratoacanthomas and squamous cell carcinomas, the clinical manifestations of RAF inhibitor induced paradoxical MAPK

activation. The increased efficacy of and reduced paradoxical MAPK activation by combined RAF and MEK inhibitor treatment has made combination therapy the front line treatment for metastatic *BRAF*^{V600E}-mutant melanoma (Grimaldi, Simeone et al. 2017).

1.3.4 MAPK inhibitors in PTC

Although MAPK inhibitors have not been as extensively studied in *BRAF*^{V600E}-mutant PTC, results from recent Phase I and II clinical trials are encouraging (Kim, Cabanillas et al. 2013, Falchook, Millward et al. 2015, Brose, Cabanillas et al. 2016). In a phase I trial of patients with *BRAF*^{V600E}-mutant, RAI-resistant PTC, vemurafenib treatment resulted in 15.6 months of PFS survival in TKI-naïve and 9.8 months of PFS in TKI-treated patients, with response rates of 58% and 36%, respectively (Kim, Cabanillas et al. 2013). A Phase II trial of vemurafenib in VEGFR-naïve and VEGFR-treated, aggressive RAI-refractory PTC resulted in 18.8 and 12.0 months of PFS, respectively (Brose, Cabanillas et al. 2016). Similarly, dabrafenib prevented disease progression in 13 out of 14 patients with metastatic *BRAF*^{V600E}-mutant PTC and extended PFS by 11.3 months, with only one patient progressing, and then only after 9.3 months of response (Falchook, Millward et al. 2015).

In addition to improving PFS, MAPK inhibitor have also been studied in a context specific to PTC, namely, to restore RAI sensitivity. RAI sensitivity is an

important factor in the treatment of PTC. As the frontline therapy for high-risk disease, RAI is a staple in the treatment of aggressive PTC. Unfortunately, *BRAF*^{V600E}-mutant PTC tend to be less differentiated and have lower expression of proteins involved in iodine metabolism (Durante, Puxeddu et al. 2007, TCGA 2014). Fortunately, both *in vitro* and *in vivo* studies have demonstrated that suppression of the MAPK pathway restores expression of iodine metabolism genes in *BRAF*^{V600E} mutant PTC (Liu, Hu et al. 2007, Chakravarty, Santos et al. 2011, Rothenberg, McFadden et al. 2015). Results from case studies and a Phase I clinical trial demonstrated that the MEK inhibitor selumetinib restored RAI sensitivity in previously RAI resistant PTC (Ho, Grewal et al. 2013, Larson, Osborne et al. 2017). Specifically, in a Phase I trial, selumetinib treatment restored RAI sensitivity in 12 of 20 patients. Eight patients reached the dosimetry threshold for RAI treatment and received RAI therapy. These patients had a mean 89% reduction in Tg levels (increasing levels correspond with disease growth) with five partial responses and three stable diseases by RECIST criteria (Ho, Grewal et al. 2013). There is now a Phase II trial testing the efficacy of selumetinib as a RAI adjuvant therapy in patients with recurrent or metastatic thyroid cancer (NCT02393690). The BRAF inhibitor dabrafenib has also been shown to restore RAI uptake in six of ten patients with *BRAF*^{V600E}-mutant PTC previously insensitive to RAI. Two of these six patients had a partial response after RAI treatment, while the other four demonstrated stable disease (Rothenberg, McFadden et al. 2015). The ability of MAPK inhibition to restore RAI sensitivity in

patients with aggressive PTC provides a new, disease-specific avenue through which MAPK inhibitors can be beneficial in the management of advanced PTC.

1.4 Shortcomings of MAPK inhibition

While the ability of MAPK inhibitors to improve PFS in *BRAF*^{V600E} malignancies is encouraging, treatment using these small molecule inhibitors is not without consequence. Treatment-associated toxicities are especially concerning in thyroid cancer because most experience with MAPK inhibitors has been restricted melanoma, a fast-paced disease with very short treatment windows. The prolonged time-course of PTC also highlights concerns surrounding financial toxicity associated with the cost of small molecule MAPK inhibitors.

1.4.1 Toxicity

While small molecule inhibitors are much safer than general chemotherapies, their toxicities remain significant. MAPK inhibitors are no exception. The most common concerns involving first- and second-generation RAF inhibitors are the keratoacanthomas and squamous-cell carcinomas that arise from paradoxical activation of the MAPK pathway. These excision-requiring skin lesions occurred in 20-30% of RAF inhibitor-treated melanoma patients (Chapman, Hauschild et al. 2011, Hauschild, Grob et al. 2012). In addition to these dermal ailments, vemurafenib also induced

photosensitivity, arthralgia, rash, fatigue, nausea, and diarrhea in melanoma patients. The severity of these toxicities required 38% of melanoma patients to undergo dose modification (Chapman, Hauschild et al. 2011). Dabrafenib was similarly challenged by adverse events. More than half of melanoma patients receiving dabrafenib treatment experienced grade 2 or higher treatment related toxicities, which is higher than the 44% of patients who received dacarbazine. The most common side-effects of dabrafenib were skin lesions, fever, fatigue, arthralgia, and headache (Hauschild, Grob et al. 2012). While the side-effect profiles of both RAF inhibitors are robust, their FDA approval was secured due to the lethal of nature of melanoma. Fortunately, some of these side-effects, especially skin lesions attributed to paradoxical MAPK pathway activation, are suppressed by MEK inhibitors (Larkin, Ascierto et al. 2014, Long, Flaherty et al. 2017).

Although the MAPK combination therapies are less subject to the keratoacanthomas and squamous-cell carcinomas associated with first- and second-generation RAF inhibitors, such combination treatments also have significant side-effects. The dabrafenib-trametinib combination therapy had a similar rate of adverse events to dabrafenib-only therapy. However, patients treated with this combination therapy experienced a greater rate of pyrexia (55%) than patients treated with dabrafenib-only (28%). In addition, dabrafenib-trametinib combination-treated patients experience more severe grade pyrexia than dabrafenib-single therapy-treated patients. Dose reductions were required in 25% and 13%, and dose interruption required in 49%

and 33% of combination and dabrafenib-single therapy patients, respectively (Long, Stroyakovskiy et al. 2014). A Phase III vemurafenib-cobimetinib combination trial was similarity affect by drug toxicities. 49% of both combination and vemurafenib-only treated groups experienced grade 3 toxicities with 13% and 9% experiencing grade 4 events, respectively. Both combination and vemurafenib-only groups also experienced similar rates (12% and 13%, respectively) of drug discontinuation (Larkin, Ascierto et al. 2014). Both combination therapies also had a ~2% rate of treatment-associated death (Larkin, Ascierto et al. 2014, Long, Stroyakovskiy et al. 2014). Despite the relief from cutaneous lesion afforded by RAF-MEK combination therapy, the percentage of melanoma patients who experienced severe adverse events remain significant.

The side-effect profile of RAF inhibitors in $BRAF^{V600E}$-mutant RAI-resistant PTC is consistent with the side-effect profile of RAF inhibitors in other $BRAF^{V600E}$-mutant malignancies. The Phase II trial showing the effectiveness of vemurafenib in patients with $BRAF^{V600E}$-mutant RAI-resistant PTC, also noted that 66% of patients experienced grade 3 or 4 treatment-related adverse events with a 62% rate of serious adverse events (Brose, Cabanillas et al. 2016). While dabrafenib treatment was better tolerated in patients with $BRAF^{V600E}$-mutant RAI-resistant PTC, the rate of adverse events such as pyrexia, fatigue, and squamous cell carcinoma was comparable to that seen in $BRAF^{V600E}$-mutant melanoma (Falchook, Millward et al. 2015). Selumetinib treatment for the restoration of RAI sensitivity resulted in the majority of patients experiencing low grade

fatigue (80%), rash (70%), and elevated liver protein levels (70%) (Ho, Grewal et al. 2013). The persistence of severe side-effect profiles associated with MAPK inhibitors fuels the continuing search for more effective and less toxic treatments, which will be especially important in the treatment of an insidiously aggressive disease such as PTC.

1.4.2 Duration

MAPK inhibitors are a class of relatively new therapies with little track record for long-term therapy. This problem is compounded by the lethal nature of melanoma, in which the safety profiles of these drugs were established. Between the short treatment window due to disease mortality and the regency of MAPK inhibitor development, the effect of enduring treatment with MAPK inhibitors remains unclear. The most extensive information on long-term MAPK inhibition is from Phase III studies on vemurafenib an dabrafenib-trametinib combination treatment. The five-year final report on the effect of vemurafenib in $BRAF^{V600E}$-mutant melanoma reported that patients who remained on treatment experienced the same initially reported treatment toxicities for the duration of their treatments (Chapman, Hauschild et al. 2011, Puzanov, Amaravadi et al. 2015). Melanoma patients who were treated with dabrafenib-trametinib combination therapy have also reached the five-year landmark. Reports from these studies document the persistence of the initially reported drug toxicities for the duration of their extended

treatments (Falchook, Millward et al. 2015, Long, Eroglu et al. 2017, Long, Flaherty et al. 2017).

Duration of treatment is a significant concern for patients with aggressive TPC. Even for stage 4 and RAI resistant disease, survival is measured in terms of years instead of months. Survival at 10-years for stage 4 and RAI resistant disease are 37% and 15%, respectively (Sciuto, Romano et al. 2009). PTC patients on RAF inhibitor therapy trials have not only shown good initial response, but also an enduring response (Kim, Cabanillas et al. 2013, Falchook, Millward et al. 2015, Brose, Cabanillas et al. 2016). While these results are encouraging for the utility of MAPK inhibitors in *BRAF* mutant thyroid cancer, the duration of disease response also projects years, if not decades, of treatment for these patients. For a disease in which current treatment toxicities are fatigue, the toxicities associated with MAPK inhibitors are significant. Compounded over the course of decades, these drug toxicities become a significant weight in the scale balancing physical and financial drug toxicities against effective treatment.

1.4.3 Cost

The rapidly climbing cost of medical care is a central concern in all fields of medicine. This concern is no different in cancer therapy, where cost of care is projected to reach $173 billion by 2020 (Mariotto, Yabroff et al. 2011). Even for patients with insurance, the out-of-pocket costs are significant (Bestvina, Zullig et al. 2014). The

impact of financial toxicity on patient quality of life and disease prognosis is becoming an increasingly sentient topic in cancer care (Zafar, McNeil et al. 2015, Zafar 2016). Given its decades long disease progression, this concern is even more true in aggressive PTC (Aschebrook-Kilfoy, Schechter et al. 2013, Lubitz, Kong et al. 2014, Lubitz and Sosa 2016). In fact, thyroid patients have one of the highest rates of personal bankruptcy due to cancer care amongst all cancer type, (Ramsey, Blough et al. 2013).

Unfortunately, the recently developed MAPK inhibitors are contributors to this rising coast of cancer care. Several studies have called into question the cost-effectiveness of MAPK inhibitors in comparison to existent chemotherapies (Curl, Vujic et al. 2014, Zhang, Yang et al. 2015). In one melanoma study, vemurafenib was calculated to cost an additional $353,993 dollars per quality-adjusted life year (QALY) gained over treatment with dacarbazine (Curl, Vujic et al. 2014). Dabrafenib was found to cost $363,136 Canadian dollars ($281,860 USD) per QALY in a separate melanoma study (Delea, Amdahl et al. 2015). A third melanoma study found vemurafenib and trametinib combination therapy to cost CHF 385,603 Swiss francs ($407,451 USD) per QALY (Matter-Walstra, Braun et al. 2015). These values all exceed the $100,000 per QALY threshold for cost-effectiveness.

These concerns around cost are especially pertinent to thyroid cancer patients, since the monthly costs for vemurafenib ($13,000 per month), dabrafenib ($9,100 per month), and trametinib ($10,400 per month) may need to be maintained over long-term

treatment (Curl, Vujic et al. 2014). In a disease where cost of treatment is already a top concern for patients (Singer, Husson et al. 2016), this exorbitant cost of MAPK inhibitors could be a significant barrier to clinical use in *BRAF*^{V600E}-mutant PTC.

1.5 Cu as therapy for BRAF^{V600E}-mutant cancers

Copper (Cu) is a trace mineral necessary for a variety of biological processes, most notably myelination and hematopoiesis. Cu was recently shown to be required for MAPK signaling, and provide a strategy to address the problem of toxicity associated with long-term MAPK inhibition, which may be required for PTC. Cu chelators are a group of drugs that have been used clinically for decades and have well-known side-effect profiles. The adaption of these drugs to the treatment of *BRAF*^{V600E} mutant PTC may provide a well-tolerated and financially sustainable method of targeting the MAPK pathway long-term.

1.5.1 Cu biology

Cu is a trace element essential to all life, from prokaryotes to mammals (Festa and Thiele 2011). In humans, Cu is absorbed through the proximal small intestine, where enterocytes absorb Cu from the gastrointestinal lumen via the copper membrane transporter 1 (CMT1). Copper-transporting P-type ATPase 7A (ATP7A) releases the enterocyte Cu into the portal vein where it become albumin bound before reaching the

liver, where 75% of the Cu is absorbed. While 20% of liver Cu is re-excreted through the gastrointestinal tract, the remaining 80% of Cu is then bound to ceruloplasmin by ATP7B in the trans-Golgi network and exported to the periphery (Bost, Houdart et al. 2016). A schematic of Cu metabolism is shown in Figure 5.

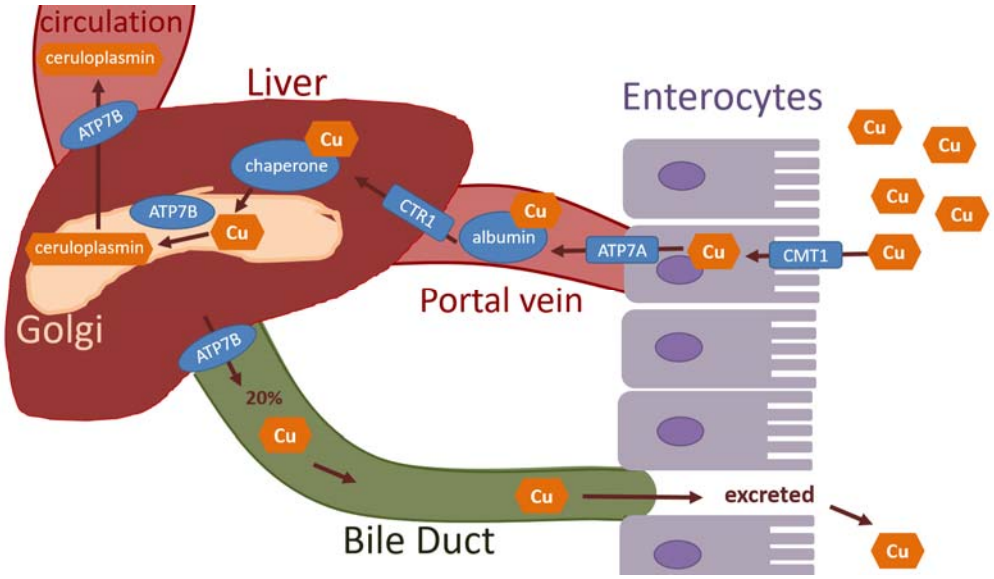

Figure 5: A schematic of Cu metabolism.
Figure created using information disrobed in Bost, *et al. J Trace Elements Med Biol.* 2016.

Ceruloplasmin bound Cu fulfills one of the major biological roles of this trace nutrient: catalyzing the oxidation of iron (Chan and Rennert 1980, Harris 1995). Since iron must be oxidized before it can be bound to the iron-transporter transferrin, Cu deficiency can lead to iron deficiency-like anemias (Halfdanarson, Kumar et al. 2008). Cu also plays a role in the final step of the electron transport chain, where its

requirement by cytochrome c oxidase (COX) IV makes it a critical element to cellular respiration (Festa and Thiele 2011). Cu is also important for the synthesis of norepinephrine (Prohaska, Bailey et al. 1990), peripheral nerve myelin sheathes (Bund, Boggs et al. 2010), collagen and elastin (Rucker, Kosonen et al. 1998), clotting Factor VIII (Tagliavacca, Moon et al. 1997), and melanin (Ebanks, Wickett et al. 2009).

The role of Cu in oxidative stress and angiogenesis is of special importance to human disease. Cu is known to be both anti- and pro-inflammatory (Berthon 1993). Maturation of holoenzyme Cu/Zinc (Zn) Erythrocyte superoxide dismutase (SOD1) through incorporation of Zn and Cu ions in a major pathway through which Cu plays a role in oxidative stress. RNAi mediated knockdown of Cu Metabolism Domain Containing 1 (COMMD1), a regulator of Cu homeostasis, has been shown to induce SOD1 activity and decrease superoxide anion concentrations while overexpression of COMMD1 was shown to have the opposite effect (Vonk, Wijmenga et al. 2010). In turn, inhibition of SOD1 has been shown to inhibit the VEGF-, EGF-, IGF1-, and FGF2-mediated activation of the MAPK pathway (Juarez, Manuia et al. 2008). In fact, inhibition of SOD1 via Cu chelator tetrathiomolybdate (TM) treatment has been shown to reduce angiogenesis and tumor growth *in vitro* (Juarez, Betancourt et al. 2006). This finding, in addition to other studies confirming the pro-angiogenic effect of Cu (Raju, Alessandri et al. 1982, Parke, Bhattacherjee et al. 1988) and the ability to inhibit angiogenesis using Cu chelators (Brem, Zagzag et al. 1990, Juarez, Betancourt et al.

2006), has led to the exploration of Cu chelators as antiangiogenic therapy in multiple cancers (Brewer, Dick et al. 2000, Brewer 2005) (See Section 1.5.4).

.

1.5.2 Cu in MEK1/2 signaling

Cu was first implicated in MAPK signaling through a genome-wide siRNA screen of MAPK pathway modifiers in the *Drosophila*. This screen revealed siRNA targeting the high-affinity Cu uptake protein 1 (Ctr1) to be one of 331 siRNAs that reduced P-Erk levels in *Drosophila* S2 cells (Friedman and Perrimon 2006). A subsequent chemical screen identified disulfiram, which binds and forms a complex with Cu, to be synergistic in suppressing the growth of transformed zebrafish melanocytes in an oncogenic-RAS-driven zebrafish melanoma model (del Ama, Jones et al. 2016). A definitive link between Cu and MAPK signaling was described by Turski et al. in 2012, when it was shown that purified recombinant Mek1 binds specifically to two molecules of Cu (Turski, Brady et al. 2012). They also showed that Cu can elicit a dose-dependent stimulation of Mek1 kinase activity by promoting the physical association of Mek1 with Erk *in vitro*. Furthermore, these effects of Cu chelation were rescuable with supplementation of excess Cu (Turski, Brady et al. 2012). They followed up these biochemical experiments by showing that genetic ablation of Cu transporter *Ctr1* in the prothoracic gland of the fly alters Ras signaling-dependent determinant of body size to produce low-Ras signaling, large bodied flies. The effect of Cu during fly development

was further confirmed in the eye and wings, where knockout of *Ctr1* in constitutively active Ras phenotypes normalized its rough-eye morphology and rescued a lethal mutation to produce flies with largely healthy wings, respectively (Turski, Brady et al. 2012). These findings were conserved in mammals, where $Ctr1^{-/-}$ mouse embryonic fibroblasts (MEF) showed a decrease in insulin-stimulated Erk1/2 phosphorylation that was rescued with expression of wild-type Ctr1. This cellular requirement was then proven physiologically important when mice with cardiac-tissue-specific ablation of *Ctr1* was shown to have decreased Erk1/2 phosphorylation in comparison to wild-type littermates (Turski, Brady et al. 2012).

Cu was subsequently shown to play a necessary role in $BRAF^{V600E}$-driven tumorigenesis when $Ctr1^{-/-}$ and $BRAF^{V600E}$-transformed MEFs were shown to have decreased Erk1/2 phosphorylation that was rescuable by wildtype CTR1, but not by transport-defective CTR1 (Brady, Crowe et al. 2014). The mechanism of Cu's effect on the MAPK pathway was isolated to the MEK level. Targeted mutagenesis was then used to identify the residues necessary for MEK1 binding of Cu as M187, H188, M230, and H239. These residues are in close proximity to the Cu binding site and conserved in the Cu-binding MEK2. MEK's requirement for Cu was then confirmed through four methods: *i*) by showing that the genetic ablation of Cu transporter CTR1 reduced phosphorylation of ERK1/2 by MEK, *ii*) by showing that a MEK1 protein with mutations at the four named residues involved in Cu-binding produced a Cu-binding

mutant (MEK^{CBM}) with decreased kinase activity in spite of concomitant constitutively activating mutations or an overabundance of Cu, *iii*) by showing that a chimeric, non-Cu-requiring MEK (MEK1–MEK5DD) engineered by fusing the ERK1/2-binding region of MEK1 to the non-Cu binding region of a constitutively active MEK5 kinase resulted in high levels of ERK1/2 phosphorylation regardless of *Ctr1* knockout, and *iv*) showing that expression of an auto-phosphorylating and phosphatase insensitive, gain-of-function ERK2 (ERK2GOF), restored tumor growth in *Ctr1* knockout cells by bypassing the need for MEK phosphorylation of ERK (Brady, Crowe et al. 2014).

These *in vitro* findings held true in *in vivo* studies, where $Ctr1^{-/-}$;$Braf^{CA/+}$;$Trp53^{fl/fl}$ mice developed fewer lung tumors and less abnormal lung tissue than $Braf^{CA/+}$;$Trp53^{fl/fl}$ *Ctr1* wild-type littermates when treated with intranasal Cre Recombinase adenovirus. Furthermore, abnormal MAPK activation by $BRAF^{V600E}$ was shown to be targetable pharmacologically when Cu chelators D-penicillamine, trientine, and ammonium tetrathimoybdate (TM) were shown to reduce the growth of $BRAF^{V600E}$-transformed MEFs, but not $BRAF^{V600E}$-transformed MEFs expressing MEK1–MEK5DD or ERK2GOF (Brady, Crowe et al. 2014). These results were further confirmed in a genetically engineered mouse model of $BRAF^{V600E}$-driven melanoma (Brady, Crowe et al. 2017). These $Braf^{CA/+}$;$Pten^{fl/fl}$;*Tyrosinase::*$CreERT2^{tg}$ mice with melanocyte specific expression of $BRAF^{V600E}$ and *Pten* deletion after topical application of 4-hydroxytamoxifen were shown to have reduced serum Cu and improved survival when treated orally with Cu chelator

TM. Genetic knockout of Cu transporter *Ctr1* in these mice also demonstrated an increased median survival (Brady, Crowe et al. 2017). Furthermore, this paper also described the ability of Cu chelator TM to counter MAPK-dependent forms of resistance to MAPK inhibitors in an *in vitro* anchorage-independent growth assay of $BRAF^{V600E}$-mutant melanoma cell line A375. As resistance to targeted therapy is a major concern in cancer therapy, the continued effectiveness of Cu chelator TM in the setting of some known resistance-imparting mutations highlighted Cu chelators' potential in combating MAPK inhibitor resistant disease. The potential of Cu chelators in a clinical setting was further emphasized by the ability of TM to enhance the anti-neoplastic effects of MAPK inhibitors vemurafenib and trametinib on the same melanoma cell line (Brady, Crowe et al. 2017).

1.5.3 Established uses for Cu chelation therapy

There are currently two FDA-approved chelators, D-penicillamine and trientine. These chelators are used for two main clinical indications: 1) in cases of heavy metal poisoning (Cao, Skaug et al. 2015) and 2) as a treatment for Wilson's Disease patients. While duration of chelation treatment is short-term for patients with heavy metal poisoning, patients with Wilson's Disease receive a longer term of treatment. Wilson's Disease patients have a mutation in the *ATP7B* gene which regulate hepatocyte Cu transport. Patients with this mutation have difficulty incorporating Cu into

ceruloplasmin and decreased ability to excrete Cu into the bile, the main mechanism for eliminating excess Cu. Thus, Wilson's Disease patients often present in mid-life when the hepatocellular accumulation of Cu reaches toxic levels. Once diagnosed, Wilson's Disease patients remain on Cu chelation for the rest of their lives (Huster 2010, Kodama, Fujisawa et al. 2012).

As mentioned, there are currently two Cu chelators FDA approved for the treatment of Wilson's Disease: penicillamine and trientine. Penicillamine was approved in 1956 and remains the frontline treatment for patients with Wilson's Disease (Walshe 1956). Trientine was subsequently approved in 1982 and is reserved for patients who had reactions to penicillamine treatment (Walshe 1982). Trientine is now commonly used as the long-term treatment for Wilson's Disease patients after initial Cu reduction with penicillamine (Scheinberg, Jaffe et al. 1987, Dahlman, Hartvig et al. 1995). Although both treatments work well at preventing the hepatic toxicities involved in Wilson's Disease, neither drug is optimal against the neurological presentations of Wilson's Disease. A new Cu chelation therapy, ammonium tetrathiomolybdate (TM), has proven to be more effective than both penicillamine and trientine at reducing these neurological symptoms (Brewer, Askari et al. 2006, Brewer, Askari et al. 2009). This drug is now approved for use in Wilson's Disease patients by the European Commission and is currently in Phase II clinical trial in the United States (NCT02273596).

The relative effectiveness of TM over penicillamine and trientine is due to its ability to form a stable tripartite complex with Cu and protein (Brewer, Dick et al. 2000). When administered with food, TM not only prevents Cu absorption like penicillamine and trientine, but also prevents reabsorption of endogenous Cu secreted in the saliva. When administered without food, TM is absorbed into the blood stream where is binds to both free and albumin bound Cu. This dual action makes the Cu-chelating properties of TM more potent than penicillamine or trientine (Brewer, Dick et al. 2000, Brewer, Askari et al. 2009). Despite this potency, treatment with TM is relatively non-toxic with 12% and 16% of patients experiencing recoverable anemia and transaminase elevations, respectively (Brewer, Askari et al. 2006, Brewer, Askari et al. 2009). A summary of Cu chelator molecular structures, mechanism of action, and use in Wilson's Disease are presented in Table 6.

Table 6: Cu chelator molecular structures, mechanism of action, and use in Wilson's Disease.

Table created using data from various sources. [1]As described in Brewer *et al. Arch Neurol.* 2006. [2]As described in Walshe *et al. Am J Med.* 1956. [3]As described in Walshe *et al. Lancet.* 1982. [4]As confirmed in the European Commission community register of orphan medicinal products. [5]In progress clinical trial number NCT02273596.

Drug	Structure	Cu-bound structure	Mechanism	Use
penicillamine	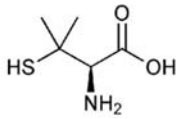	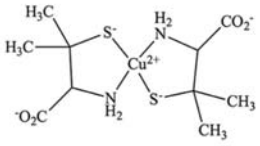	Prevents intestinal absorption of Cu.[1]	- FDA approved as frontline therapy for Wilson's Disease.[2] - Not effective against neurological symptoms.[1]
trientine	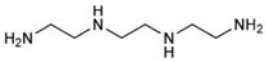	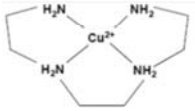	Prevents intestinal absorption of Cu.[1]	-FDA approved in patients who do not tolerate penicillamine.[3] - Not effective against neurological symptoms. [1]
TM	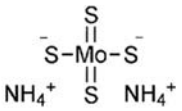	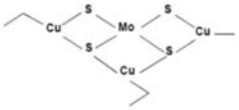	With food- Prevents intestinal Cu absorption and reabsorption of endogenous Cu.[1] Without food- binds both free and albumin-bound Cu in the serum.[1]	- European Commission approved for Wilson's Disease. [4] - In Phase II clinical trial as therapy for neurological symptoms of Wilson's Disease.[5]

1.5.4 Cu chelation in cancer therapy

Cu chelators, especially TM, have been explored in cancer therapy for over a decade with inconclusive results (Brewer, Dick et al. 2000, Redman, Esper et al. 2003, Pass, Brewer et al. 2008). These trials were initiated due to the importance of Cu in the tumor microenvironment (Jain, Cohen et al. 2013, Chan, Willis et al. 2017) and during angiogenesis (Brem, Zagzag et al. 1990, Finney, Vogt et al. 2009). Unfortunately, these

clinical trials did not significantly reduce tumor load or improve patient survival. However, these trials did provide invaluable evidence that TM treatment can be well tolerated even in seriously ill cancer patients (Hou, Dick et al. 2007).

The most common side-effects suffered by cancer patients treated with TM was the same as symptoms of iatrogenic Cu depletion Wilson's Disease patients on Cu chelation therapy: mild fatigue, sulfurous burps, anemia, and neutropenia (Brewer, Dick et al. 2000, Redman, Esper et al. 2003, Pass, Brewer et al. 2008) (Table 7). 12.5% and 20.9% of patients experienced mild anemia and neutropenia, respectively, with only 0.07% and 3.7% of patients suffering grade 3 or higher events (Chan, Willis et al. 2017). These adverse events tended to occur as mild and transient anemia during the first two weeks of treatment that resolved spontaneously or with dose adjustment in grade 3/4 events (Brewer, Dick et al. 2000, Redman, Esper et al. 2003, Pass, Brewer et al. 2008). In addition to this encouragingly mild side-effect profile, TM was also found to be well-tolerated long-term. In one Phase I study, one patient with metastatic breast cancer received TM thrice daily for >65 months (Jain, Cohen et al. 2013).

Table 7: Trials of TM in cancer therapy.
Table created using data from various sources. [1]As described in Brewer et al. *Clin Cancer Res*. 2000. [2]As described in Redman et al. *Clin Cancer Res*. 2003. [3]As described in Pass et al. *Ann Thorac Surg*. 2008. [4]As described in Chan et al. *Clin Cancer Res*. 2017. [5]As described in Jain et al. *Ann Oncol*. 2013.

Disease	Side-effects	Severe events	Treatment Duration	Phase
Metastatic Cancers[1]	mild reversible anemia, and sulfurous eructation	11% anemia	8-15 months	Phase I
Renal Cancer[2]	granulocytopenia, fatigue, and sulfurous eructation	26% granulocytopenia	Median of 7.9 months	Phase II
Malignant Mesothelioma[3]	dizziness, anemia, granulocytopenia, and thrombocytopenia	13% anemia 3% thrombocytopenia	2 months to 57 months	Phase II
Breast Cancer[4]	neutropenia, sulfur eructation, and fatigue	3.7% neutropenia 1.6% leukopenia	up to 24 months	Phase II
Breast Cancer[5]	anemia, neutropenia, leukopenia, sulfurous eructation, and fatigue	3.1% neutropenia 0.2% anemia	1 month to >65 months	Phase II

1.5.5 Potential for Cu chelation therapy in *BRAF^{V600E}*-mutant PTC

The benign safety-profile and long-term tolerability of Cu chelators make them an attractive treatment for diseases with a prolonged time course. PTC is such a disease. Even patients with advanced, RAI-refractory PTC have prognoses that extend for decades (Sciuto, Romano et al. 2009). Indeed, the average time to recurrence is 8.1 years for all stages of PTC, with 17% of deaths occurring after 20 years (Grogan, Kaplan et al. 2013). This poses unique challenges to targeting the MAPK pathway in PTC, as cost and toxicities are amplified over prolonged treatment. During this time, PTC patients must balance the value gained from toxic treatment against a slowly advancing, often

asymptomatic disease (Lubitz and Sosa 2016, Gild, Topliss et al. 2017). For these patients with aggressive PTC, there are currently two FDA approved TKIs, sorafenib and lenvatinib, which although less toxic than chemotherapy, still have significant side-effect profile (Brose, Nutting et al. 2014, Lorusso, Pieruzzi et al. 2016). Sorafenib and lenvatinib also do not directly target the instigating $BRAF^{V600E}$ mutation (Costa, Herrero et al. 2008, Elisei, Viola et al. 2012). Cu chelators present a possible less toxic method of targeting $BRAF^{V600E}$-mutated PTC.

Although RAF and MEK inhibitors have proven effective against $BRAF^{V600E}$-mutated PTC in early clinical trials, treatment with these inhibitors has significant toxicities that led to dose reduction in ~38% of patients (Brose, Cabanillas et al. 2016). Conversely, previous trials testing Cu chelator TM in cancer have shown that the drug is ineffective at limiting disease progression, but are well tolerated in cancer patients (Brewer, Dick et al. 2000, Redman, Esper et al. 2003, Pass, Brewer et al. 2008). The discovery that MEK requires Cu to mediate $BRAF^{V600E}$ oncogenic signaling (Turski, Brady et al. 2012, Brady, Crowe et al. 2014) presents a potential solution to both problems. Namely, the use of well-tolerated Cu chelators as targeted therapy against $BRAF^{V600E}$ mutant PTC could resolved the toxicity issues associated with MAPK inhibitors in this disease, where long-term quality of life is of special importance.

2. Copper chelation as targeted therapy in a mouse model of oncogenic BRAF-driven papillary thyroid cancer

NOTE: Chapter 2 was modified from a manuscript of the same title accepted for publication in Clinical Cancer Research. The authors were MengMeng Xu, Michael Casio, Danielle E. Range, Julie A. Sosa, and Christopher M. Counter. Michael Casio helped H&E stain and scan in thyroid sections. Danielle E. Range delineated the tumors in H&E stained thyroid sections. I performed all the other experiments.

2.1 Introduction

As discussed in Chapter 1, the incidence of thyroid has more than tripled over the past four decades, with the papillary thyroid cancer (PTC) histologic subtype accounting for the overwhelming majority of this rising incidence (Davies and Welch 2014, Howlader N 2017). Fortunately, most PTC patients are diagnosed with early stage disease, which responds well to surgical resection with or without radioactive iodine (RAI) therapy. However, a subset of PTC cases does not respond to conventional therapy. The therapeutic options for patients with progressive or symptomatic disease not amenable to surgical resection or RAI are limited to the tyrosine kinase inhibitors (TKIs) sorafenib or lenvatinib (Harris and Bible 2011, Haugen, Alexander et al. 2016). While these therapies extend progression free survival, they are associated with well-documented toxicities (Brose, Nutting et al. 2014, Schlumberger, Tahara et al. 2015).

Additionally, PTC is typically diagnosed in patients under 55 years of age, yet disease-specific death peaks in the 70s (Kitahara and Sosa 2016). This presents a unique, decades-long clinical challenge between balancing appropriate therapy with patient quality of life (Lubitz, Kong et al. 2014, Lubitz and Sosa 2016).

In the United States, 40% to 60% of PTC tumors have an oncogenic (V600E) mutation in the kinase BRAF (Xing 2013), which is associated with a 2-fold increase in recurrent/persistent disease and increased mortality (Xing 2010, Xing 2013). MAPK inhibitors have been approved for the treatment of $BRAF^{V600E}$-mutant melanoma (Chapman, Hauschild et al. 2011, Larkin, Ascierto et al. 2014, Ascierto, McArthur et al. 2016) and show encouraging early results in patients with $BRAF^{V600E}$-mutant RAI-resistant PTC. BRAF inhibitor vemurafenib improved progression-free survival by 15.6 and 9.8 months in TKI-naïve and TKI-treated patients with response rates of 58% and 36%, respectively (Kim, Cabanillas et al. 2013). Another BRAF inhibitor, dabrafenib extended progression-free survival by 11.3 months, with only one patient progressing, and then only after 9.3 months of response (Falchook, Millward et al. 2015). MEK inhibitors are also showing promise in the management of advanced PTC by restoring tumor sensitivity to RAI (Leijen, Soetekouw et al. 2011, Ho, Grewal et al. 2013, Larson, Osborne et al. 2017).

While these results are encouraging, clinical adoption of MAPK inhibitors for long-term treatment of $BRAF^{V600E}$-mutant PTC may be complicated by the protracted

PTC disease course, which may necessitate years of continuous treatment. Current phase II clinical data suggest that 66% of *BRAF*^{V600E}-mutant PTC patients treated with vemurafenib experienced serious adverse events with 28% of patients choosing to discontinue treatment due to these adverse events (Brose, Cabanillas et al. 2016). Such toxicities must be weighed against the quality of life and cost of therapy, especially in a disease like PTC for which patients can remain asymptomatic for decades (Ramsey, Blough et al. 2013, Lubitz, Kong et al. 2014, Lubitz and Sosa 2016, Zafar 2016, Gild, Topliss et al. 2017).

Previous work by Donita Brady and Matt Crowe in our lab and Michelle Turski in the lab of Dennis Thiele showed that MEK1/2 require the metal Cu for kinase activity and to mediate the oncogenic signaling and tumorigenic activity of BRAF^{V600E}. They also demonstrated that MEK1/2 can be pharmacologically targeted with existing Cu chelating drugs (Turski, Brady et al. 2012, Brady, Crowe et al. 2014, Brady, Crowe et al. 2017). Cu chelators have a history of low toxicity from their use as long-term therapy in Wilson's Disease, a disease of Cu overload (Das and Ray 2006, Ala, Walker et al. 2007). This low toxicity profile presents a potential niche opportunity to provide a relatively non-toxic method of targeting *BRAF*^{V600E}-mutant PTC using Cu chelation. The experiments in this chapter are designed to explore a possible solution to targeting the MAPK pathway in a relatively non-toxic fashion by using Cu chelation as a targeted therapy against *BRAF*^{V600E}-mutant PTC.

2.2 Materials and Methods

2.2.1 Cell lines

BCPAP (Schweppe, Klopper et al. 2008) and K1 (Saiselet, Floor et al. 2012) cells were purchased from ATCC in March 2014 and maintained in RPMI supplemented with 10% fetal bovine serum, 1% penicillin, and 1% streptomycin. The identity of both cell lines was confirmed in January 2018 by DNA profiling of polymorphic short tandem repeat (STR) markers, which were obtained through the Duke University DNA Analysis Facility's human cell line authentication analysis service using the GenePrint 10 kit (Promega). The resultant STR makers were compared to those available for BCPAP (CVCL_0153) and K1 (CVCL_2537) cells lines through Cellosaurus (Schweppe, Klopper et al. 2008). Both cell lines were also confirmed to be free of mycoplasma infection in February 2018, as assessed by the Duke Cell Culture Facility using the MycoAlert PLUS kit (Lonza). BCPAP cell lines were engineered to express $ERK2^{GOF}$ by stable infection using established methods (O'Hayer and Counter 2006) of a retrovirus derived from the plasmid pBABEpuro-HA-$ERK2^{GOF}$ encoding the $ERK2^{R67S,D321N}$ mutant form of ERK2, termed ERK^{GOF} (Brady, Crowe et al. 2014).

2.2.2 Drug preparation

Trametinib, vemurafenib, sorafenib (Chemitek), lenvatinib (Selleckchem), and ammonium tetrathiomolybdate (Sigma-Aldrich), termed TM, were dissolved in DMSO

for *in vitro* experiments and 1% DMSO / 1% methylcellulose for *in vivo* experiments, as described (Brady, Crowe et al. 2014, Brady, Crowe et al. 2017).

2.2.3 Soft agar assay

Soft agar assays were performed as previously described (Brady, Crowe et al. 2014). In brief, 1 ml of 0.3% bactoagar-RPMI solution containing $2.0x10^4$ BCPAP cells or $1.0x10^4$ K1 cells and the indicated concentration of drug or vehicle was plated into each well of a 6-well plate already containing a solidified 2 ml bottom layer of 0.6% bactoagar-RPMI solution also containing the relevant vehicle or drug. Cells were fed weekly with 250 μl of media containing vehicle or drug. After 3 weeks, colonies containing > 50 cells were counted in a blinded fashion. Drug concentrations were determined based on effective concentration. Specifically, we first empirically identified the lowest concentrations of each drug that inhibited colony formation (see below) to the maximum level, and termed this the EC_{100}. Based on this, the EC_0, $EC_{12.5}$, EC_{25}, EC_{50}, EC_{100}, and EC_{200} and are as follows: 0, 50, 100, 200, 400, or 800 nM for TM; 12.5, 25, 50, 100, or 200 nM for sorafenib; 12.5, 25, 50, 100, or 200 nM for lenvatinib; 12.5, 25, 50, 100, or 200 nM for vemurafenib; and 0.625, 1.25, 2.5, 5.0, or 10.0 nM for trametinib (Table 8). Each drug was serially diluted from the highest concentration so that the total volume of DMSO added was identical in each well with the 0 nM control, namely the total volume of DMSO per well was 200 μl for TM, 50 μl for sorafenib, lenvatinib, and vemurafenib, and 25 μl for trametinib, regardless of the dilution. The concentrations of drugs in

combinations experiments were combined in fixed-ratio doses in order to calculate therapeutic synergy.

Table 8: Drug concentrations corresponding to each effective concentration.

Drug	$EC_{6.25}$	$EC_{12.5}$	EC_{25}	EC_{50}	EC_{100}	EC_{200}
lenvatinib	not determined	12.5 nM	25 nM	50 nM	100 nM	200 nM
sorafenib	not determined	12.5 nM	25 nM	50 nM	100 nM	200 nM
TM	25 nM	50 nM	100 nM	200 nM	400 nM	800 nM
trametinib	not determined	0.625 nM	1.25 nM	2.5 nM	5 nM	10 nM
trientine	not determined	12.5 nM	25 nM	50 nM	100 nM	200 nM
vemurafenib	6.25 nM	12.5 nM	25 nM	50 nM	100 nM	200 nM

2.2.4 Immunoblot analysis

Whole cell lysates were isolated using standard RIPA buffer containing proteases and phosphatases and quantified using the Lowery protein assay (BioRad). 50 μg of lysates from BCPAP cells treated with DMSO vehicle or increasing concentrations (25 nM, 50 nM, or 100 nM) of TM for 7 days or TM ($EC_{6.25}$, 25 μM), vemurafenib ($EC_{6.25}$, 6.25 μM) or both drugs at the same concentrations for 7 days were resolved by SDS-PAGE and immunoblotted with a rabbit anti-phospho(Thr 202/Tyr 204)-ERK1/2 antibody (Cell Signaling Technology, antibody # 3700 at a 1:1000 dilution), a mouse anti-ERK1/2 antibody (Cell Signaling Technology, antibody # 9101 at a 1:1000 dilution), a mouse anti-HA-Tag antibody (Cell Signaling Technology, antibody # 2367 at a 1:1000 dilution), a

rabbit anti-phospho-S6 ribosomal protein (Ser235/236) antibody (Cell Signaling Technology, antibody #4858S at a 1:1000 dilution), a rabbit anti-S6 ribosomal protein (Cell Signaling Technology, antibody #2217 at a 1:1000 dilution), or a mouse anti-β-tubulin (Sigma-Aldrich, antibody # 2367 at a 1:5000 dilution) followed by a goat anti-rabbit IgG (Cell Signaling Technology, antibody # 7076 at a 1:10,000 dilution) or a goat anti-mouse IgG (Cell Signaling Technology, antibody # 7074 at a 1:10,000 dilution) horseradish peroxidase-conjugated secondary antibody and visualized using enhanced chemiluminescence detection (Cell Signaling Technology).

2.2.5 8-week treatment TBP mouse study

Mice with *Braf*^{CA} (Dankort, Filenova et al. 2007), *Pten*^{fl} (Lesche, Groszer et al. 2002), and *Thyro::CreER*^{T2} (Undeutsch, Lof et al. 2014) alleles were obtained from the Jackson Laboratory or as a kind gift from the laboratories of David Kirsch (Duke University), or Martin McMahon (University of Utah). *Braf*$^{CA/CA}$;Pten$^{fl/fl}$ and *Thyro::CreER*$^{T2/+}$ mice were crossed to generate ***T****hyro::CreER*$^{T2/+}$;***B****raf*$^{CA/+}$;***P****ten*$^{fl/+}$ (TBP) mice (Charles, Silva et al. 2014). Mice in this study were derived from a mixed BL6 and Sv129 background and littermates were used regardless of sex. At 40 days of age, TBP mice received a single 100 μl intraperitoneal injection of a 10 mg/ml tamoxifen (Sigma-Aldrich) dissolved in peanut oil to activate CreER in thyrocytes and induce tumorigenesis. 8 weeks later, cohorts of 10 mice each were randomly assigned to one of three treatment groups receiving daily oral gavage of vehicle (250 μl of 1% DMSO/1%

methylcellulose), vemurafenib (50 mg/kg), or TM (80 mg/kg). The appearance, behavior, and weight of mice were monitored daily and drug holidays provided if weight dropped below 10% of the animal's maximum weight. Drug holiday was maintained until the mouse reached its previous weight. There was only a one-day difference in the average number of treatment days between the three cohorts (Table 9). Mice were euthanized at the end of the 8-week treatment period and their thyroids removed for analysis. Studies involving mice were conducted in accordance with protocols approved by the Duke University Institutional Animal Care and Use Committee.

2.2.6 24-week treatment TBP mouse study

At 40 days of age TBP mice were injected with tamoxifen as above to induce thyroid tumorigenesis. Mice in this study were derived from a mixed BL6 and Sv129 background and littermates were used regardless of sex. 8 weeks later, mice were randomly assigned into cohorts of 17 mice that were treated by daily oral gavage with vemurafenib (50 mg/kg) and either vehicle (250 μl of 1% DMSO/1% methylcellulose) or TM (80 mg/kg) for 4 weeks. Vemurafenib treatments were then terminated while vehicle or TM treatments were continued for a further 20 weeks. Mice were monitored as above and given drug holidays if required. All mice were humanely euthanized at the end of the 24-week treatment period and their tumors removed for analysis. Study was conducted in accordance with protocols approved by the Duke University Institutional Animal Care and Use Committee.

Table 9: Days per week (up to 7) mice (1-10) were treated with vehicle, vemurafenib, or TM in the 8-week study.

	Mouse	Week of treatment (days per week treated)								Total days treated
		1	2	3	4	5	6	7	8	
vehicle treatment	1	7	7	7	5	5	5	7	7	50
	2	7	7	7	5	5	5	7	7	50
	3	7	7	7	5	5	5	7	7	50
	4	7	7	7	5	5	5	7	7	50
	5	7	5	7	7	7	6	7	7	53
	6	7	5	7	7	7	5	7	7	52
	7	7	7	5	7	7	5	7	7	52
	8	7	7	5	7	7	5	7	7	52
	9	7	6	7	5	7	5	7	7	51
	10	7	7	5	7	7	5	7	5	50
	Average	**7.0**	**6.5**	**6.4**	**6.0**	**6.2**	**5.1**	**7.0**	**6.8**	**51.0**
Vemurafenib treatment	1	7	7	7	5	5	5	5	7	48
	2	7	6	7	5	5	5	7	7	49
	3	7	5	5	5	5	7	6	7	47
	4	7	5	5	5	5	7	7	7	48
	5	5	5	5	5	6	6	5	7	44
	6	7	5	7	7	7	7	6	7	53
	7	7	5	7	7	7	7	7	7	54
	8	7	5	7	7	7	7	7	7	54
	9	7	7	5	7	7	5	7	7	52
	10	7	6	7	6	5	7	6	7	51
	Average	**6.8**	**5.6**	**6.2**	**5.9**	**5.9**	**6.3**	**6.3**	**7.0**	**50.0**
TM treatment	1	7	7	5	5	4	5	7	7	47
	2	7	6	7	4	5	5	7	6	47
	3	5	5	5	6	7	6	5	7	46
	4	7	7	5	7	6	7	7	6	52
	5	7	7	5	6	5	6	7	6	49
	6	7	5	7	7	5	6	7	7	51
	7	7	7	6	5	7	7	6	7	52
	8	7	6	5	7	6	7	6	7	51
	9	5	7	6	7	6	7	7	6	51
	10	7	5	7	5	6	7	7	6	50
	Average	**6.6**	**6.2**	**5.8**	**5.9**	**5.7**	**6.3**	**6.6**	**6.5**	**49.6**

2.2.7 *Ctr1*$^{fl/fl}$ TBP mouse study

Mice with a *Ctr1*^{fl} allele (Kuo, Zhou et al. 2001), a kind gift of Dennis Thiele (Duke University), were used to generate *Braf*$^{CA/CA}$;*Pten*$^{fl/fl}$;*Ctr1*$^{fl/+}$ and *Ctr1*$^{fl/+}$;*Thyro::*CreER^{T2} mice, which were crossed to generate 23 *Ctr1*$^{+/+}$ versus 8 *Ctr1*$^{fl/fl}$ TBP littermates. Mice in this study were derived from a mixed BL6 and Sv129 background and littermates were used regardless of sex. At 40 days of age, thyroid tumorigenesis was induced by injection of tamoxifen as above, after which the appearance, behavior, and weight of these mice were monitored weekly. Mice were humanely euthanized upon reaching a maximum tumor volume (1 cm^3), 15% weight loss, or moribund. Studies involving mice were conducted in accordance with protocols approved by the Duke University Institutional Animal Care and Use Committee.

2.2.8 Determining tumor volumes in thyroids

Thyroids removed from the above TBP mice at the end of the 8- or 24-week treatment period were fixed in formalin for 24 hours and paraffin embedded. Each thyroid was sectioned in its entirety on a RM2125 RTS microtome (Leica Biosystems Incorporated). Multiple serial slices from every 200 μM throughout the depth of the gland were mounted on slides. Two slides from each depth were reserved for immunohistochemical analysis (see below) while another one was hematoxylin and eosin (H&E) stained and the tumor perimeter delineated by an endocrine pathologist blinded to the genotype. One pathologist performed all tumor delineations over the

span of two months and referenced control slides from a normal and 8-week post-induction thyroid from TBP mice to reduce intra-rater variability. Tumor volume was calculated based on the delineated tumor area for each slide. The tumor load, as defined by percent tumor occupying the total thyroid area, was calculated for each slide and then used to calculate the volume of thyroid occupied by tumor for each mouse.

2.2.9 Immunohistochemistry

The slides reserved for immunohistochemical analysis were de-paraffinized, dehydrated, and stained with a rabbit anti-phospho (Thr 202/Tyr204)-Erk1/2 (Cell Signaling Technology, antibody # 4376, 1:400 dilution) or a rabbit anti-CD31 (Abcam, antibody #28364, 1:100 dilution) by the Duke Pathology Research Histology Laboratory. A breast cancer slide and a mouse spleen slide were used as positive control for p-Erk1/2 and CD31, respectively. High-powered, stitch photographs were taken of the entire tissue on a Vanox S microscope (Olympus Corporation of the Americas). Percentage of immuno-mutant area per tumor was then quantified in a blinded fashion using Image J (NIH). Both thresholding and/or optical density analyses was performed.

2.2.10 Generation of TBP mouse PTC cell lines

Thyroids initially removed en bloc were further dissected to isolate tumors from each lobe. The tumors were rinsed in sterile PBS then macerated into a homogenous paste. Tumor tissue from each lobe where then divided in three and suspended in solutions of 0.2 mg/mL collagenase in RPMI. The suspended tumors were incubated

over night at 37°C with 5% CO_2. Solutions were transferred to 10 cm cell culture plates containing RPMI supplemented with 10% fetal bovine serum, 1% penicillin, and 1% streptomycin. Plates containing the tumor suspension were incubated undisturbed for 48 hours before media as removed and replenished. Adherent cells were allowed to reach 80% confluence before the plates were trypsinized and split at 1:3. This process was repeated until the cell population attained homogenous morphology.

2.2.11 Xenograft model

The cell lines generated from TBP mice were trypsinized, collected, and washed three times using sterile PBS. The cells were resuspended in PBS at a concentration of $5.0x10^7$ cells/mL. 200 mL of this $5.0x10^7$ cells/mL solution was then injected subcutaneously into the flanks of 8- to 12-week-old female SCID/beige mice (Charles River Laboratory) as previously described (Hamad, Elconin et al. 2002). Tumor size was assessed every-other-day using calipers to measure width and length. Tumor volume was calculated using the standard practice: xenograft volume = height x $(width)^2/2$ (Tomayko and Reynolds 1989).

2.2.12 Statistics

Statistical analysis of tumor load, tumor volume, and metastases was performed with two-way analysis of variance (ANOVA) using Prism 6 software (GraphPad Software Incorporated). Kaplan-Meier survival curve analysis was performed using the Mantel-Cox log-rank method to compare survival curves between $Ctr1^{+/+}$ versus $Ctr1^{fl/fl}$

TBP littermates using Prism 6 software (GraphPad Software Incorporated). Synergy between drug combinations was calculated using the previously described Bliss and Combination Indexes (Chou and Talalay 1984, Foucquier and Guedj 2015). Statistical analysis of metastatic lesions, growth in soft agar, and immunohistochemical staining of P-Erk1/2 and CD31 was performed with two-way *t*-test using Prism 6 software (GraphPad Software Incorporated).

2.3 Results

2.3.1 TM reduces growth of human *BRAF*^{V600E}-mutant PTC cell lines through inhibition of MEK1/2

Given the rapidly evolving landscape of targeted therapies for *BRAF*^{V600E}-mutant cancers, we sought to evaluate the therapeutic potential of TM relative to both standard-of-care treatment for progressive and/or symptomatic advanced iodine-resistant PTC, sorafenib and lenvatinib (Gild, Topliss et al. 2017), and the promising MAPK inhibitor, vemurafenib, dabrafenib, and trametinib (Kim, Cabanillas et al. 2013, Falchook, Millward et al. 2015, Brose, Cabanillas et al. 2016, Grimaldi, Simeone et al. 2017). We elected to use a more long-term assay of soft agar growth over traditional proliferation assays. BCPAP cells, one of the very few *BRAF*^{V600E}-mutant human PTC cell lines available (Schweppe, Klopper et al. 2008), were seeded in triplicate in soft agar containing either vehicle or a five-step dose escalation of each of the aforementioned five drugs. The dosages of these drugs were based on the effective concentration, as defined

by the lowest concentration that inhibited colony formation to the maximum level for each drug (EC_{100}). After three weeks of drug treatment, the number of anchorage-independent colonies was counted in a blinded fashion. This analysis revealed that TM was as or more effective than sorafenib and lenvatinib at reducing the anchorage-independent growth of BCPAP cells (Figure 6A). The small effect seen by sorafenib and lenvatinib was not unexpected, as both drugs are TKI inhibitors while the tested cells are *BRAF*^{V600E}-mutant. The relative effectiveness of TM compared to vemurafenib and trametinib tracked with previous studies using *BRAF*^{V600E}-mutant melanoma cell lines (Brady, Crowe et al. 2017), suggesting that TM targets the MAPK pathway with similar effectiveness in *BRAF*^{V600E}-mutant PTC. Similar results were observed in another *BRAF*^{V600E}-mutant human PTC cell line, K1 (Figure 6B). This suggests that TM's effect on cell growth is not restricted to BCAP cells and likely targets the MAPK pathway of *BRAF*^{V600E}-mutant PTC with similar effectiveness as seen in other *BRAF*^{V600E}-mutant cancers.

The only drug in K1 cells that did not track with findings from BCPAP cells was lenvatinib (Figure 6B). Instead of mildly inhibiting transformed cell growth, lenvatinib increased the growth of K1 cells by approximately 40%. This could be attributed to the additional glutamic acid to lysine mutation at position 542 of *PI3KCA* found in the K1 cell line (Schweppe, Klopper et al. 2008, Saiselet, Floor et al. 2012), which leads to increased binding affinity for negatively charged phosphatidylinositol substrates and

subsequent increase in cell growth and invasion (Karakas, Bachman et al. 2006, Gustin, Cosgrove et al. 2008). Mutations in this region of *PI3KCA* have been associated with poor prognosis (Li, Rong et al. 2006, Barbareschi, Buttitta et al. 2007, Kato, Iida et al. 2007) and increased PI3K signaling has been linked to drug resistance in a number of cancers (Tang and Ling 2014, Guerrero-Zotano, Mayer et al. 2016, Lindblad, Cordero et al. 2016). While lenvatinib targets many kinases, this drug does not target the PI3K or MAPK pathways active in K1 cells (Lorusso, Pieruzzi et al. 2016, Hussein, Mizuo et al. 2017) and could account for its ineffectiveness in soft-agar assay.

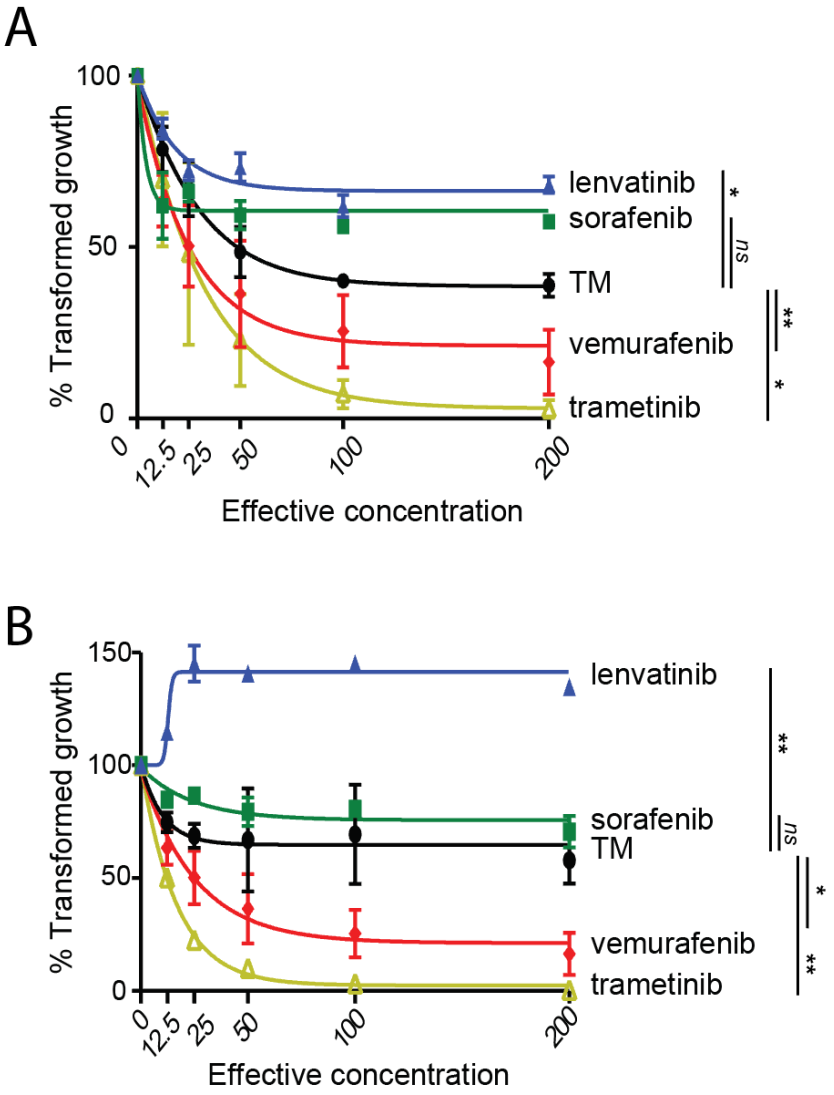

Figure 6: TM reduces anchorage-independent growth of BCPAP cells an and K1 cells.
A) % transformed growth in soft agar (mean ± SEM, triplicate samples, three experiments) normalized to vehicle control of BCPAP cells treated with increasing doses (effective concentration) of lenvatinib (▲), sorafenib (■), TM (●), vemurafenib (♦), or trametinib (△).
B) % transformed growth in soft agar (mean ± SEM, triplicate samples, three experiments) normalized to vehicle control of K1 cells treated with increasing doses (effective concentration) of lenvatinib (▲), sorafenib (■), TM (●), vemurafenib (♦), or trametinib (△).
*p<0.05, **p<0.01, *ns*= not significant.

To assess whether the effect of TM on transformed growth was through inhibition of MEK1/2 rather than other potential Cu-dependent proteins or pathways, BCPAP cells were engineered and confirmed by immunoblot to stably express ERK^{GOF}, an activated version of this kinase (Brady, Crowe et al. 2014) (Figure 7A). The cells were then treated with TM and the levels of phosphorylation ERK1/2 (P-ERK1/2), the substrates of MEK1/2, and phosphorylated S6 (P-S6), an ERK1/2 substrate, were assessed by immunoblot analysis and transformed growth was assessed by a soft agar assay. As controls, vehicle-treated vector cells (negative control) were shown to exhibit lower P-ERK1/2 and P-S6 levels compared to vehicle-treated ERK^{GOF} cells (positive control). In agreement with previous studies in other $BRAF^{V600E}$-mutant tumor and cancer cell lines (Brady, Crowe et al. 2014, Brady, Crowe et al. 2017), P-ERK1/2 levels were reduced in cells treated with TM (Figure 7A), and furthermore, TM failed to reduce the anchorage-independent growth of BCPAP cells expressing ERK^{GOF} (Figure 7B). Similar results were found with another Cu chelator, trientine, which also reduced anchorage-independent growth of BCPAP cells that was rescued by expression of ERK^{GOF} (Figure 7C). We conclude that TM inhibits MEK1/2 kinase activity and correspondingly retards the transformed growth of the human $BRAF^{V600E}$-mutant PTC cell line BCPAP.

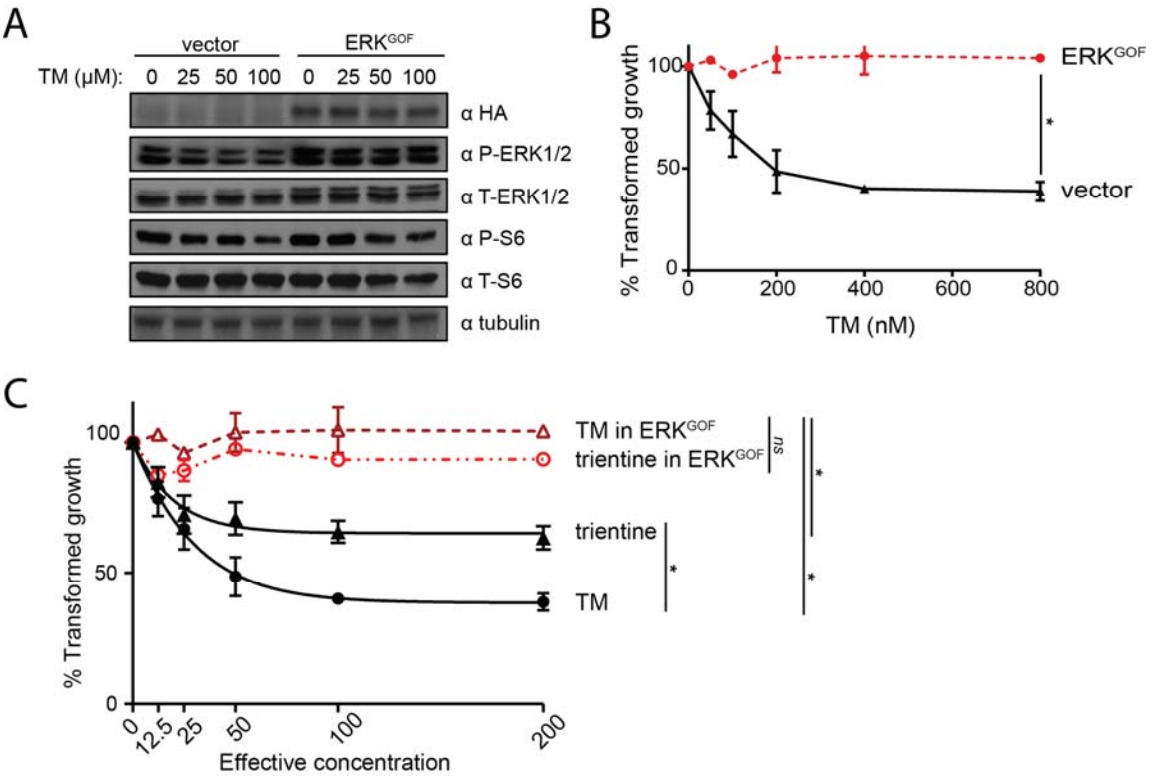

Figure 7: TM inhibits MAPK signaling in BCPAP cells

A) Immunoblot detection of HA epitope-tagged ERK^{GOF}, phosphorylated (P-) and total (T-) Erk1/2 or S6, and tubulin in BCPAP cells transduced with an expression vector encoding no transgene (vector) or ERK^{GOF} treated with the indicated increasing concentrations of TM.

B) % transformed growth in soft agar (mean ± SEM, triplicate samples, three experiments) normalized to vehicle control of BCPAP cells stable transduced with a control vector (▲) or one encoding ERK^{GOF} (●) at the indicated increasing concentrations of TM.

C) % transformed growth in soft agar (mean ± SEM, triplicate samples, three experiments) normalized to vehicle control of BCPAP cells treated with trientine (▲) in comparison to cells treated with TM (●) and BCPAP cells stably transduced with ERK^{GOF} treated with trientine (○) in comparison to cells treated with TM (Δ).

* $p<0.05$, *ns*= not significant.

2.3.2 Oral TM reduces tumor load in a *Braf^{V600E}*-driven mouse model of aggressive PTC

To address whether TM exhibits antineoplastic activity in a more relevant *in vivo* setting, we turned to the genetically engineered ***T****hyro::CreER$^{T2/+}$*;***B****raf$^{CA/+}$*;***P****ten$^{fl/+}$*(TBP) mouse model of PTC. In this model, administration of tamoxifen activates CreER recombinase in the thyrocytes, leading to recombination of the *Braf^{CA}* and *Pten^{fl}* alleles. This results in expression of oncogenic *Braf^{V600E}* and inactivation of the tumor suppressor *Pten* in these cells, which leads to aggressive metastatic PTC (Charles, Silva et al. 2014). Indeed, longitudinal analysis of the thyroids from TBP mice after injection with tamoxifen revealed a stepwise progression from normal thyroid (Figure 8A, B, and C). At two weeks post-injection, gross goiter (Figure 8D, E, and F) was detected. At eight weeks, histologically confirmed PTC with the diagnostic papillary structures and nuclear pallor, grooves, and enlargement were present (Figure 8G, H, and I). At 12 weeks, enlarged tumors were observed (Figure 8J, K, and L) with half of the mice developing metastasis to the lung. The primary tumors retained their PTC characteristics (diagnostic papillary structures, and nuclear pallor, grooves, and enlargement). This lack of dedifferentiation into ATC and tumor aggression confirms the validity of TBP as a model for aggressive *Braf^{V600E}*-mutant PTC.

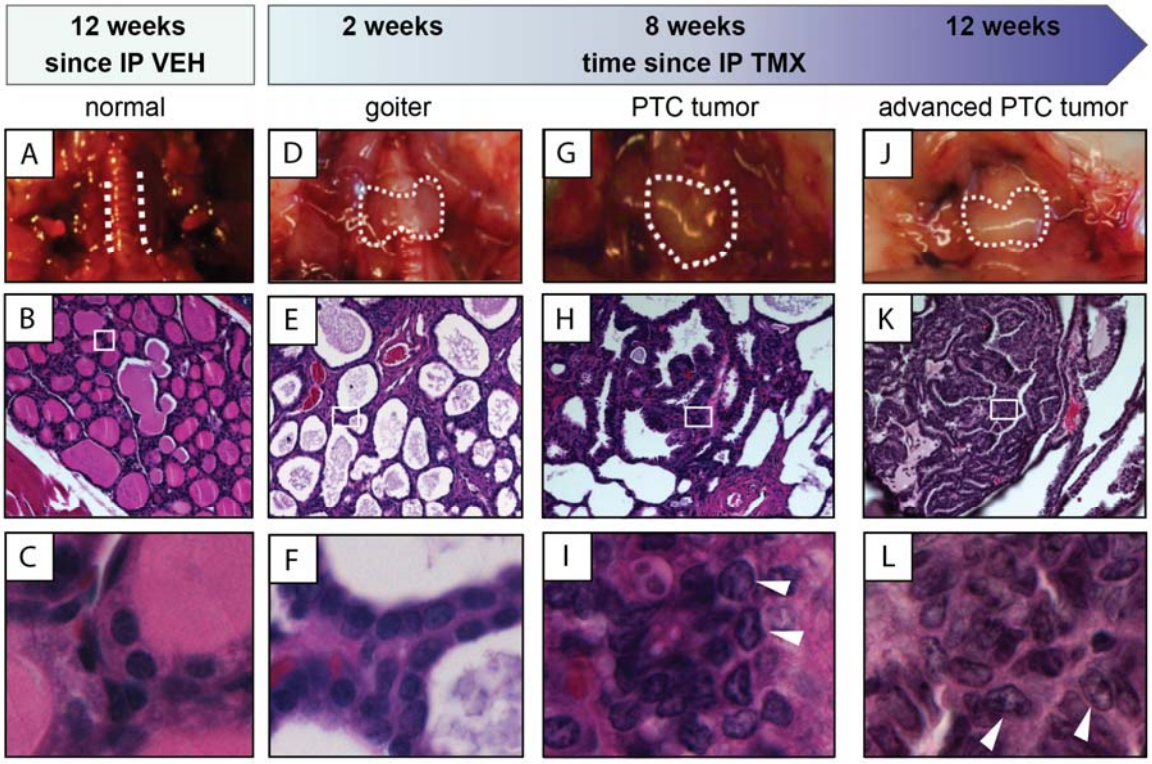

Figure 8: Gross pathology and histology of thyroid tumor development in TBP mice. Samples from euthanized TBP mice at the indicated time points after an intraperitoneal (IP) injection of vehicle (VEH, **A** to **C**) or tamoxifen (TMX, **D** to **L**). *Top*: Gross pathology (dotted lines demark border of thyroid), *Middle*: H&E staining of thyroid section at 20x magnification, and *Bottom*: 63x magnification of boxed region in corresponding 20x images. Arrows indicate nuclear clearing and grooves characteristic to PTC.

At 40 days of age, TBP mice were injected with tamoxifen and then randomly assigned to one of three treatment groups of ten mice each: *i*) a negative-control vehicle-treated cohort; *ii*) a positive-control vemurafenib-treated cohort (given that this drug shows clinical promise in phase II trials of RAI-resistant PTC) (Brose, Cabanillas et al. 2016); and finally, *iii*) the experimental TM-treated cohort. As noted above, histologically confirmed PTC was not established until eight weeks after tamoxifen

injection (Figure 8). Thus, to ensure the presence of established disease, treatments were not initiated until eight weeks post-tamoxifen injection. As TM requires up to four weeks to reduce Cu to therapeutically low levels in both rodents and humans (Mills, El-Gallad et al. 1981, Mills, El-Gallad et al. 1981, Bremner, Mills et al. 1982, Brewer, Dick et al. 2000), mice were treated for a total eight weeks in order to provide four weeks of therapeutic TM dosing. This dose of TM has previously been shown to reduce serum ceruloplasmin activity by 20% in mice (Brady, Crowe et al. 2017), which compares favorably to human clinical cancer trials that reduce serum ceruloplasmin activity by up to 50% (Chan, Willis et al. 2017). To ensure the same effective treatment time, mice in the vemurafenib arm were treated for the first four weeks, then provided vehicle control for the final four weeks. After eight weeks, all mice were humanely euthanized and their thyroids were removed en-bloc, paraffin embedded, and serially sectioned every 200 μm (amounting to roughly 15 sections per thyroid). Necropsy revealed a similar number of mice with grossly visible metastatic lung lesions (Figure 9).

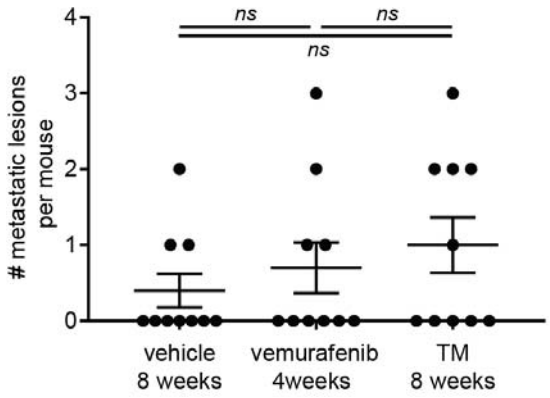

Figure 9: Number of lung metastases in TBP mice receiving indicated drug treatments. All metastases were between 0.5-1.0 mm in diameter. *ns*= not significant.

The region of the thyroid occupied by tumor was then circumscribed by a pathologist who was blinded to the genotype of the samples. All mice were confirmed by the pathologist to have PTC. The tumor versus total thyroid area was determined for each section, and the total volume occupied by the tumor calculated from all sections and recorded as either the tumor volume or as a percentage of total thyroid occupied by tumor (Figure 10A). Most thyroids contained one tumor per lobe, as demonstrated in three-dimensional reconstructions of a sample thyroid from each study cohort (Figure 10B). As expected, vemurafenib treatment significantly reduced the average tumor load by 22% (Figure 10C) and tumor volume by 39% (Figure 10D) in comparison to vehicle control. Similarly, TM treatment significantly reduced the average tumor load by 34% (Figure 10C) and tumor volume by 40% (Figure 10D). Thus, oral TM treatments in mice with established PTC reduces tumor load as well as treatment with the clinical BRAF inhibitor vemurafenib.

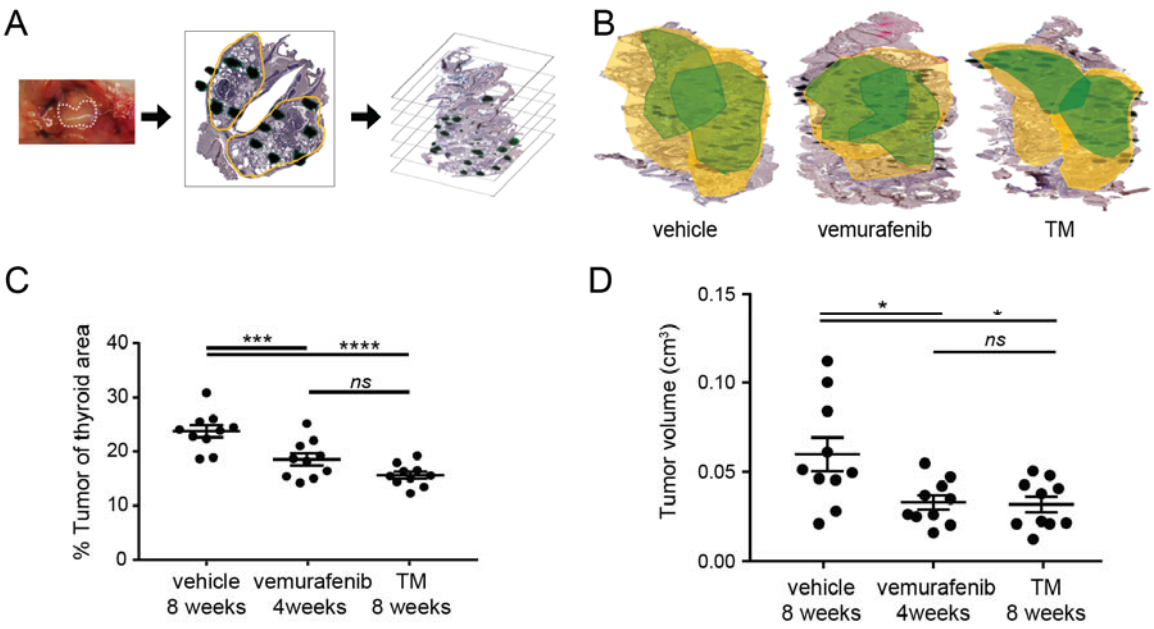

Figure 10: TM treatment reduced tumor load in TBP mice.

A) Diagram of tumor volume analysis. *Left panel:* Thyroids (dotted line) were removed from TBP mice euthanized 8 weeks after being treated with vehicle, vemurafenib, or TM. *Middle panel:* Thyroids were fixed enblock, paraffin mounted, sections taken every 200 microns, and H&E stained. *Right panel:* Tumor area (dark green regions) in the thyroid (yellow outline) was determined by a pathologist blinded to the mouse genotype to calculate the tumor load (percentage of the ratio of tumor area/thyroid area of all sections).

B) A representative 3-dimensional reconstruction of a thyroid en bloc from a TBP mouse euthanized 8 weeks after being treated with vehicle, vemurafenib, or TM. Yellow outlines the thyroid area while green outlines the tumor boundaries. Both lobes of the thyroid are shown.

C) % tumor load (% of thyroid occupied by tumor, each sample is a filled circle, mean ± SEM shown as bars) at the 8-week fixed endpoint in three cohorts of 10 TBP mice orally treated with vehicle, vemurafenib, or TM.

D) Tumor volume (cm^3, each sample is a filled circle, mean ± SEM shown as bars) at the 8-week fixed endpoint in three cohorts of 10 TBP mice orally treated with vehicle, vemurafenib, or TM.

*p<0.05, ***p<0.005, ****p<0.0001, *ns*= not significant.

2.3.3 Oral TM inhibits Mek1/2 kinase activity in PTC tumors

To explore the mechanism of TM, we performed immunohistochemical staining for phosphorylated (P) Erk1/2. MEK1/2 kinases are well established to transmit oncogenic BRAF signaling by phosphorylating their substrates ERK1/2 (Xing 2013). As such, reduction in P-Erk1/2 levels in tumors has been used to validate on-target effects of MAPK inhibitors. 36 thyroid sections from 20 TBP mice treated with TM or vehicle were stained with an anti-P-Erk1/2 antibody, after which the positive-stained area of tumors was circumscribed and expressed as a percent of the total tumor. In agreement with the effects of TM on P-Erk1/2 levels in tumors from other oncogenic $Braf^{V600E}$ cancer mouse models (Brady, Crowe et al. 2014), there was a statistically significant reduction in percent P-Erk1/2 staining in the thyroid tumors of mice treated with TM, as assessed by threshold analysis (Figure 11A and B), although not by optical density analysis (Figure 11C). In agreement with previous observations that chelating Cu reduces angiogenesis (Badet, Soncin et al. 1989, Brem, Zagzag et al. 1990, Brewer 2005, Juarez, Betancourt et al. 2006, Finney, Vogt et al. 2009), CD31 staining was also statistically reduced in the thyroid tumors of mice treated with TM compared to those treated with vehicle, as assessed by threshold analysis (Figure 11D and E). Thus, TM appears to inhibit Mek1/2 kinase activity in BrafV600E-mutant PTC lesions.

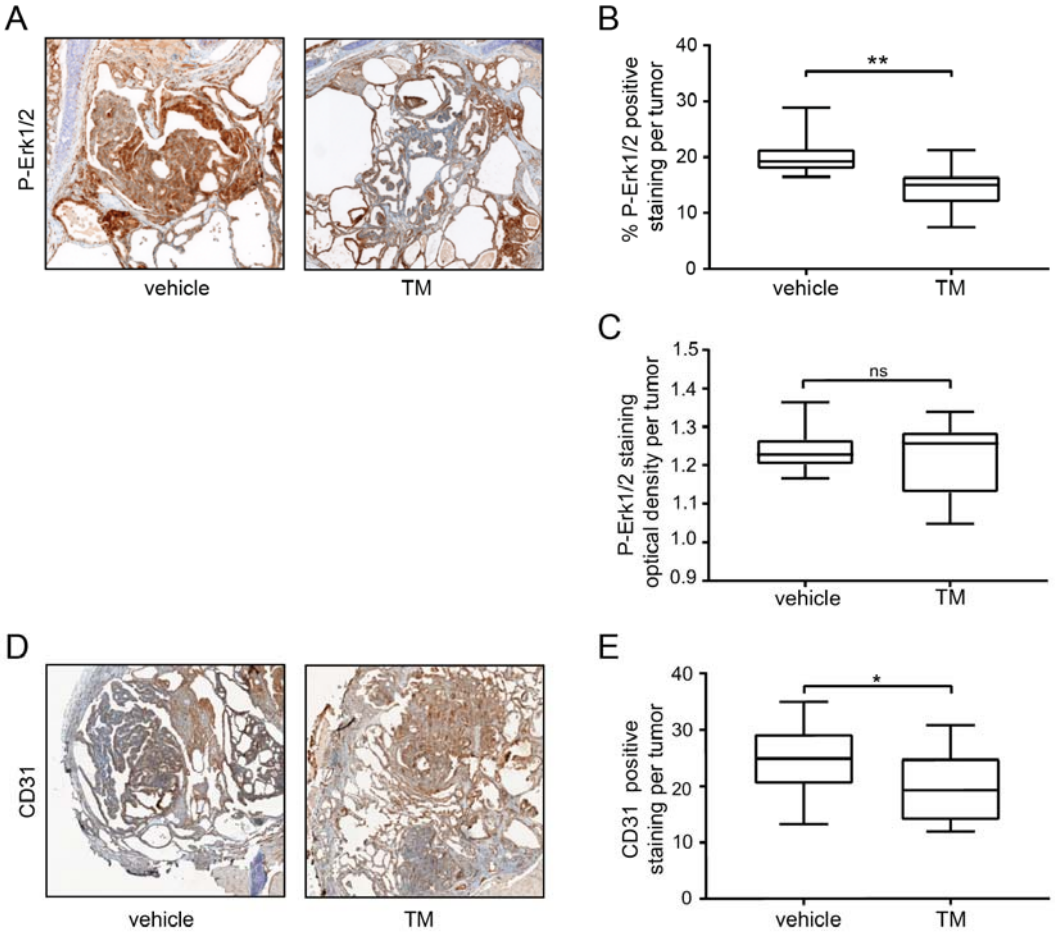

Figure 11: Oral TM inhibits Mek1/2 kinase and CD31 activity in PTC tumors

A) Representative image of a thyroid section H&E stained (purple) and immunohistochemically stained with an anti-P-Erk1/2 antibody (brown) isolated from a TBP mouse euthanized at the 8-week fixed endpoint after being treated with vehicle (*left*) or TM (*right*).

B) Threshold analysis boxplot of % P-Erk1/2 staining per tumor (36 sections from each cohort of 10) at the 8-week fixed endpoint in TBP mice treated with either vehicle or TM.

C) Optical density boxplot of % P-Erk1/2 staining per tumor (36 sections from each cohort of 10) at the 8-week fixed endpoint in TBP mice treated with either vehicle or TM.

D) Representative image of a thyroid section H&E stained (purple) and immunohistochemically stained with an anti-CD31 antibody (brown) isolated from a TBP mouse euthanized at the 8-week fixed endpoint after being treated with vehicle (*left*) or TM (*right*).

E) Threshold analysis boxplot of % CD31 staining per tumor (36 sections from each cohort of 10) at the 8-week fixed endpoint in TBP mice treated with either vehicle or TM.

* $p<0.05$, ** $p<0.001$.

2.3.4 TM-vemurafenib combination-therapy does not convey additional tumor reduction benefit in TBP mice

In addition to the comparison between TM and vemurafenib alone, the monotherapies were also compared to combination therapy with both TM and vemurafenib. Mice in the combination-therapy cohort began treatment at eight weeks post tumor induction and received treatment for a total of eight weeks, with the first four weeks consisting of both vemurafenib and TM, followed by four weeks of TM only. By allowing TM four weeks to reduce Cu to therapeutically low levels (Brewer, Dick et al. 2000), this study design allowed for four weeks of effective treatment by both vemurafenib and TM (Figure 12A). The combination-therapy did not result in a difference in lung metastases (Figure 12B), but did reduce the average tumor load by 33% (Figure 12C) and tumor volume by 26% (Figure 12D) in comparison to vehicle control. This reduction was not significantly different from the 22% and 34% reduction in tumor load or the 39% and 40% reduction in tumor volume in the vemurafenib and TM treatment arms, respectively (Figure 12C and D). Thus, TM-vemurafenib combination-therapy does not seems to be more efficacious than monotherapy with either drug in mice with established PTC.

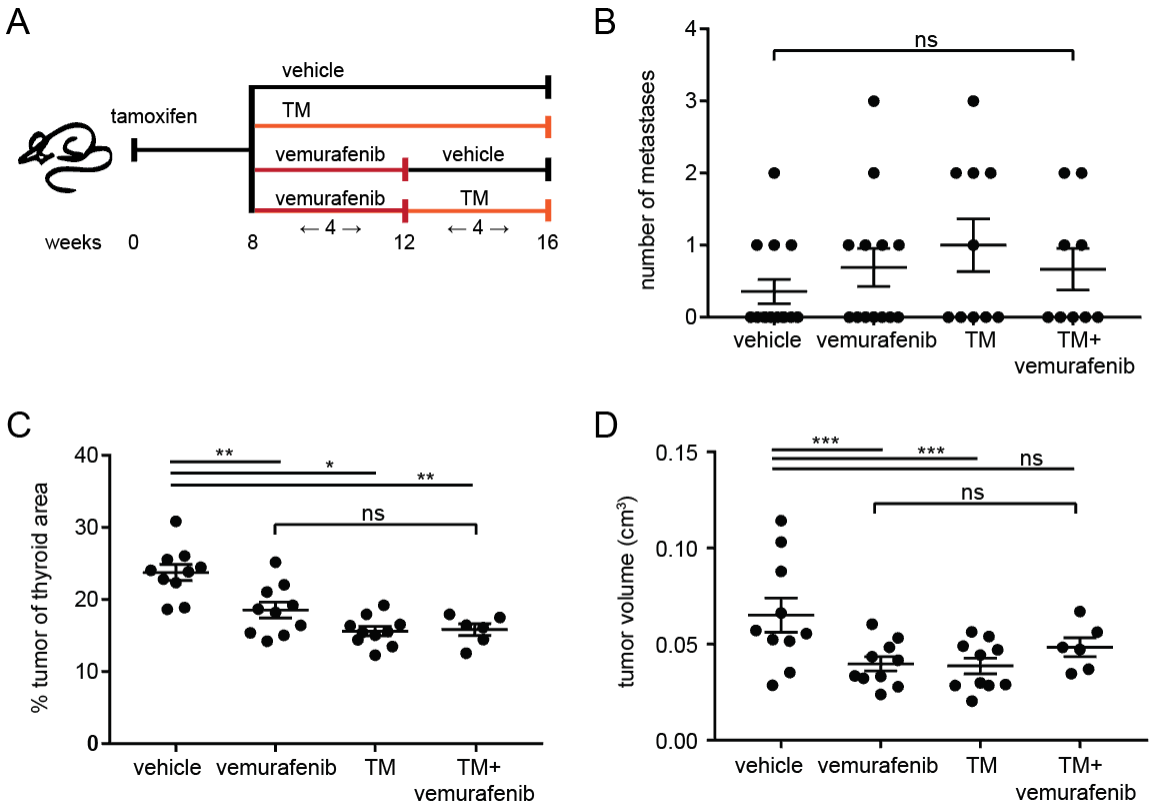

Figure 12: TM-vemurafenib combination-therapy does not convey additional tumor reduction benefit in TBP mice.

A) Schematic of study and treatment time course. Once mice reach the 8-week time point, their thyroids are prepared as described in Figure 10A.

B) Number of gross metastases found in the lungs of mice in each arm. All metastases were between 0.5-1.0 mm in diameter.

C) % tumor load (% of thyroid occupied by tumor, each sample is a filled circle, mean ± SEM shown as bars) at the 8-week fixed endpoint in TBP mice orally treated with vehicle (n=10), vemurafenib (n=10), TM (n=10), or TM and vemurafenib (n=6).

D) Tumor volume (cm^3, mean ± SEM shown as bars) at the 8-week fixed endpoint in TBP mice orally treated with vehicle (n=10), vemurafenib (n=10), TM (n=10), or TM and vemurafenib (n=6).

* $p<0.05$. ** $p<0.01$, *** $p<0.005$, *ns*= not significant.

This study design was chosen because it most closely models the clinical scenario, in which patients would receive therapy upon diagnosis of the disease (modeled by tumor establishment at 8 weeks post tamoxifen injection in TBP mice) (Figure 13A). Another valid method of TM-vemurafenib combination treatment would be to begin the eight weeks of TM treatment at the 8-week time point and begin the four weeks of vemurafenib treatment at the 12-week time point (Figure 13B). While this study design would allow the analysis of concomitant TM-vemurafenib combination treatment, this is a clinically unlikely scenario since it is ethically ambiguous and practically difficult to withhold an effective treatment from patients after initial diagnosis. Finally, both TM and vemurafenib could be administered for all eight weeks (Figure 13C). However, since vemurafenib would be effective for all eight weeks, this method would not present a impartial comparison between the combination cohort and TM- and vemurafenib-single therapy cohorts, which each only received four weeks of effective therapy. An entirely alternative approach in which TM treatment is begun at four weeks post tamoxifen induction was also considered (Figure 13D). However, this approach was dismissed because it is a poor model of clinical scenarios, in which patients would never begin therapy before diagnosis. This study design presents an additional confounding factor in that beginning TM early may have an inhibitory effect during tumor development. Thus, due to these considerations, the study design presented in Figure 12A and 13A was selected for its advantages in accurate clinical

representation, comparison between groups, and reduction of confounding effects on tumor development.

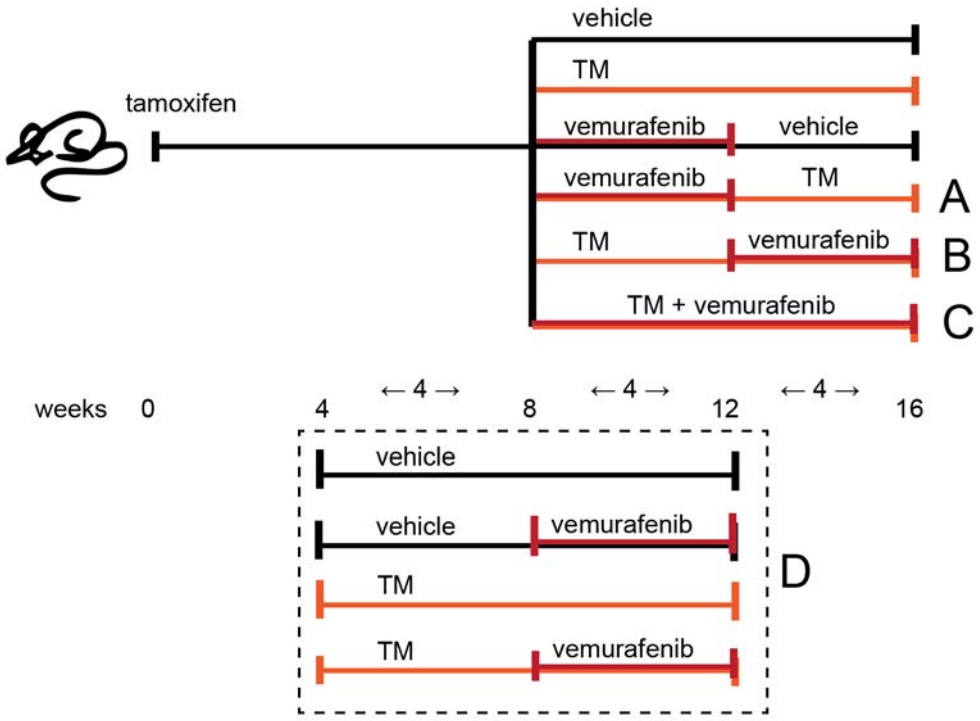

Figure 13: Schematic of possible treatment time courses.
A) Mice receive vemurafenib and TM for the first four weeks, followed by TM alone for four weeks.
B) Mice receive TM alone for the first four weeks, followed by vemurafenib and TM for four weeks.
C) Mice receive both vemurafenib and TM for all eight weeks.
D) The time course is move forward by four weeks to give TM time to lower Cu levels, so that the combination treatment portion occurs at 8- to 12-weeks after tamoxifen.

2.3.5 Long-term oral TM enhances the ability of vemurafenib to reduce tumor volume in a BrafV600E-driven GEMM of aggressive PTC

As TM enhances the antineoplastic activity of vemurafenib and can be dosed for extended periods of time in late-stage cancer patients, we surmised that one clinical scenario that TM may prove valuable is long-term maintenance therapy following vemurafenib treatment. To this end, we treated mice with vemurafenib and TM for four weeks, and then continued TM treatments for a further four weeks, but saw no advantage over TM or vemurafenib alone (Figure 12C and D). We therefore extended TM treatment for a total of 20 weeks. Specifically, TBP mice were injected with tamoxifen at 40 days of age as above, and eight weeks later when PTC was established to be present (*e.g.* Figure 8), two cohorts of 17 mice each were treated with *i*) vemurafenib and vehicle for four weeks, followed by 20 weeks of vehicle or *ii*) vemurafenib and TM for four weeks, followed by 20 weeks of TM. All mice were humanely euthanized and tumor volumes determined exactly as described above. Mice treated with vemurafenib and TM followed by maintenance therapy with TM exhibited an average tumor volume of 0.20 ± 0.01 cm^3 whereas mice treated with vemurafenib and vehicle followed by vehicle exhibited an average tumor volume of 0.40 ± 0.04 cm^3, or roughly a 50% reduction in tumor volume (Figure 14B). The number of metastatic lesions was similar between the two cohorts (Figure 14C). The ability of TM to reduce tumor volume only after extending follow up TM treatment to 20 weeks (Figure 14B) from the previous 4 weeks (Figure 12D) suggests that the effects of TM therapy is more

pronounced over long-term therapy. This could be due to the slow-growing nature of PTC, which may have required an extended growth period to achieve tumor sizes that was measurably different in the TM and vehicle treated groups. This tumor volume reduction by prolonged TM therapy after cessation of vemurafenib treatment suggests that TM may be effective as a long-term therapy in aggressive $BRAF^{V600E}$-mutant PTC.

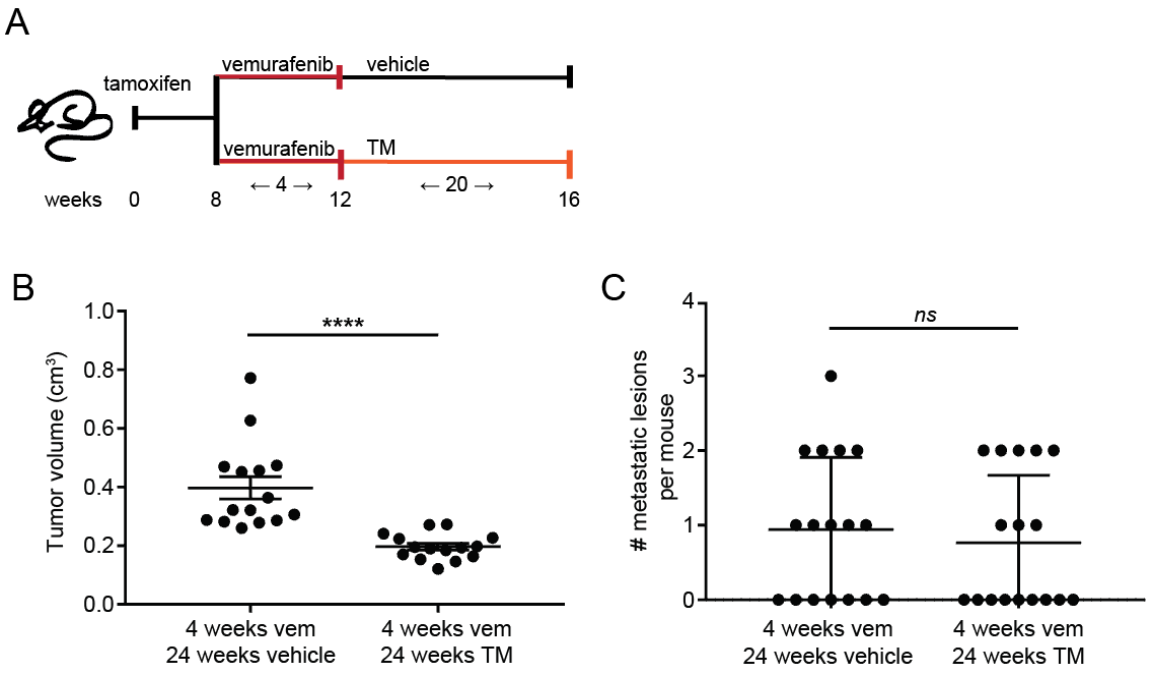

Figure 14: Long-term TM treatment after cessation of vemurafenib (vem) treatment reduces tumor volume and has no effect on metastases in TBP mice.
A) Schematic of study and treatment time course. Once mice reach the 8-week time point, their thyroids are prepared as described in Figure 10A.
B) Tumor volume (cm^3, each sample is a filled circle, mean ± SEM shown as bars) at the 24-week fixed endpoint in cohorts of 17 TBP mice orally treated with vemurafenib (vem) and vehicle, or vemurafenib (vem) and TM as indicated.
C) Number of gross metastases found in the lungs of mice in each arm. All metastases were between 0.5-1.0 mm in diameter.
**** $p<0.0001$, *ns*=not significant.

2.3.6 Inactivating the *Ctr1* gene in the thyroid trended towards an extended lifespan in a *Braf*^{V600E}-driven GEMM of aggressive PTC

To genetically test whether the antineoplastic activity of TM was due to a reduction of Cu in PTC lesions, we compared the lifespan of TBP mice with or without a functional *Ctr1* gene in their tumors. *Ctr1* encodes the primary Cu-specific transporter in mammalian cells, and inactivation of this gene has been shown to reduce Cu levels in cells (Kuo, Zhou et al. 2001, Lee, Prohaska et al. 2001), including in tumors (Brady, Crowe et al. 2014, Brady, Crowe et al. 2017). A floxed version of the *Ctr1* gene (Kuo, Zhou et al. 2001) was therefore crossed into the TBP background. TBP littermates homozygous for the wild-type (+/+, *n*=23) versus the floxed (*fl*/*fl*, *n*=8) *Ctr1* alleles were treated with tamoxifen to both induce PTC and inactivate the *Ctr1*^{fl} alleles when present. All mice were then regularly monitored and euthanized upon reaching disease endpoint where all mice were confirmed to have thyroid tumors. Analysis of the Kaplan-Meier survival curve revealed a trend towards an 18% increase in median survival of the *Ctr1*$^{fl/fl}$ cohort. Moreover, the near absence of mice reaching endpoint in the *Ctr1*$^{fl/fl}$ cohort until around 400 days suggests a true survival benefit until a sudden decline due to age, although admittedly all mice reached endpoint with thyroid cancer (Figure 15). As a caveat, I note here that I did not confirm recombination of the *Ctr1* alleles in the tumors.

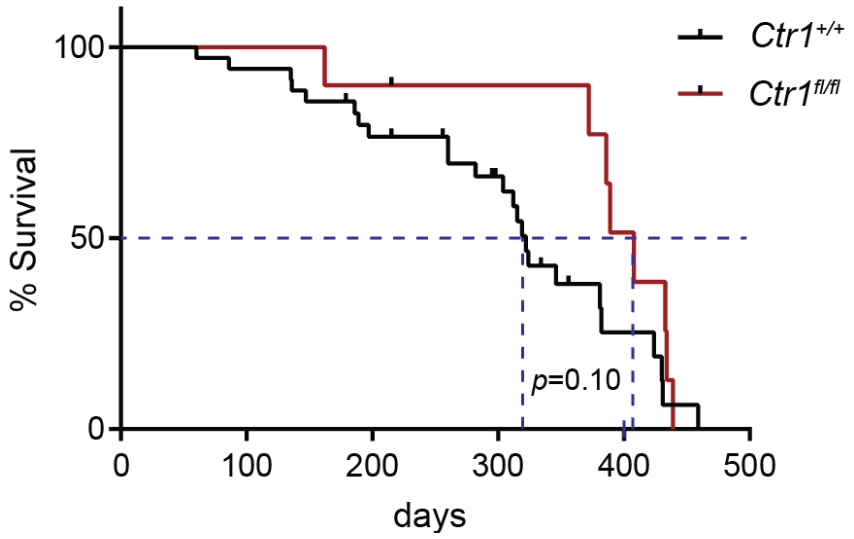

Figure 15: *Ctr1*$^{fl/fl}$ in thyrocytes of TBP mice trend towards a survival advantage. Kaplan-Meier survival curve of Ctr1$^{+/+}$ (n=23, 12 in study, red line) versus Ctr1$^{fl/fl}$ (n=8, 2 in study, black line) TBP mice. Dotted line: median survival. Censor marks: mice still on study. p=0.10.

2.3.7 Sex has no significant effect on tumor size, metastasis, or survival in TBP mice.

PTC is a disease that occurs far more frequently in women than men, but tends to be more aggressive when diagnosed in men (Kumar, Abbas et al. 2010). Although some preliminary studies suggest an imbalance of estrogen receptors isoforms to be the culprit for these epidemiological statistic, the underlying mechanisms for this discrepancy between sexes remains unclear (Yao, Chiu et al. 2011). Thus, to explore whether sex had an effect TBP mouse studies, the tumor volumes, metastases, and survival curves of the above studies were divided into female and male cohorts (Figure 16). Although the tumor volume of male mice appeared to be slightly greater in all but the TM-treated

cohort in the 8-week study, there was no statistically significant difference between the two sexes in any cohort. However, the larger size of the tumors in the male vehicle-treated mice led to statistically significant differences only between the male vehicle-treated mice and female mice in all other drug cohorts. The TM-treated cohort was the only group in which both male and female mice had statistically significant reductions in tumors size compared to male vehicle-treated mice (Figure 16A). There was also no difference in tumor size between the males and females of each cohort in the 24-week study. However, unlike the 8-week study, the tumors of both male and female mice maintained on TM were significantly smaller than the tumors of both male and female mice without TM maintenance therapy (Figure 16C). Segregating mice by sex did not elucidate any difference in numbers of metastases in either study (Figure 16B and D). Finally, dividing the genetic survival study by sex did not result in new statically significant differences between Kaplan-Meier survival curves of $Ctr^{+/+}$ and $Ctr1^{fl/fl}$ littermates (Figure 16E). However, it is interesting to note that the female $Ctr1^{fl/fl}$ mice had a very flat survival curve until around 400 days while the male mice showed a more gradual decline, which follows the clinical trend of more aggressive disease in men.

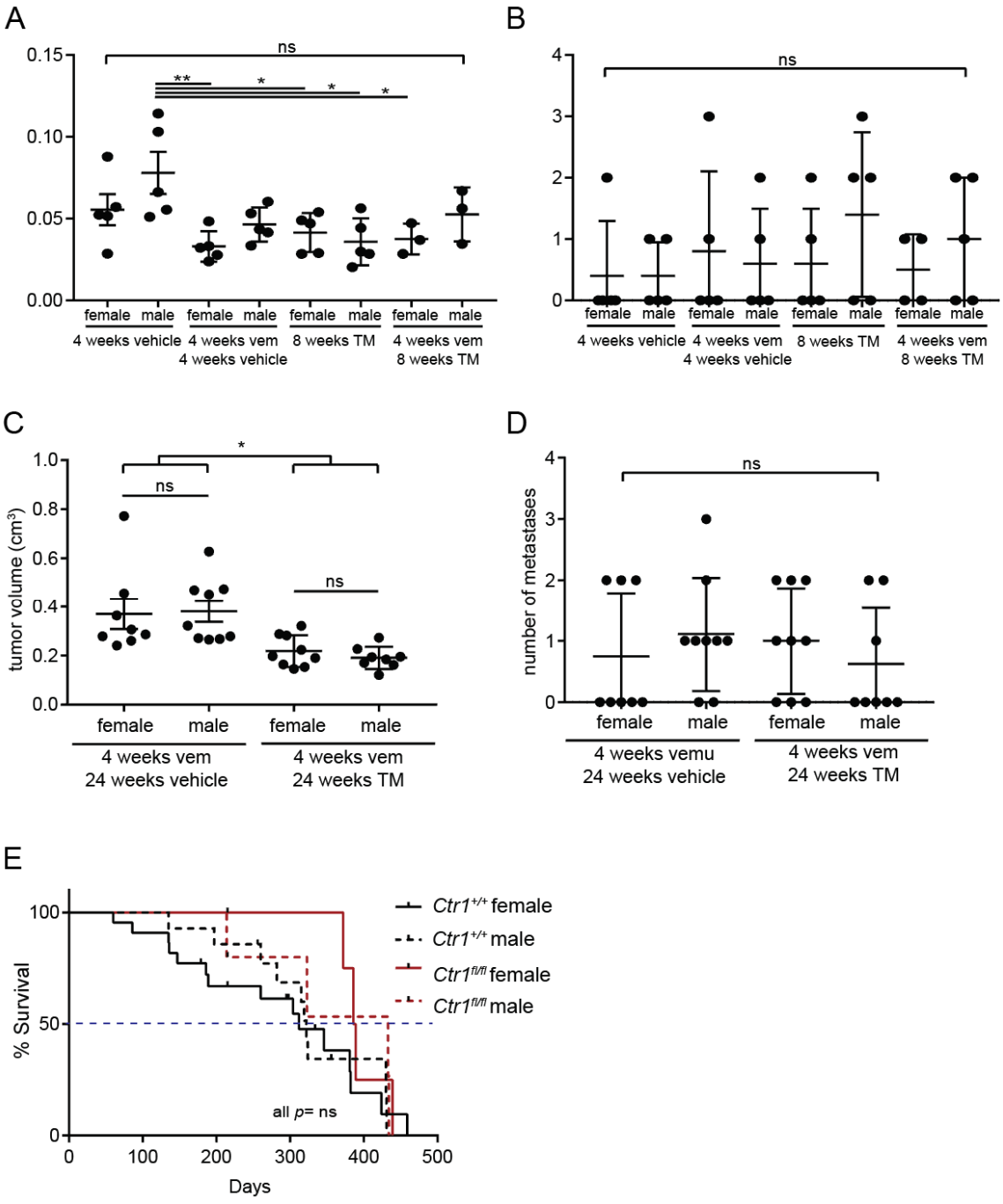

Figure 16: Sex of TBP mice has no effect on tumor size and response to TM treatment. Full figure legend on next page.

Figure 16: Sex of TBP mice has no effect on tumor size and response to TM treatment.
A) Tumor volume (cm^3, each sample is a filled circle, mean ± SEM shown as bars) at the 8-week fixed endpoint in female and male TBP mice orally treated with vemurafenib (vem) and vehicle, or vemurafenib (vem) and TM as indicated.
B) Number of gross metastases found in the lungs of 8-week study mice in each arm. All metastases of mice were between 0.5-2.0 mm in diameter.
C) Tumor volume (cm^3, each sample is a filled circle, mean ± SEM shown as bars) at the 24-week fixed endpoint in female and male TBP mice orally treated with vemurafenib (vem) and vehicle, or vemurafenib (vem) and TM as indicated.
D) Number of gross metastases found in the lungs of 24-week study mice in each arm. All metastases of mice were between 0.5-2.0 mm in diameter.
E) Kaplan-Meier survival curve of $Ctr1^{+/+}$ female (*n*=15, 7 in study, solid black line), $Ctr1^{+/+}$ male (*n*=10, 4 in study, dotted black line), $Ctr1^{fl/fl}$ female (*n*=4, 1 in study, solid red line), and $Ctr1^{fl/fl}$ male (*n*=4, 1 in study, dotted red line) TBP mice. Dotted line: median survival. Censor marks: mice still on study.
* $p<0.05$, ** $p<0.01$, *ns*=not significant.

2.3.8 TM enhances the antineoplastic activity of sorafenib and vemurafenib

Given the potential of TM to therapeutically target the MAPK pathway and an increasing emphasis on multi-drug therapy, we evaluated the therapeutic potential of TM when combined with current standard-of-care drugs, sorafenib and lenvatinib, or the clinically assessed MAPK inhibitors vemurafenib and trametinib, again using the long-term assay of growth in soft agar. BCPAP cells were seeded in triplicate in soft agar containing one of these five drugs at their $EC_{12.5}$, EC_{25}, and EC_{50} concentrations, or in combinations with TM, again at these three concentrations. Given the known effect of combining BRAF and MEK inhibitors, we also tested a triple combination of TM with vemurafenib and trametinib. Vehicle-treated cells served to normalize transformed

growth to 100%. After three weeks of drug treatment, the number of anchorage-independent colonies was counted in a blinded fashion, and the percent transformed growth was determined and used to calculate the Combination and BLISS indices to assess drug synergy. The Combination Index was calculated using CalcuSyn software, which was based on the logarithmic conversion and linear regression methods developed by Chou and Talalay (Chou and Talalay 1984). The BLISS index (Foucquier and Guedj 2015) is a fractional product method calculated from the observed effect relative to expected effect:

$$\text{Bliss Index} = \text{Effect}_{\text{Observed}}/\text{Effect}_{\text{Expected}}$$

where the expected effect is defined as:

$$\text{Effect}_{\text{Expected}} = \text{Effect}_{A} + \text{Effect}_{B} - (\text{Effect}_{A}*\text{Effect}_{B}).$$

TM was synergistic with vemurafenib by both indices at $EC_{12.5}$ and by BLISS index at EC_{25} (Figure 17 and Table 10). This agrees with the synergy observed between TM and vemurafenib in other *BRAF*^{V600E}-mutant cancer cell lines (Brady, Crowe et al. 2017), and the clinical superiority of BRAF and MEK inhibitor combination therapy in comparison to either drug alone (Robert, Karaszewska et al. 2015, Long, Hauschild et al. 2017). This was attributed to a reduction in MAPK signaling, as the addition of TM at an $EC_{6.25}$ to vemurafenib at an $EC_{6.25}$ reduced P-ERK1/2 and P-S6 levels in BCPAP cells below those of the same cells treated with either drug alone (Figure 18). TM was also synergistic with sorafenib by both indices at $EC_{12.5}$ and the Combination Index at EC_{25}

with an additive effect by the BLISS Index (Table 10), which is perhaps not unexpected as sorafenib was originally designed to target BRAF paralog, CRAF (Adnane, Trail et al. 2006). The lack of synergy at EC_{50} in both sorafenib and vemurafenib was expected as synergy is calculated based on relative reduction in colony growth, which is reduced as higher concentration of single drug therapy achieve greater growth inhibition. TM was not consistently synergistic with lenvatinib, trametinib, or in the triple combination. The synergistic Combination Index value at EC_{25} for lenvatinib, and $EC_{12.5}$ and EC_{50} for triple combination between vemurafenib, trametinib, and TM are likely to be artifacts since they are not accompanied by less than additive BLISS Index values. In summary, TM enhances the antineoplastic activity of the standard-of-care sorafenib and the BRAF inhibitor vemurafenib, this suggests a possible avenue to evaluate TM clinically.

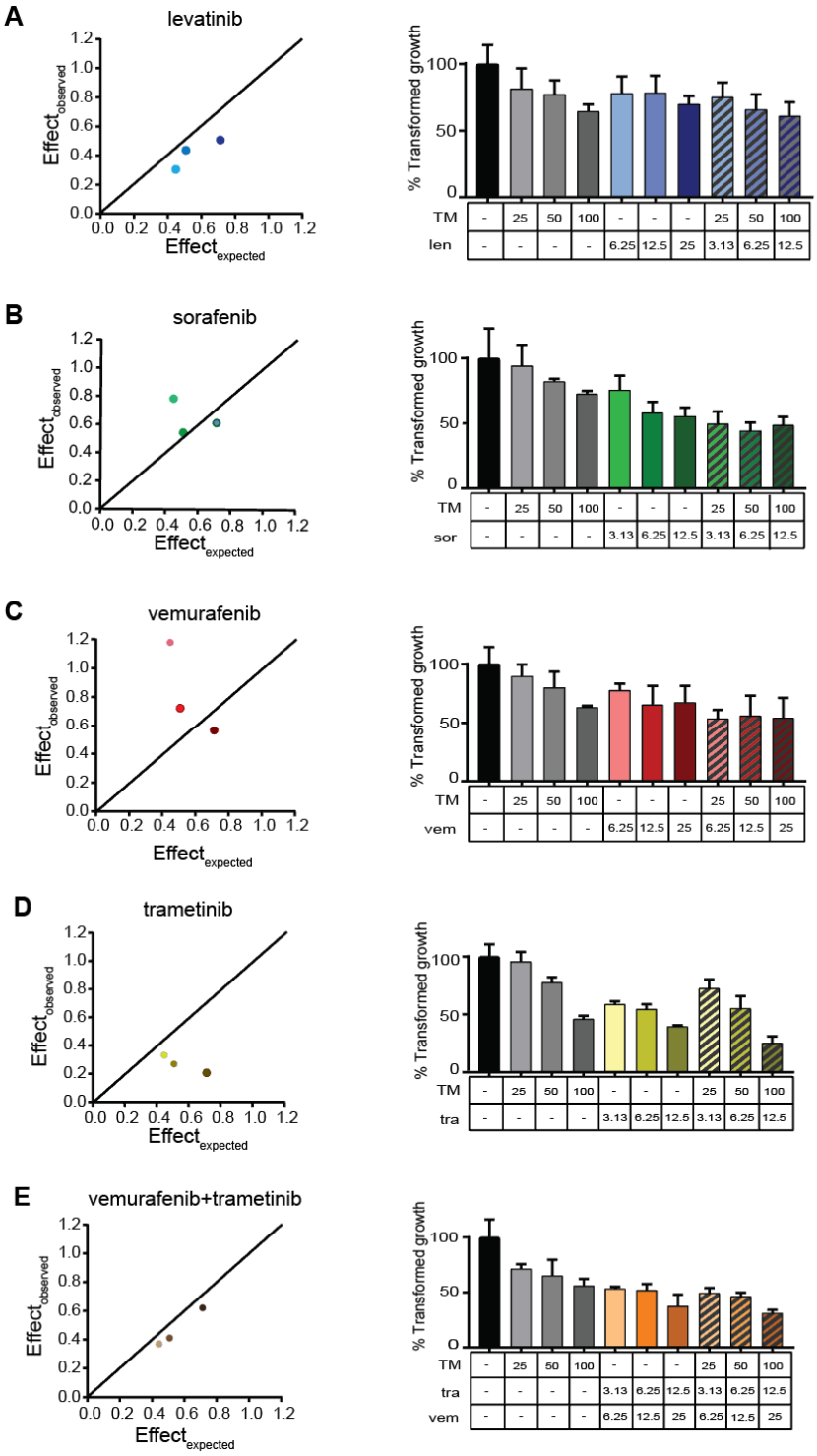

Figure 17: Effect of combining TM with standard-of-care and emerging therapies. Full figure legends on next page.

Figure 17: Effect of combining TM with standard-of-care and emerging therapies.
Left: Graphical representation of corresponding BLISS index values, with points lying above the bisecting line indicating synergy of that concentration of drug combination. *Right:* % transformed growth in soft agar (mean ± SEM, triplicate samples) normalized to vehicle control of BCPAP cells treated with the indicated concentrations to achieve an EC_{10}, EC_{20}, and EC_{50} dose of (**A**) TM, lenvatinib (Len), or both drugs, (**B**) TM, sorafenib (Sor), or both drugs, (**C**) TM, vemurafenib (Vem), or both drugs, (**D**) TM, trametinib (Tra), or both drugs, and (**E**) TM, trametinib (Tra), vemurafenib (Vem) or all three drugs.

Table 10: TM is synergistic with sorafenib and vemurafenib at $EC_{12.5}$ and EC_{25}.
Summary of BLISS and Combination Index (CI) values for anchorage independent growth of BCPAP cells at increasing fixed-ratio doses (EC12.5, 25, and 50). BLISS Index is presented in grey rows and CI in white rows. BLISS Index vales 1-1.2 are considered additive, while BLISS Index >1.2 are considered synergistic. CI Index vales 0.8-1 are considered additive, while CI Index <0.8 are considered synergistic. Synergistic vales are bolded.

TM with	Combination Index	$EC_{12.5}$	EC_{25}	EC_{50}
lenvatinib	BLISS	0.68	0.86	0.71
	CI	0.97	**0.72**	0.95
sorafenib	BLISS	**1.75**	1.07	0.86
	CI	**0.34**	**0.52**	1.28
vemurafenib	BLISS	**2.63**	**1.42**	0.79
	CI	**0.51**	0.88	1.44
trametinib	BLISS	0.74	0.53	0.29
	CI	0.88	2.95	8.27
vemurafenib trametinib	BLISS	0.82	0.81	0.87
	CI	**0.72**	1.13	**0.57**

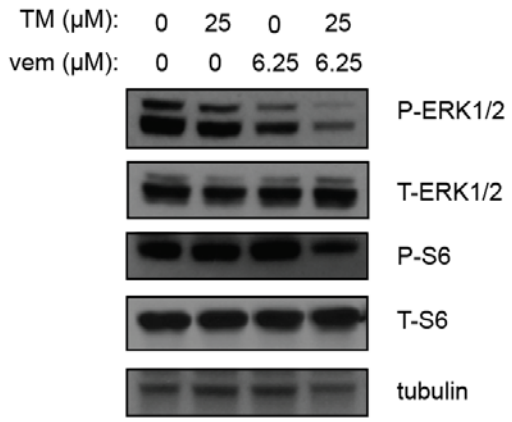

Figure 18: Reduction in MAPK signaling of BCPAP cells treated with vemurafenib and TM.
Immunoblot detection of phosphorylated (P-) and total (T-) Erk1/2 protein and downstream effector protein S6, and tubulin in BCPAP cells treated with the indicated concentrations of TM and vemurafenib (vem).

2.3.9 Characterization of tumor cell lines derived from TBP mice

To develop a model through which a large number of drug combinations can be more efficiently tested, we sought to generate tumor cell lines from the primary PTC tumors and lung metastases of TBP mice. While multiple samples from each lobe and lung metastases of each mouse were collected (see materials and methods subsection 2.2.8), only six cell lines were successfully established. Three cell lines were derived from the left lobe primary tumor of TBP mouse # 462 (T462 L1, T462 L2, and T462 L3) and three lines were derived from the right lobe primary tumor of TBP CTR1$^{-/-}$ mouse # 580 (T580 R1, T580 R2, and T580 R3). These lines were then sent to the lab of Dr. Bryan Haugen (University of Colorado), whose lab is responsible for characterizing and

revealing cell line redundancy of over 40 thyroid cancer cell lines (Schweppe, Klopper et al. 2008).

Quantitative reverse transcription-polymerase chain reaction was used to characterize the expression of thyrocyte specific genes in our TBP cell lines. The levels of sodium-iodide symporter (NIS), paired box gene 8 (PAX8), and thyroid globulin (TG) were relatively low in comparison to mouse thyroid tissue positive controls (Figure 19, top row) and significantly higher than that of negative control lung samples (Figure 19, bottom row). NIS, the main transporter of iodide into the thyrocyte (Kogai and Brent 2012), remains relatively low. This phenomenon is expected as NIS expression in thyrocytes is elicited by thyroid stimulating hormone, which is was not present in the cell culture setting (Kogai and Brent 2012). Apart from cell line T462 L1, expression of PAX8, a nuclear protein involved in thyroid follicular cell development and expression of thyroid-specific genes (Fabbro, Di Loreto et al. 1994, Rosignolo, Sponziello et al. 2016), was higher than lung tissue negative controls (Figure 19 bottom row). Expression of TG protein in all cell lines was also unsurprisingly low, as TG is responsible for iodination and thyroxine synthesis. Without TSH to stimulate iodide intake by the NIS and thyroid hormone production, TG would not be produced in large amounts in cultured PTC cell lines (Figure 19 bottom row).

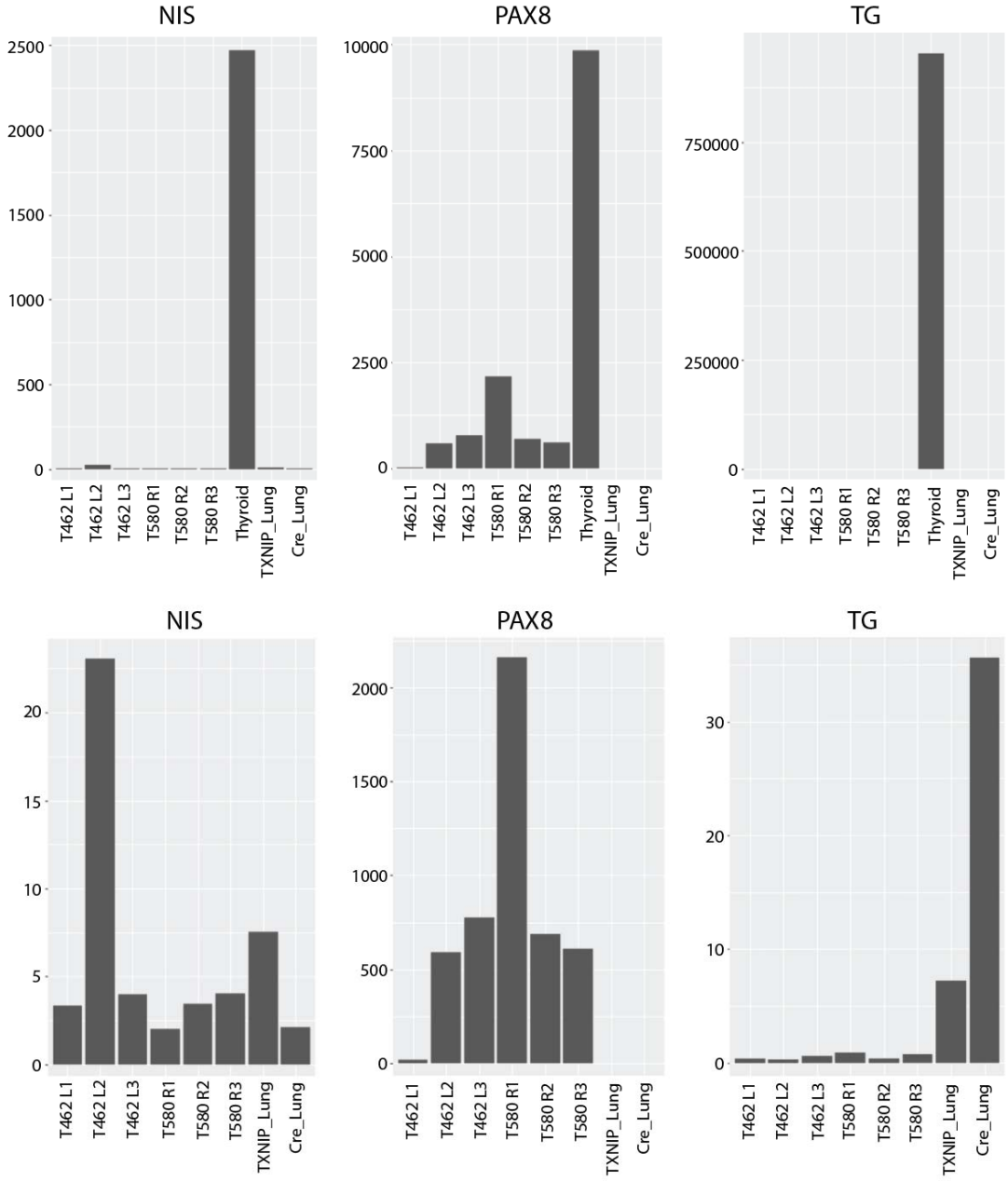

Figure 19: TBP cell line expression of thyro-specific markers, NIS, PAX8, and TG.
Top row: qRT-PCR of sodium-iodide symporter (NIS), paired box gene 8 (PAX8), and thyroid globulin (TG) with mouse thyroid tissue as a positive control and lung as a negative control.
Bottom row: to elucidate the differences between low expression cell lines and negative control lung tissue, the same qRT-PCR data presented without the mouse thyroid tissue positive control.

Analysis of cytokeratin 7 (KER7), thyroid transcription factor 1 (TTF-1), and mesenchymal marker vimentin (VIM) expression further confirmed the thyrocyte origin of the generated cell lines (Bejarano, Nikiforov et al. 2000). High KER7 and low VIM expression indicate cells of epithelial origin and not derived from mesenchymal cells, respectively. Finally, TTF-1 levels comparable to the mouse thyroid positive control line support the identification of these six TBP cell lines as thyrocyte of origin and still retaining some thyroid-specific gene expression (Figure 20).

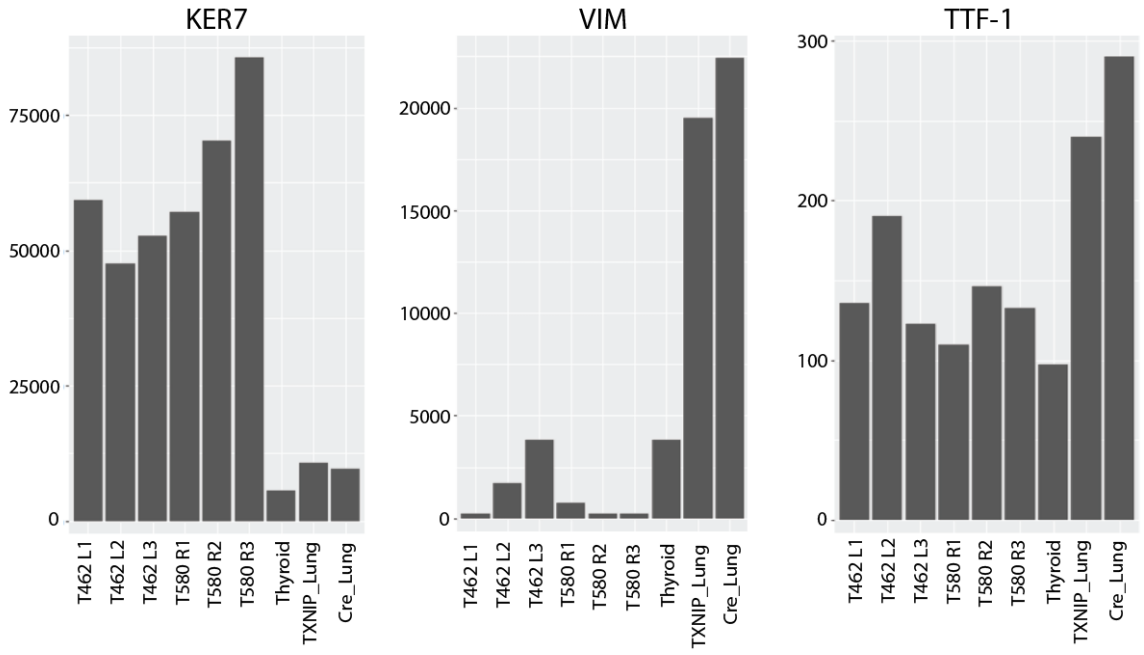

Figure 20: TBP cell line expression of KER7, VIM, and TTF-1.
qRT-PCR of epithelial marker keratin 7 (KER7), thyroid transcription factor 1 (TTF-1), and mesenchymal marker vimentin (VIM) with mouse thyroid tissue as a positive control and lung as a negative control.

2.3.10 TBP mouse tumor cell lines as an allograft model for PTC

The requirement of thyrocytes for TSH hormone has made an animal model of the disease difficult to establish. Robust subcutaneous growth of a human PTC cells line has only been achieved with the concurrent injection of human adipose tissue-derived stromal/stem cells (ASCs) (Kandil, Hauch et al. 2013). While orthotopic and metastatic xenograft models have been established for ATC (Sewell, Reeb et al. 2013, Zhang, Gaskins et al. 2014, Morrison, Pike et al. 2015), FTC (Zhang, Gaskins et al. 2014), and PTC (Ahn, Henderson et al. 2008, Morrison, Pike et al. 2015), these models rely on the growth of highly passaged human cells lines in immunodeficient mice. While genetically engineered mouse models (Charles, Iezza et al. 2011, Charles, Silva et al. 2014) allow the study of PTC in immunocompetent mice, their versatility in preclinical investigation is limited by slow tumor growth. While a recent study has successfully implanted mouse cell lines derived from *Thyro::CreER$^{T2/+}$;Braf$^{CA/+}$;Pten$^{fl/fl}$* and *Thyro::CreER$^{T2/+}$;Braf$^{CA/+}$;P53$^{fl/fl}$* mouse models of PTC into the thyroids of immunocompetent mice, this orthotopic method is still limited by the need for surgical implantation and the inability to monitor growing tumors (Vanden Borre, McFadden et al. 2014).

Given the above, T462 L1, L2, and L3 TBP mouse tumor cell lines were evaluated as potential candidates for a sub-cutaneous allograft model for potential future use to compare the effectiveness of TM against standard-of-care drugs sorafenib and

lenvatinib, and MAPK inhibitors vemurafenib and trametinib *in vivo*. All three cell lines successfully formed tumors by two weeks after injection into the flanks of SCID/beige mice (Figure 21). Although there was no statistical difference between the growth between all three cell lines, the growth patterns between T462 L1 and T462 L2 tracked closely. These data indicate that all three cell lines are viable candidates for allograft models of $BRAF^{V600E}$-mutant PTC. Combining this data with the genetic expression data (see Subsection 2.3.10) showing the lack of PAX8 expression in T462 L1, suggest cell lines T462 L2 and L3 to be the best candidates for a xenograft model of PTC.

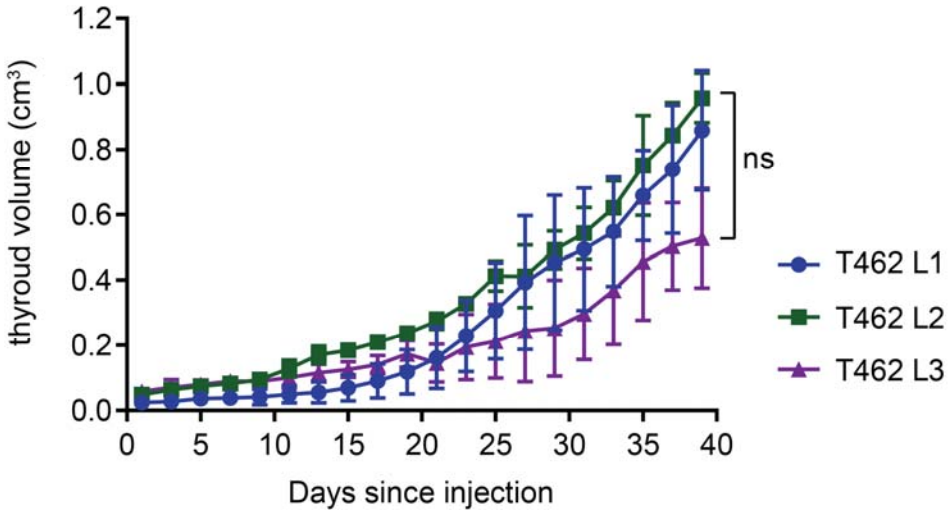

Figure 21: TBP mouse cell lines generate tumors in a subcutaneous xenograft model.
Tumour volume (cm^3, mean ± s.e.m.) days after 10^7 cells were injected subcutaneously into the flanks of SCID/beige mice (*n*=5). All three lines T462 L1, L2, and L3, derived from the primary thyroid tumor of a TBP mouse sucessfully formed tumors.
ns= not significant.

2.4 Discussion

The finding that 40 to 60% of PTC tumors have a *BRAF*^{V600E} mutation (Xing 2010) in the United States prompted the clinical evaluation of BRAF and MEK inhibitors, originally developed for the treatment of *BRAF*^{V600E}-mutant melanoma (Robert, Karaszewska et al. 2015, Grimaldi, Simeone et al. 2017, Long, Hauschild et al. 2017), for the treatment of advanced *BRAF*^{V600E}-mutant PTCs (Leijen, Soetekouw et al. 2011, Ho, Grewal et al. 2013, Kim, Cabanillas et al. 2013, Falchook, Millward et al. 2015, Larson, Osborne et al. 2017). However, melanoma and PTC behave very differently; PTC is known to be much more indolent overall, with longer associated survival observed for patients with unresectable or metastatic disease. Indeed, the average time to recurrence is 8.1 years for all stages of PTC, with 17% of deaths occurring after 20 years (Grogan, Kaplan et al. 2013). This poses unique challenges to targeting the MAPK pathway in PTC, as cost and toxicities may be amplified if prolonged treatment is required. Unlike most other cancers, where costs are largely incurred in the final year of life, 78% of the cost of thyroid cancer treatment accumulates over the initial and surveillance phases of the disease (Lubitz, Kong et al. 2014, Lubitz and Sosa 2016). The cost of targeted therapies administered over a long period of time can be prohibitively expensive for patients and payers (Ramsey, Blough et al. 2013, Lubitz, Kong et al. 2014, Lubitz and Sosa 2016, Zafar 2016, Gild, Topliss et al. 2017). In additional to financial toxicity, drug treatment itself often comes with non-negligible side effects. In a recent clinical trial of

vemurafenib, 66% of PTC patients experienced Grade 3 and 4 adverse events (Brose, Cabanillas et al. 2016). These toxicities are especially concerning for patients with PTC who are often asymptomatic from their disease for long periods of time. As such, quality of life considerations are of special importance in their treatment decisions (Ramsey, Blough et al. 2013, Lubitz, Kong et al. 2014, Lubitz and Sosa 2016, Zafar 2016, Gild, Topliss et al. 2017).

Here we show that TM was as effective as the BRAF inhibitor vemurafenib in terms of inhibiting Mek1/2 kinase activity and the growth of established PTC lesion in a $BRAF^{V600E}$-driven mouse model of this disease. Additionally, TM enhanced the antineoplastic activity of both the standard-of-care sorafenib and the clinical BRAF inhibitor vemurafenib. TM is typically a well-tolerated drug. Unlike vemurafenib, which caused 66% of PTC patients to experience Grade 3 and 4 adverse events (Brose, Cabanillas et al. 2016), the only side-effect of treatment with TM is a small likelihood of mild and transient anemia in the first week of treatment (Brewer, Dick et al. 2000, Redman, Esper et al. 2003, Pass, Brewer et al. 2008, Jain, Cohen et al. 2013, Hordyjewska, Popiolek et al. 2014, Chan, Willis et al. 2017). Regular surveillance of Cu levels using the simple serum assay of ceruloplasmin activity has allowed TM to be dosed chronically in humans with few ill-effects (Brewer, Dick et al. 2000, Redman, Esper et al. 2003, Pass, Brewer et al. 2008, Jain, Cohen et al. 2013, Hordyjewska, Popiolek et al. 2014, Chan, Willis et al. 2017). In fact, TM has been continually dosed thrice daily for as long as 65

months in a Phase I breast cancer trial (Jain, Cohen et al. 2013). This feature makes TM particularly well suited for management of advanced PTC, especially in terms of chronic inhibition of the MAPK pathway. The synergy of TM with sorafenib *in vitro* suggests an immediate clinical pathway to evaluating this drug in PTC patients. Alternatively, the combination of BRAF and MEK inhibitors is known to be clinically superior to either drug alone in the treatment of melanoma (Long, Hauschild et al. 2017). Thus, TM could be added to current efforts testing BRAF inhibitors in PTC patients (Brose, Cabanillas et al. 2016). Although combining TM with a MEK inhibitor or both BRAF and a MEK inhibitors was not synergistic *in vitro*, there may still be value in adding TM to these modalities as a long-term maintenance therapy after initial treatment with these more toxic drugs. Indeed, when TM was provided as a maintenance therapy after vemurafenib treatments were terminated, tumor volume was reduced compared to control mice (Figure 14). As such, there are several potential clinical venues to explore TM for the treatment of $BRAF^{V600E}$-mutant PTC.

Mechanistically, we ascribe the antineoplastic effects of TM in large part to inhibition of the Cu-dependent activity of MEK1/2 in the PTC tumors themselves. This is supported by three lines of evidence. First, the ability of TM to inhibit PTC transformed growth was rescued by ERK^{GOF} *in vitro*, an activated version of the MEK1/2 substrate ERK2. If TM inhibited transformation by other Cu-dependent pathways, this would not have been the case. This also highlights the specificity of this drug. Namely,

like other MAPK inhibitors, *BRAF* mutation status predicts sensitivity to TM (Brady, Crowe et al. 2014). Although TM has been evaluated across a broad spectrum of cancers with modest effects (Brewer, Dick et al. 2000, Redman, Esper et al. 2003, Brewer 2005, Pass, Brewer et al. 2008, Jain, Cohen et al. 2013, Chan, Willis et al. 2017), it has never been matched to the $BRAF^{V600E}$ mutation, which will be an important inclusion criterion. Second, in TBP mice treated with TM, there was a reduction in the level of P-Erk1/2 by one criteria, a direct measure of Mek1/2 kinase activity *in vivo*, which was similar to what has been reported in other mouse models of oncogenic *Braf*-driven tumorigenesis (Brady, Crowe et al. 2017). Third, crossing a floxed version of Cu-specific transporter *Ctr1* into TBP mice phenocopied the effect of TM in this same mouse model of $Braf^{V600E}$-mutant PTC. This argues that the effect of TM on tumorigenesis lies in a reduction of Cu in the tumor rather than the stroma. Admittedly however, how TM specifically inhibits MEK1/2 remains to be fully elucidated. It is worth noting that a disulfiram metabolite has been shown to have copper-binding properties and is antineoplastic (Skrott, Mistrik et al. 2017) and we also detected a reduction of CD31 staining in the thyroid tumors of TM-treated mice. These findings collectively suggest that TM inhibits the Cu-dependent activity of MEK1/2 kinases to reduce oncogenic BRAF-driven signaling.

In summary, TM represents a unique clinical opportunity in PTC. Its ability to inhibit MEK1/2 kinases while having low toxicity makes it particularly well suited for

long-term inhibition of the MAPK pathway in *BRAF*^{V600E}-mutant PTC, either in combination with current or emerging therapies and/or as a maintenance therapy.

3. Discussion

3.1 Cu chelation in $BRAF^{V600E}$ *thyroid cancer*

3.1.1 Advantages of Cu chelation as targeted therapy for PTC

I have shown in Chapter 2 that Cu chelator TM was as effective as the BRAF inhibitor vemurafenib at inhibiting the growth of established PTC lesions in a $BRAF^{V600E}$-driven mouse model of this disease. TM was also more effective than frontline drugs sorafenib and lenvatinib at reducing anchorage-independent growth of two human $BRAF^{V600E}$-mutant PTC cell lines. These findings support the use of Cu chelators as targeted inhibitors of $BRAF^{V600E}$-driven PTC. However, the true advantage to clinical treatment with Cu chelators lies in their benign side-effect profile and cost-effectiveness.

In comparison to vemurafenib, which gave 66% of PTC patients Grade 3 or 4 adverse events (Brose, Cabanillas et al. 2016), the side-effects of TM treatment in cancer patients was restricted almost entirely to sulfurous burps and mild (Grade 1/2) anemia/neutropenia (Brewer, Dick et al. 2000, Redman, Esper et al. 2003, Pass, Brewer et al. 2008). Although considerations of drug toxicity are not generally in the forefront of considerations for cancer treatment strategies, patient quality of life plays a significant role in determining thyroid cancer therapy. This is because even aggressive PTC is considered a relatively indolent disease, with an average time to recurrence of 8.1 years for all stages. Indeed, 17% of deaths occur after 20 years (Grogan, Kaplan et al. 2013). Patients receiving targeted therapy against their $BRAF^{V600E}$ mutant PTC may required

chronic treatment, and thus suffer the associated drug toxicities potentially for decades. Thus, the ability to inhibit the MAPK pathway with non-toxic Cu chelators in *BRAF*^{V600E} mutant PTC may be especially valuable to the chronic management of aggressive thyroid cancer.

Cu chelation therapy also presents an opportunity to reduce the cost of care for PTC. Unlike most cancers, where costs are largely incurred at initial treatment or in the final year of life, 78% of the cost of thyroid cancer treatment accumulates over the initial and surveillance phases of the disease (Mariotto, Yabroff et al. 2011, Lubitz, Kong et al. 2014, Lubitz and Sosa 2016). Quality-adjusted life year (QALY) analysis have shown MAPK inhibitors to be highly cost ineffective, with QALYs three times higher than the threshold for cost-effectiveness (Curl, Vujic et al. 2014, Delea, Amdahl et al. 2015, Matter-Walstra, Braun et al. 2015). Thus, the addition of long-term MAPK inhibitor therapy would add to the severe financial burden already weighing on PTC patients (Ramsey, Blough et al. 2013). Cu chelation could be a solution to this prohibitively high cost of treatment because these drugs have been on the market for decades. Previous experience in Wilson's Disease patients also suggest that Cu levels can be maintained with oral zinc after initial chelation (Brewer, Hedera et al. 2003), an option that would be much less financially toxic than long-term MAPK inhibitor therapy.

3.1.2 Cu chelation as a maintenance therapy for PTC

One of the unique challenges facing treatment of PTC is the choice between active treatment and active surveillance. Once a patient has undergone the initial surgical ablation and possible RAI therapy, they are reevaluated for disease every six to twelve months. If a patient is found to have residual or new disease after the initial treatment, the care team must decide between further treatment or active surveillance. This decision is made based on a variety of clinical characteristics, including tumor size, growth rate, and RAI avidity (Wells, Asa et al. 2015, Haugen, Alexander et al. 2016). For patients with tumors that are <1 cm or slow growing, inoperable tumors insensitive to RAI, the best treatment option is often to "watch and wait", even if the presence of $BRAF^{V600E}$ markers indicate a likelihood of aggressive disease. Although MAPK inhibitors would specifically target these diseases, their use may result in physical and financial toxicities that could decrease the quality of life in patients who would otherwise remain asymptomatic. Cu chelation may play a pivotal role in these scenarios by providing a method of inhibiting the MAPK pathway that is less expensive and less physically taxing. This ability to undergo "maintenance therapy" with Cu chelation would allow for the peace of mind active treatment provides without sacrificing quality of life and financial solvency.

3.1.3 Cu chelation as a combination therapy for PTC

Dabrafenib-trametinib (Long, Stroyakovskiy et al. 2014, Robert, Karaszewska et al. 2015) and vemurafenib-cobimetinib (Ascierto, McArthur et al. 2016) combination therapies have shown that potent inhibition of the MAPK pathway yields better tumor inhibition than single therapy alone. I show here that Cu chelation using TM may be a synergistic combination therapy partner to both vemurafenib and sorafenib. This synergistic property may be more clinically applicable than applying Cu chelation single therapy over the FDA-approved sorafenib or vemurafenib, as combination therapies have proven to be more effective in *BRAF*^{V600E}-mutant melanoma (Robert, Karaszewska et al. 2015, Ascierto, McArthur et al. 2016). Since the results of *BRAF*^{V600E}-mutant melanoma trials inform clinical treatments in less well-studied *BRAF*^{V600E}-mutant malignancies, combination therapies targeting the MAPK pathway will be a likely treatment of choice for *BRAF*^{V600E}-mutant PTC as well. Since MEK inhibitors themselves are not without toxicities and combination therapies also combine toxicities, Cu chelation will still be at an advantage over other MEK inhibitors in combination therapy because they impart fewer drug toxicities. This lack of toxicities may permit Cu chelator-RAF inhibitor combination treatments to reduce skin ailments associated with paradoxical MAPK activation with an overall reduction in adverse events seen in RAF-MEK inhibitor combination therapy.

3.1.4 Cu chelation adjuvant to RAI treatment

The MEK inhibitor selumetinib (Ho, Grewal et al. 2013, Larson, Osborne et al. 2017) and BRAF inhibitor dabrafenib (Rothenberg, McFadden et al. 2015) have both been shown in clinical trials to restore RAI sensitivity in previously RAI resistant PTC. As a MEK inhibitor, Cu chelation should also be able to accomplish this feat in *BRAF*^{V600E}-mutant PTC. Since *BRAF*^{V600E}-mutant PTC are more likely to be of aggressive variants (Adeniran, Zhu et al. 2006, Elisei, Viola et al. 2012) that would benefit from RAI treatment but are simultaneously likely to be RAI insensitive due to a greater level of dedifferentiation (Durante, Puxeddu et al. 2007, TCGA 2014), the implementation of Cu chelators earlier in the treatment flow would allow for more efficacious treatment. Since evaluation for RAI treatment occurs shortly after initial surgery, the gentler Cu chelators may be preferable to the more toxic MEK inhibitors when providing an adjuvant therapy for increasing RAI uptake. Of course, whether Cu chelators could be as effective as MEK inhibitors in this setting remains to be determined.

3.1.5 Clinical challenge of adapting Cu to PTC treatment

Although the above sections highlight the benefits of targeting *BRAF*^{V600E}-mutant PTC with Cu chelation, there is a significant barrier to clinical adoption (Brewer, Dick et al. 2000, Redman, Esper et al. 2003, Pass, Brewer et al. 2008). This barrier is that TM, the Cu chelator used in this study, is not approved in the United States. Although the drug

is approved for use by the European Commission, TM is currently in phase II FDA trials (NCT02273596). Thus, although TM has proven to be non-toxic in phase II cancer trials (Redman, Esper et al. 2003, Jain, Cohen et al. 2013, Chan, Willis et al. 2017), it is difficult to initiate a clinical trial using TM as this drug cannot be administered off-label. This problem is compounded by the crowded arena of *BRAF*^{V600E}-mutant disease. There are currently multiple clinical trials using BRAF and MEK inhibitors as single or combination therapy *BRAF*^{V600E}-mutant PTC. One method of bypassing this lack of FDA approval is to design clinical trials using trientine, which is FDA approved for the treatment of Wilson's Disease (Walshe 1982). Although this drug is not as potent as TM (Brewer, Askari et al. 2006), trientine reduced anchorage dependent growth in *BRAF*^{V600E}-mutant PTC cell lines *in vitro* (Figure 7), a combination of this drug, a Cu restricted diet, and the slow-growing nature of PTC may allow the drug to lower Cu levels enough to be effective in a long-term disease like PTC.

3.1.6 Future directions

The evidence for adopting Cu chelation as targeted therapy in *BRAF*^{V600E}-mutant PTC can be enhanced on all the fronts described in sections 3.1.1-4. To address the general barrier erected by a lack of FDA approval for TM, the long-term 24-week experiment can be repeated by with trientine in place of TM. In combination with Cu-free food and water, this study design would allow time for trientine to reduce Cu levels

to therapeutically low levels and address whether other Cu chelators can be substituted for TM *in vivo.* Additionally, trientine is a drug that can be dissolved in water and dosed to mice long-term. Thus, this drug can be used to extend this pharmacological tumor burden study into a survival study that could further enhance the current genetic survival data.

The confirmation of cell lines derived from TBP as viable allografts establishes a platform through which Cu chelators can be quickly and reliably evaluated against a full panel of stand-of-care drugs, MAPK inhibitors, and other relevant therapies. Using this system, TM and trientine can both be compared against these drugs alone and in combination. This flexibility would also allow evaluation of Cu chelation against other emerging therapies, such as immunotherapies, which have become prominent in *BRAF*^{V600E}-mutant melanoma (Hu-Lieskovan, Robert et al. 2014). In addition, the TBP mouse model can be leveraged to address the emerging problem of immunotherapy associated thyroid toxicities (Min 2016, Alhusseini and Samantray 2017, Illouz, Briet et al. 2017).

Additionally, the ability to allograft TBP cells would also allow for investigation into whether Cu chelation can be used to restore RAI sensitivity. The described TBP cell lines are likely to be RAI resistant as they carry the BRAF^{V600E} mutation often associated with RAI resistance and qRT-PCR of these lines show a low expression of NIS and PAX8, genes responsible for iodine uptake. The large and easily accessible nature of

allografts would allow for imaging of RAI uptake, which was previously prohibited by the size of mouse thyroids. Since RAI is an essential treatment for PTC, the ability to restore RAI response would be immensely useful as it may allow treatment of previously RAI resistant resectable disease.

Finally, although current clinical data show BRAF inhibitors to be effective for relatively long terms in *BRAF*^{V600E}-mutant PTC (Falchook, Millward et al. 2015, Brose, Cabanillas et al. 2016), the history of resistance to targeted therapy in other *BRAF*^{V600E}-mutant cancers (Lito, Rosen et al. 2013) suggests that *BRAF*^{V600E}-mutant PTC will eventually develop resistance to BRAF inhibitors as well. The cell lines and mouse models used in this study provide an avenue through which BRAF inhibitor resistant *BRAF*^{V600E}-mutant PTC can be developed (through long-term low-dose BRAF inhibitor treatment of cells, TBP mice, or allograft) and their mechanisms dissected. The resulting BRAF inhibitor resistant disease can be used to determine whether, and in which resistance mechanism, Cu chelation may remain an effective therapy.

3.2 Cu chelation in other diseases of chronic MAPK activation

The MAPK pathway is important to a wide spectrum of cellular activities and is ubiquitous throughout the body. Dysregulation in this pathway can be seen in a large variety pathologic processes. Here I discuss two chronic disorders (RASopathies, and

obsessive-compulsive disorder) attributable to abnormal MAPK pathway activation in which Cu chelation may provide possible therapeutic relief.

3.2.1 RASopathies

3.2.1.1 Genetics of RASopathies

The RASopathies, one of the largest groups of congenital diseases, derive their namesake from a shared disease mechanism: dysregulation of the RAS/mitogen activated protein kinase (RAS/MAPK) pathway (Schubbert, Bollag et al. 2007, Schubbert, Shannon et al. 2007, Aoki, Niihori et al. 2008, Rauen 2013). RAS is a membrane associated GTPase essential for cellular response to extracellular stimuli. RAS is responsible for a variety of cell functions, especially cell proliferation, differentiation, and survival. Due this survival role, overactive RAS mutations have long been known to play an important role in oncogenesis (Bos 1989, Downward 2003). However, the role of hyperactive RAS has only recently come into focus in developmental disorders.

RASopathies are composed of Noonan Syndrome (NS), Neurofibromatosis Type I (NF1), Costello Syndrome (CS), Cardio-Facio-Cutaneous Syndrome (CFC), Legius Syndrome (LS), and LEOPARD Syndrome (Schubbert, Bollag et al. 2007, Schubbert, Shannon et al. 2007, Rauen 2013). Due to the common underlying mechanism, these diseases present with similar craniofacial dysmorphology, cardiac malformations, growth, and neurological abnormalities, as well as increased cancer risk (Gelb and

Tartaglia 2006, Schubbert, Bollag et al. 2007, Schubbert, Shannon et al. 2007, Aoki, Niihori et al. 2008, Buday and Downward 2008, Rauen 2013). Despite the similarities, distinct phenotypic differences exist between each disease, and even within a disease, depending on where mutations occur in the RAS/MAPK cascade. For instance, Noonan Syndrome patients with RAF1 mutations present with hypertrophic cardiomyopathy (HCM), while those with SHP2 mutations present with valvuloseptal defects (Aoki, Niihori et al. 2008).

RAS proteins are activated when growth factors bind to cell surface receptors, activating the receptor complex, which consists of intracellular adaptor molecules such as Shc (SH2-containing protein), Grb2 (growth-factor-receptor bound protein 2) and Gab (GRB2-associated binding). When activated, these proteins recruit SHP2 and SOS1. SOS1, a guanine nucleotide-exchange factor (GNEFs), activates the inactive RAS-GDP by catalyzing nucleotide exchange; leading to the formation of active RAS-GTP. Conversely, GTPase-activating proteins (GAPs), such as neurofibromin (NF1), bind to RAS-GTP and accelerates reversion back to the inactive RAS-GDP form (Schubbert, Shannon et al. 2007, Aoki, Niihori et al. 2008). Activated RAS-GTP can affect cellular response through several pathways, including the RAF/MEK/ERK cascade, which plays a prominent role in cellular proliferation (Schubbert, Bollag et al. 2007).

RASopathies can have mutations at various levels in this signaling cascade, specific mutations have been identified in *NF1*, *SHP2*, *SOS1*, *RAS*, *RAF*, *MEK*, and *ERK*.

Some syndromes, such as Noonan Syndrome, are caused by single mutations spread across most the RAS/MAPK signaling pathway, while other syndromes caused by single mutations in very few affecters (Figure 22). With the exception of Neurofibromatosis Type I, which is the result of NF1 loss-of-function leading to loss of RAS inhibition, all known RASopathies are caused by direct gain-of-function mutations (Schubbert, Bollag et al. 2007, Schubbert, Shannon et al. 2007, Rauen 2013).

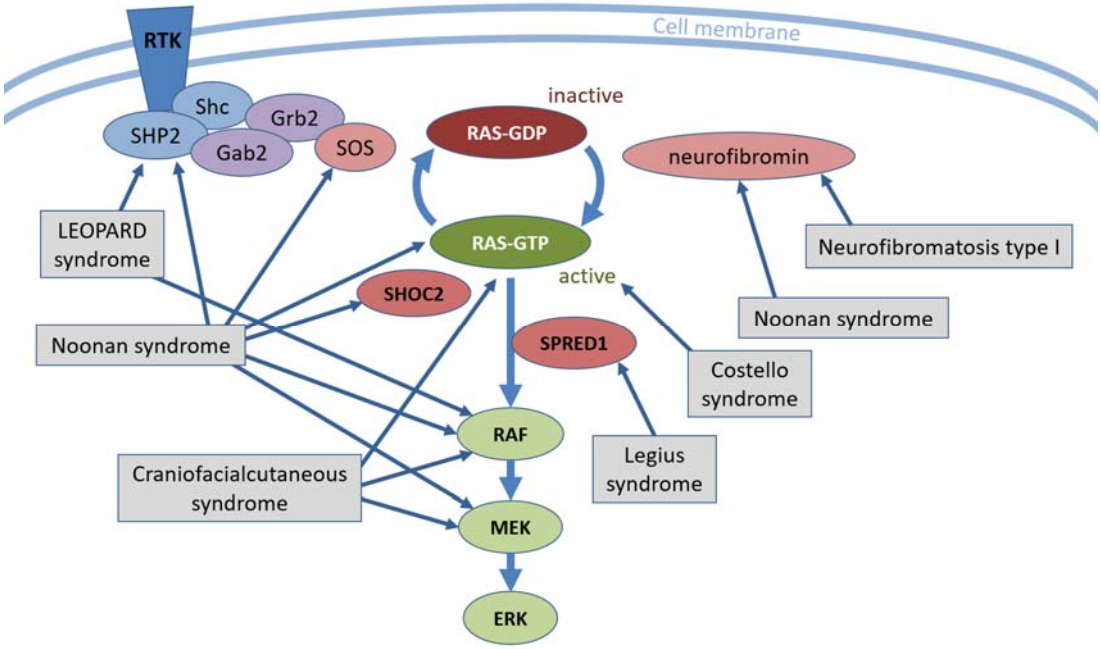

Figure 22: Schematic of RAS/MAPK pathway and locations of RASopathy mutations. Figure adapted from the Swedish information center for Rare Disease.

The large number of specific RAS/MAPK pathway mutations found in RASopathies presents both a confounding factor in treatment and a great opportunity to better understand the subtleties of RAS/MAPK signaling. For instance, although all RASopathies are the result of increased RAS/MAPK activation, mutations at different

levels of the pathway are linked to certain phenotypic subtypes. Cardiac defects found in Noonan Syndrome mouse models harboring different mutations clearly demonstrate this phenomenon. Mice with phosphatase-activating PTPN11 mutations present with valvuloseptal defects without hypertrophic cardiomyopathy (HCM) (Araki, Mohi et al. 2004, Krenz, Gulick et al. 2008, Araki, Chan et al. 2009). However, mice with SOS1 activating mutations present with left ventricular hypertrophy (LVH) and incomplete penetrance of aortic stenosis (Chen 2010). And lastly, mice with RAF1 activating mutations presented with HCM only (Wu, Simpson et al. 2011). Note that the PTPN11 gene encodes the SHP2 protein, the first effector in activating the RAS/MAPK pathway, SOS1 the second effector protein, and RAF1 further downstream. The gradual loss of valvuloseptal defects and emergence of HCM as the responsible mutation occurs further down-stream could be a manifestation of the subtleties in RAS/MAPK signaling. Genes of interest and the specific RASopathy mutations are detailed in Table 11. These mutants represent each RASopathy based on commonality in the clinical setting, proven cause of RASopathy phenotype *in vivo,* and representation of mutations seen in the gene of interest (Rasmussen and JFriedman 2000, Araki, Mohi et al. 2004, Gelb and Tartaglia 2006, Oishi, Gaengel et al. 2006, Rodriguez-Viciana, Tetsu et al. 2006, Pandit, Sarkozy et al. 2007, Schubbert, Bollag et al. 2007, Tartaglia, Pennacchio et al. 2007, Aoki, Niihori et al. 2008, Araki, Chan et al. 2009, Nakamura, Gulick et al. 2009, Chen 2010, Wu, Simpson et al. 2011, Rauen 2013, Vanden Borre, McFadden et al. 2014, Chan, Willis et al. 2017).

Table 11: The genes mutated in RASopathies.

Mutations are organized by syndrome, mutated gene, gene function, and mutational affect. Last column highlights the mutations that will be explored. (Rasmussen and JFriedman 2000, Araki, Mohi et al. 2004, Gelb and Tartaglia 2006, Oishi, Gaengel et al. 2006, Rodriguez-Viciana, Tetsu et al. 2006, Pandit, Sarkozy et al. 2007, Schubbert, Bollag et al. 2007, Tartaglia, Pennacchio et al. 2007, Aoki, Niihori et al. 2008, Araki, Chan et al. 2009, Nakamura, Gulick et al. 2009, Chen 2010, Wu, Simpson et al. 2011, Rauen 2013, Vanden Borre, McFadden et al. 2014, Chan, Willis et al. 2017).

Mutation		Function	Mutations type (s)	Select Mutations
Noonan Syndrome	PTPN11 (50%)	Codes for SHP2 a nonreceptor protein tyrosine phosphatase	Missense mutation disturbs catalytic stability of inactive SHP2→ more RAS/MAPK signaling	PTPN11 D61G PTPN11 A72S PTPN Y62D PTPN11 I282V PTPN11 N308D
	SOS1 (15%)	Codes for SOS1 a RasGEF (guanine nucleotide exchange factor)	Missense disrupts auto-inhibition of SOS1 RasGEF activity→ more RAS in active GTP form→ more RAS/MAPK signaling	SOS1 E846K SOS W552G SOS1 W729L
	RAF1 (3-5%)	Serine/threonine kinase in RAS/MAPK pathway	1) Conserved region 2 (S259) 2) Conserved region 3 (activation segment)	RAF1 L613V RAF1 S257L/A RAF1 D468N
	KRAS (1-2%)	Phosphorylates and activates RAF in RAS/MAP Kinase cascade	1) mutations reducing intrinsic and GAP stimulated GTPase activity 2) mutations interfering with guanine nucleotide binding	KRAS V14I KRAS T58I KRAS G12D (cancer)
	NRAS (<1%)	Phosphorylates and activates RAF in RAS/MAPK pathway	- Found in switch II region of NRAS - are thought to interfere with GTPase function.	NRAS T50I NRAS G60E
	SHOC2 (<1%)	A scaffold protein that binds RasGTP and mediates PP1C translocation to the cell membrane	S2G mutation leads to abnormal prolonged translocation of SHOC2 to the cell membrane→ increased RAF1 dephosphorylating and activation	SHOC2 S2G SHOC2 S2A
NF1	NF1	Neurofibromin, a RasGAP (negative regulator of RAS)	dominant negative loss of function→ increased RasGTPase activity	NF1 R1947X
CFC	BRAF, MEK1/2	Serine/threonine kinases in RAS/MAP Kinase cascade	BRAF- mutations in cysteine rich domain of exon 6 MEK1/2- activating heterozygous missense mutations	BRAF Q257R BRAF S467A BRAF V600E (Cancer) MEK 1 S218D MEK1/2 S222D
Costello Syndrome	HRAS	Serine/threonine kinase in RAS/MSAPK pathway	Heterozygous activating mutations in HRAS disturb guanine nucleotide binding→ reduction in intrinsic and GAP-induced GTPase activity→ RAS remains activated	HRAS G12S HRAS G12A

3.2.1.2 Potential of Cu chelation in RASopathies

As a family of congenital diseases characterized by increased signaling in the RAS/mitogen activated protein kinase (MAPK) pathway (Aoki, Niihori et al. 2008, Rauen 2013), RASopathies are a perfect target for long-term MAPK inhibition through Cu chelation. Although this group of diseases share similar cardiac and craniofacial malformations, growth and neurological abnormalities, and increased cancer risk caused by the underlying increase in MAPK signaling, symptomatic management, not systematic treatment, remains the standard of care (Schubbert, Bollag et al. 2007, Schubbert, Shannon et al. 2007). RAS/MAPK pathway inhibitors have been successfully implemented for cancers with hyperactive RAS/MAPK signaling (Chapman, Hauschild et al. 2011, Falchook, Millward et al. 2015, Ascierto, McArthur et al. 2016, Long, Eroglu et al. 2017). Following these encouraging results, RASopathy researchers have treated RASopathy symptoms using MEK inhibitors in a variety of animal models (Nakamura, Gulick et al. 2009, Pagani, Oishi et al. 2009, Wu, Simpson et al. 2011, Anastasaki, Rauen et al. 2012, Stinchcombe and Johnson 2014). Despite promising preliminary results, MEK inhibitors possess innate barriers to clinical application. MEK inhibitors have high toxicity that render them unattractive for use in RASopathies as they are untested in children, toxic, and may be too expensive for the long-term dosing necessary in treating a congenital disease.

As MEK1/2 require Cu to phosphorylate ERK (Turski, Brady et al. 2012, Brady, Crowe et al. 2014), chelating this metal may be a potential target through which RASopathies could be treated. Both genetic reduction and pharmacologic reduction of Cu has been shown to decrease ERK phosphorylation, resulting in decreased cell growth of cancers with a hyperactive MAPK pathway. As inexpensive drugs whose long-term use in Wilsons Disease (disease of abnormal copper accumulation) have proven low toxicity profiles, Cu chelators could be an ideal long-term treatment for RASopathies patients.

3.2.2 Obsessive-compulsive disorder

Obsessive-compulsive disorder (OCD), a neuropsychiatric disease characterized by repeated, intrusive thoughts or ritualized behaviors, affects 2% of the population (Leckman, Grice et al. 1997). Although neuroimaging has localized the disease to the cortico-striato-thalamo-cortical (CSTC) circuits, the underlying disease mechanism remains largely unknown (Aouizerate, Guehl et al. 2004). However, a recent study has linked the MAPK pathway with the brain-derived neurotrophic factor (BDNF) and showed that a deficiency of SPRED2, a regulator of RAS/MAPK pathway, in the amygdala can cause OCD-like behavior in mice. These OCD symptoms were rescuable by treatment with MEK inhibitor selumetinib, which was shown to suppress the MAPK pathway in treated mice (Ullrich, Weber et al. 2018). These results indicated another

clinical setting in which chronic MAPK inhibition with Cu chelators may be advantageous.

4. Conclusion

The ability of Cu chelator TM to inhibit tumor growth of *BRAF*^{V600E}-driven human PTC *in vitro* and reduce tumor load in a genetically engineered mouse model of *BRAF*^{V600E}-mutant PTC *in vivo* presents an potential opportunity for the development of an effective, well-tolerated targeted therapy for *BRAF*^{V600E}-mutant PTC. Cu chelators possess several advantages over conventional and MAPK inhibitor therapies in PTC. As drugs with a well-known and benign long-term toxicity profile (Jain, Cohen et al. 2013), Cu chelators have a baseline advantage over the more toxic conventional MAPK inhibitors (Chapman, Hauschild et al. 2011, Hauschild, Grob et al. 2012, Ascierto, McArthur et al. 2016, Long, Flaherty et al. 2017). This asset is further compounded in PTC as its decades-long disease progression creates a potential need for enduring treatment, which further highlights the quality of life benefits Cu chelation therapy could provide. The adaption of Cu chelation to *BRAF*^{V600E}-mutant PTC may present an additional financial advantage as these drugs are less expensive than MAPK inhibitors, which have been shown to be very cost ineffective (Curl, Vujic et al. 2014, Delea, Amdahl et al. 2015, Matter-Walstra, Braun et al. 2015, Zhang, Yang et al. 2015). Cu chelation could be adapted to PTC treatment in three distinct methods: *i*) as a less toxic monotherapy for *Braf*^{V600E}-mutant PTC, *ii*) as maintenance therapy after initial treatment in patients with intermediate- or high-risk disease, and *ii*) as a combination-therapy amplifying the antineoplastic effects of standard-of-care sorafenib or BRAF inhibitor

vemurafenib. The success of other MAKP inhibitors at restoring RAI sensitivity, also suggest that Cu chelation could be evaluated as a RAI adjuvant therapy. These options could allow Cu chelation to add value in PTC treatment at multiple stages of disease management.

The ubiquitous nature of the MAPK pathway throughout all cell types presents a variety of additional diseases in which Cu chelation may be beneficial. Two such long-term diseases of MAPK hyperactivation, RASopathies (Rauen 2013) and OCD (Ullrich, Weber et al. 2018), have been attributed to abnormal MAPK pathway activation. As patients suffering from congenital diseases of MAPK pathway activation and a chronic neuropsychiatric disease, both RASopathies and OCD patients, respectively, could benefit from a therapy that targets the root pathophysiology of their disease. While MAPK inhibitors have shown efficacy in animal models of both disease (Wu, Simpson et al. 2011, Ullrich, Weber et al. 2018), clinical adaption of these drugs is unlikely because of their toxic side-effect profiles and prohibitive cost. Cu chelation presents a therapeutic option that may allow long-term inhibition of the MAPK pathway without reducing the patient's quality of life or introducing an untenable financial burden.

In short, Cu chelation represents a unique clinical opportunity in PTC. The ability of Cu chelator TM to inhibit MEK1/2 kinases while maintaining a benign drug toxicity profile makes it particularly well-suited for long-term inhibition of the MAPK pathway in $BRAF^{V600E}$-mutant PTC. This benign drug can be leveraged either in

combination with current or emerging therapies and/or as a chronic maintenance therapy. The low-toxicity of Cu chelator TM may also be beneficial in other diseases of chronic MAPK activation.

References

Adeniran, A. J., Z. Zhu, M. Gandhi, D. L. Steward, J. P. Fidler, et al. (2006). "Correlation between genetic alterations and microscopic features, clinical manifestations, and prognostic characteristics of thyroid papillary carcinomas." Am J Surg Pathol **30**(2): 216-222.

Adnane, L., P. A. Trail, I. Taylor and Wilhelm, S. M. (2006). "Sorafenib (BAY 43-9006, Nexavar), a dual-action inhibitor that targets RAF/MEK/ERK pathway in tumor cells and tyrosine kinases VEGFR/PDGFR in tumor vasculature." Methods Enzymol **407**: 597-612.

Ahn, S., Y. Henderson, Y. Kang, C. Chattopadhyay, P. Holton, et al. (2008). "An orthotopic model of papillary thyroid carcinoma in athymic nude mice." Arch Otolaryngol Head Neck Surg **134**(2): 190-197.

Ala, A., A. P. Walker, K. Ashkan, J. S. Dooley and M. L. Schilsky (2007). "Wilson's Disease." Lancet **369**(9559): 397-408.

Alhusseini, M. and J. Samantray (2017). "Hypothyroidism in cancer patients on immune checkpoint inhibitors with anti-PD1 agents: insights on underlying mechanisms." Exp Clin Endocrinol Diabetes **125**(4): 267-269.

Anastasaki, C., K. A. Rauen and E. E. Patton (2012). "Continual low-level MEK inhibition ameliorates cardio-facio-cutaneous phenotypes in zebrafish." Dis Model Mech **5**(4): 546-552.

Aoki, Y., T. Niihori, Y. Narumi, S. Kure and Y. Matsubara (2008). "The RAS/MAPK syndromes: novel roles of the RAS pathway in human genetic disorders." Hum Mutat **29**(8): 992-1006.

Aouizerate, B., D. Guehl, E. Cuny, A. Rougier, B. Bioulac, et al. (2004). "Pathophysiology of obsessive-compulsive disorder: a necessary link between phenomenology, neuropsychology, imagery and physiology." Prog Neurobiol **72**(3): 195-221.

Araki, T., G. Chan, S. Newbigging, L. Morikawa, R. T. Bronson, et al. (2009). "Noonan syndrome cardiac defects are caused by PTPN11 acting in endocardium to enhance endocardial-mesenchymal transformation." Proc Natl Acad Sci USA **106**(12): 4736-4741.

Araki, T., M. G. Mohi, F. A. Ismat, R. T. Bronson, I. R. Williams, et al. (2004). "Mouse model of Noonan syndrome reveals cell type- and gene dosage-dependent effects of Ptpn11 mutation." Nat Med **10**(8): 849-857.

Are, C. and A. R. Shaha (2006). "Anaplastic thyroid carcinoma: biology, pathogenesis, prognostic factors, and treatment approaches." Ann Surg Oncol **13**(4): 453-464.

Aschebrook-Kilfoy, B., R. B. Schechter, Y. C. Shih, E. L. Kaplan, B. C. Chiu, et al. (2013). "The clinical and economic burden of a sustained increase in thyroid cancer incidence." Cancer Epidemiol Biomarkers Prev **22**(7): 1252-1259.

Ascierto, P. A., G. A. McArthur, B. Dreno, V. Atkinson, G. Liszkay, et al. (2016). "Cobimetinib combined with vemurafenib in advanced BRAF(V600)-mutant melanoma (coBRIM): updated efficacy results from a randomised, double-blind, phase 3 trial." Lancet Oncol **17**(9): 1248-1260.

Badet, J., F. Soncin, J. D. Guitton, O. Lamare, T. Cartwright, et al. (1989). "Specific binding of angiogenin to calf pulmonary artery endothelial cells." Proc Natl Acad Sci USA **86**(21): 8427-8431.

Barbareschi, M., F. Buttitta, L. Felicioni, S. Cotrupi, F. Barassi, et al. (2007). "Different prognostic roles of mutations in the helical and kinase domains of the PIK3CA gene in breast carcinomas." Clin Cancer Res **13**(20): 6064-6069.

Bejarano, P. A., Y. E. Nikiforov, E. S. Swenson and P. W. Biddinger (2000). "Thyroid transcription factor-1, thyroglobulin, cytokeratin 7, and cytokeratin 20 in thyroid neoplasms." Appl Immunohistochem Mol Morphol **8**(3): 189-194.

Berthon, G. (1993). "Is copper pro- or anti-inflammatory? A reconciling view and a novel approach for the use of copper in the control of inflammation." Agents Actions **39**(3-4): 210-217.

Bestvina, C. M., L. L. Zullig and S. Yousuf Zafar (2014). "The implications of out-of-pocket cost of cancer treatment in the USA: a critical appraisal of the literature." Future Oncol **10**(14): 2189-2199.

Bischoff, L. A., J. Curry, I. Ahmed, E. Pribitkin and J. L. Miller (2013). "Is above age 45 appropriate for upstaging well-differentiated papillary thyroid cancer?" Endocr Pract **19**(6): 995-997.

Bollag, G., P. Hirth, J. Tsai, J. Zhang, P. N. Ibrahim, et al. (2010). "Clinical efficacy of a RAF inhibitor needs broad target blockade in BRAF-mutant melanoma." Nature **467**(7315): 596-599.

Bos, J. L. (1989). "ras oncogenes in human cancer: a review." Cancer Res **49**(17): 4682-4689.

Bost, M., S. Houdart, M. Oberli, E. Kalonji, J.-F. Huneau, et al. (2016). "Dietary copper and human health: Current evidence and unresolved issues." J Trace Elements Med Biol **35**: 107-115.

Brady, D. C., M. S. Crowe, D. N. Greenberg and C. M. Counter (2017). "Copper chelation inhibits *BRAF*^{V600E}-driven melanomagenesis and counters resistance to *BRAF*^{V600E} and mek1/2 inhibitors." Cancer Res **77**(22): 6240-6252.

Brady, D. C., M. S. Crowe, M. L. Turski, G. A. Hobbs, X. Yao, et al. (2014). "Copper is required for oncogenic BRAF signalling and tumorigenesis." Nature **509**(7501): 492-496.

Brem, S. S., D. Zagzag, A. M. Tsanaclis, S. Gately, M. P. Elkouby, et al. (1990). "Inhibition of angiogenesis and tumor growth in the brain. Suppression of endothelial cell turnover by penicillamine and the depletion of copper, an angiogenic cofactor." Am J Pathol **137**(5): 1121-1142.

Bremner, I., C. F. Mills and B. W. Young (1982). "Copper metabolism in rats given di- or trithiomolybdates." J Inorganic Biochem **16**(2): 109-119.

Brewer, G. J. (2005). "Copper lowering therapy with tetrathiomolybdate as an antiangiogenic strategy in cancer." Curr Cancer Drug Targets **5**(3): 195-202.

Brewer, G. J., F. Askari, R. B. Dick, J. Sitterly, J. K. Fink, et al. (2009). "Treatment of Wilson's Disease with tetrathiomolybdate: V. Control of free copper by tetrathiomolybdate and a comparison with trientine." Transl Res **154**(2): 70-77.

Brewer, G. J., F. Askari, M. T. Lorincz, M. Carlson, M. Schilsky, et al. (2006). "Treatment of Wilson disease with ammonium tetrathiomolybdate: IV. Comparison of tetrathiomolybdate and trientine in a double-blind study of treatment of the neurologic presentation of Wilson disease." Arch Neurol **63**(4): 521-527.

Brewer, G. J., R. D. Dick, D. K. Grover, V. LeClaire, M. Tseng, et al. (2000). "Treatment of metastatic cancer with tetrathiomolybdate, an anticopper, antiangiogenic agent: Phase I study." Clin Cancer Res **6**(1): 1-10.

Brewer, G. J., P. Hedera, K. J. Kluin, M. Carlson, F. Askari, et al. (2003). "Treatment of Wilson disease with ammonium tetrathiomolybdate: III. Initial therapy in a total of 55 neurologically affected patients and follow-up with zinc therapy." Arch Neurol **60**(3): 379-385.

Brose, M. S., M. E. Cabanillas, E. E. Cohen, L. J. Wirth, T. Riehl, et al. (2016). "Vemurafenib in patients with BRAF(V600E)-mutant metastatic or unresectable papillary thyroid cancer refractory to radioactive iodine: a non-randomised, multicentre, open-label, phase 2 trial." Lancet Oncol **17**(9): 1272-1282.

Brose, M. S., C. M. Nutting, B. Jarzab, R. Elisei, S. Siena, et al. (2014). "Sorafenib in radioactive iodine-refractory, locally advanced or metastatic differentiated thyroid cancer: a randomised, double-blind, phase 3 trial." Lancet **384**(9940): 319-328.

Buday, L. and J. Downward (2008). "Many faces of Ras activation." Biochim Biophys Acta **1786**(2): 178-187.

Bund, T., J. M. Boggs, G. Harauz, N. Hellmann and D. Hinderberger (2010). "Copper uptake induces self-assembly of 18.5 kda myelin basic protein (MBP)." Biophysical J **99**(9): 3020-3028.

Cao, Y., M. A. Skaug, O. Andersen and J. Aaseth (2015). "Chelation therapy in intoxications with mercury, lead and copper." J Trace Elem Med Biol **31**: 188-192.

Casaluce, F., A. Sgambato, P. Maione, P. C. Sacco, G. Santabarbara, et al. (2017). "Selumetinib for the treatment of non-small cell lung cancer." Expert Opin Investig Drugs **26**(8): 973-984.

Casara, D., D. Rubello, G. Saladini, G. Masarotto, A. Favero, et al. (1993). "Different features of pulmonary metastases in differentiated thyroid cancer: natural history and multivariate statistical analysis of prognostic variables." J Nucl Med **34**(10): 1626-1631.

Castellone, M. D., V. De Falco, D. M. Rao, R. Bellelli, M. Muthu, et al. (2009). "The beta-catenin axis integrates multiple signals downstream from RET/papillary thyroid carcinoma leading to cell proliferation." Cancer Res **69**(5): 1867-1876.

Catalanotti, F., D. B. Solit, M. P. Pulitzer, M. F. Berger, S. N. Scott, et al. (2013). "Phase II trial of MEK inhibitor selumetinib (AZD6244, ARRY-142886) in patients with BRAFV600E/K-mutant melanoma." Clin Cancer Res **19**(8): 2257-2264.

Chakravarty, D., E. Santos, M. Ryder, J. A. Knauf, X. H. Liao, et al. (2011). "Small-molecule MAPK inhibitors restore radioiodine incorporation in mouse thyroid cancers with conditional BRAF activation." J Clin Invest **121**(12): 4700-4711.

Chan, N., A. Willis, N. Kornhauser, M. M. Ward, S. B. Lee, et al. (2017). "Influencing the tumor microenvironment: a phase II study of copper depletion using tetrathiomolybdate in patients with breast cancer at high risk for recurrence and in preclinical models of lung metastases." Clin Cancer Res **23**(3): 666-676.

Chan, W. Y. and O. M. Rennert (1980). "The role of copper in iron metabolism." Ann Clin Lab Sci **10**(4): 338-344.

Chandra, A. K., L. H. Singh, S. Tripathy, A. Debnath and J. Khanam (2006). "Iodine nutritional status of children in North East India." Indian J Pediatr **73**(9): 795-798.

Chapman, P. B., A. Hauschild, C. Robert, J. B. Haanen, P. Ascierto, et al. (2011). "Improved survival with vemurafenib in melanoma with BRAF V600E mutation." N Engl J Med **364**(26): 2507-2516.

Charles, R. P., G. Iezza, E. Amendola, D. Dankort and M. McMahon (2011). "Mutationally activated BRAF(V600E) elicits papillary thyroid cancer in the adult mouse." Cancer Res **71**(11): 3863-3871.

Charles, R. P., J. Silva, G. Iezza, W. A. Phillips and M. McMahon (2014). "Activating BRAF and PIK3CA mutations cooperate to promote anaplastic thyroid carcinogenesis." Mol Cancer Res **12**(7): 979-986.

Chen, P. C., W. Hiroko, C. David, A. Toshiyuki, and Y. Tao (2010). "Activation of multiple signaling pathways causes developmental defects in mice with a Noonan syndrome-associated Sos1 mutation." J Clin Invest **120**(12): 12.

Chiu, A. C., E. S. Delpassand and S. I. Sherman (1997). "Prognosis and treatment of brain metastases in thyroid carcinoma." J Clin Endocrinol Metab **82**(11): 3637-3642.

Chou, T. C. and P. Talalay (1984). "Quantitative analysis of dose-effect relationships: the combined effects of multiple drugs or enzyme inhibitors." Adv Enzyme Regul **22**: 27-55.

Costa, A. M., A. Herrero, M. F. Fresno, J. Heymann, J. A. Alvarez, et al. (2008). "BRAF mutation associated with other genetic events identifies a subset of aggressive papillary thyroid carcinoma." Clin Endocrinol **68**(4): 618-634.

Curl, P., I. Vujic, L. J. van 't Veer, S. Ortiz-Urda and J. G. Kahn (2014). "Cost-effectiveness of treatment strategies for BRAF-mutant metastatic melanoma." PLoS One **9**(9): e107255.

Dahlman, T., P. Hartvig, M. Lofholm, H. Nordlinder, L. Loof, et al. (1995). "Long-term treatment of Wilson's Disease with triethylene tetramine dihydrochloride (trientine)." QJM **88**(9): 609-616.

Dankort, D., E. Filenova, M. Collado, M. Serrano, K. Jones, et al. (2007). "A new mouse model to explore the initiation, progression, and therapy of BRAFV600E-induced lung tumors." Genes Dev **21**(4): 379-384.

Das, S. K. and K. Ray (2006). "Wilson's Disease: an update." Nat Clin Pract Neurol **2**(9): 482-493.

Davies, H., G. R. Bignell, C. Cox, P. Stephens, S. Edkins, et al. (2002). "Mutations of the BRAF gene in human cancer." Nature **417**(6892): 949-954.

Davies, L. and H. G. Welch (2014). "Current thyroid cancer trends in the United States." JAMA Otolaryngol Head Neck Surg **140**(4): 317-322.

de Biase, D., V. Cesari, M. Visani, G. P. Casadei, N. Cremonini, et al. (2014). "High-sensitivity BRAF mutation analysis: BRAF V600E is acquired early during tumor development but is heterogeneously distributed in a subset of papillary thyroid carcinomas." J Clin Endocrinol Metab **99**(8): E1530-1538.

del Ama, L. F., M. Jones, P. Walker, A. Chapman, J. A. Braun, et al. (2016). "Reprofiling using a zebrafish melanoma model reveals drugs cooperating with targeted therapeutics." Oncotarget **7**(26): 40348-40361.

Delea, T. E., J. Amdahl, A. Wang, M. M. Amonkar and M. Thabane (2015). "Cost effectiveness of dabrafenib as a first-line treatment in patients with BRAF V600 mutation-mutant unresectable or metastatic melanoma in Canada." Pharmacoeconomics **33**(4): 367-380.

Downward, J. (2003). "Targeting RAS signalling pathways in cancer therapy." Nat Rev Cancer **3**(1): 11-22.

Durante, C., E. Puxeddu, E. Ferretti, R. Morisi, S. Moretti, et al. (2007). "BRAF mutations in papillary thyroid carcinomas inhibit genes involved in iodine metabolism." J Clin Endocrinol Metab **92**(7): 2840-2843.

Ebanks, J. P., R. R. Wickett and R. E. Boissy (2009). "Mechanisms regulating skin pigmentation: the rise and fall of complexion coloration." Int J Molec Sci **10**(9): 4066-4087.

Elisei, R., D. Viola, L. Torregrossa, R. Giannini, C. Romei, et al. (2012). "The BRAF(V600E) mutation is an independent, poor prognostic factor for the outcome of patients with low-risk intrathyroid papillary thyroid carcinoma: single-institution results from a large cohort study." J Clin Endocrinol Metab **97**(12): 4390-4398.

Enewold, L., K. Zhu, E. Ron, A. J. Marrogi, A. Stojadinovic, et al. (2009). "Rising thyroid cancer incidence in the United States by demographic and tumor characteristics, 1980-2005." Cancer Epidemiol Biomarkers Prev **18**(3): 784-791.

Escudier, B., T. Eisen, W. M. Stadler, C. Szczylik, S. Oudard, et al. (2007). "Sorafenib in advanced clear-cell renal-cell carcinoma." N Engl J Med **356**(2): 125-134.

Fabbro, D., C. Di Loreto, C. A. Beltrami, A. Belfiore, R. Di Lauro, et al. (1994). "Expression of thyroid-specific transcription factors TTF-1 and PAX-8 in human thyroid neoplasms." Cancer Res **54**(17): 4744-4749.

Falchook, G. S., K. D. Lewis, J. R. Infante, M. S. Gordon, N. J. Vogelzang, et al. (2012). "Activity of the oral MEK inhibitor trametinib in patients with advanced melanoma: a phase 1 dose-escalation trial." Lancet Oncol **13**(8): 782-789.

Falchook, G. S., M. Millward, D. Hong, A. Naing, S. Piha-Paul, et al. (2015). "BRAF inhibitor dabrafenib in patients with metastatic BRAF-mutant thyroid cancer." Thyroid **25**(1): 71-77.

Festa, R. A. and D. J. Thiele (2011). "Copper: an Essential Metal in Biology." Curr Biol **21**(21): R877-R883.

Finney, L., S. Vogt, T. Fukai and D. Glesne (2009). "Copper and angiogenesis: unravelling a relationship key to cancer progression." Clin Exp Pharmacol Physiol **36**(1): 88-94.

Flaherty, K. T., C. Robert, P. Hersey, P. Nathan, C. Garbe, et al. (2012). "Improved survival with MEK inhibition in BRAF-mutant melanoma." N Engl J Med **367**(2): 107-114.

Foucquier, J. and M. Guedj (2015). "Analysis of drug combinations: current methodological landscape." Pharmacol Res Perspect **3**(3): e00149.

Freeman, A. K., D. A. Ritt and D. K. Morrison (2013). "The importance of RAF dimerization in cell signaling." Small GTPases **4**(3): 180-185.

Friedman, A. and N. Perrimon (2006). "A functional RNAi screen for regulators of receptor tyrosine kinase and ERK signalling." Nature **444**(7116): 230-234.

Gallop, K., C. Kerr, S. Simmons, B. McIver and E. E. Cohen (2015). "A qualitative evaluation of the validity of published health utilities and generic health utility measures for capturing health-related quality of life (HRQL) impact of differentiated thyroid cancer (DTC) at different treatment phases." Qual Life Res **24**(2): 325-338.

Gelb, B. D. and M. Tartaglia (2006). "Noonan syndrome and related disorders: dysregulated RAS-mitogen activated protein kinase signal transduction." Hum Mol Genet **15**(2): R220-226.

Ghofrani, M. and I. T. Ocal (2015). "Medullary thyroid carcinoma: a brief review of pathogenesis, diagnosis, and treatment." AJSP **20**(5): 204-209.

Ghossein, R. and V. A. Livolsi (2008). "Papillary thyroid carcinoma tall cell variant." Thyroid **18**(11): 1179-1181.

Ghossein, R. A., R. Leboeuf, K. N. Patel, M. Rivera, N. Katabi, et al. (2007). "Tall cell variant of papillary thyroid carcinoma without extrathyroid extension: biologic behavior and clinical implications." Thyroid **17**(7): 655-661.

Gild, M. L., D. J. Topliss, D. Learoyd, F. Parnis, J. Tie, et al. (2017). "Clinical guidance for radioiodine refractory differentiated thyroid cancer." Clin Endocrinol (Oxf) **88**(4): 529-537.

Gooneratne, S. R., J. M. Howell and J. M. Gawthorne (1981). "An investigation of the effects of intravenous administration of thiomolybdate on copper metabolism in chronic Cu-poisoned sheep." Br J Nutr **46**(3): 469-480.

Grimaldi, A. M., E. Simeone and P. A. Ascierto (2014). "The role of MEK inhibitors in the treatment of metastatic melanoma." Curr Opin Oncol **26**(2): 196-203.

Grimaldi, A. M., E. Simeone, L. Festino, V. Vanella, M. Strudel, et al. (2017). "MEK inhibitors in the treatment of metastatic melanoma and solid tumors." Am J Clin Dermatol **18**(6): 745-754.

Grogan, R. H., S. P. Kaplan, H. Cao, R. E. Weiss, L. J. Degroot, et al. (2013). "A study of recurrence and death from papillary thyroid cancer with 27 years of median follow-up." Surgery **154**(6): 1436-1446. .

Guerrero-Zotano, A., I. A. Mayer and C. L. Arteaga (2016). "PI3K/AKT/mTOR: role in breast cancer progression, drug resistance, and treatment." Cancer Metastasis Rev **35**(4): 515-524.

Gustin, J. P., D. P. Cosgrove and B. H. Park (2008). "The PIK3CA gene as a mutated target for cancer therapy." Curr Cancer Drug Targets **8**(8): 733-740.

Halfdanarson, T. R., N. Kumar, C. Y. Li, R. L. Phyliky and W. J. Hogan (2008). "Hematological manifestations of copper deficiency: a retrospective review." Eur J Haematol **80**(6): 523-531.

Hamad, N. M., J. H. Elconin, A. E. Karnoub, W. Bai, J. N. Rich, et al. (2002). "Distinct requirements for Ras oncogenesis in human versus mouse cells." Genes Dev **16**(16): 2045-2057.

Harris, E. D. (1995). "The iron-copper connection: the link to ceruloplasmin grows stronger." Nutr Rev **53**(6): 170-173.

Harris, P. J. and K. C. Bible (2011). "Emerging therapeutics for advanced thyroid malignancies: rationale and targeted approaches." Expert Opin Investig Drugs **20**(10): 1357-1375.

Haugen, B. R., E. K. Alexander, K. C. Bible, G. M. Doherty, S. J. Mandel, et al. (2016). "2015 american thyroid association management guidelines for adult patients with thyroid nodules and differentiated thyroid cancer: the american thyroid association guidelines task force on thyroid nodules and differentiated thyroid cancer." Thyroid **26**(1): 1-133.

Hauschild, A., J. J. Grob, L. V. Demidov, T. Jouary, R. Gutzmer, et al. (2012). "Dabrafenib in BRAF-mutant metastatic melanoma: a multicentre, open-label, phase 3 randomised controlled trial." Lancet **380**(9839): 358-365.

Ho, A. L., R. K. Grewal, R. Leboeuf, E. J. Sherman, D. G. Pfister, et al. (2013). "Selumetinib-enhanced radioiodine uptake in advanced thyroid cancer." N Engl J Med **368**(7): 623-632.

Hoffman, K., A. Lorenzo, C. M. Butt, S. C. Hammel, B. B. Henderson, et al. (2017). "Exposure to flame retardant chemicals and occurrence and severity of papillary thyroid cancer: A case-control study." Environ Int **107**: 235-242.

Hordyjewska, A., L. Popiolek and J. Kocot (2014). "The many "faces" of copper in medicine and treatment." Biometals **27**(4): 611-621.

Hou, G., R. Dick, C. Zeng and G. J. Brewer (2007). "Antitumor and antiinflammatory effects of tetrathiotungstate in comparison with tetrathiomolybdate." Transl Res **149**(5): 260-264.

Howell, G. M., S. P. Hodak and L. Yip (2013). "RAS mutations in thyroid cancer." Oncologist **18**(8): 926-932.

Howlader N, N. A., Krapcho M, Miller D, Bishop K, Kosary CL, et al. (2017, April 2017). "SEER cancer statistics review, 1975-2014." Retrieved Oct 5th, 2017, from https://seer.cancer.gov/csr/1975_2014/.

Hu-Lieskovan, S., L. Robert, B. Homet Moreno and A. Ribas (2014). "Combining Targeted Therapy With Immunotherapy in BRAF-Mutant Melanoma: Promise and Challenges." J Clin Oncol **32**(21): 2248-2254.

Hussein, Z., H. Mizuo, S. Hayato, M. Namiki and R. Shumaker (2017). "Clinical pharmacokinetic and pharmacodynamic profile of lenvatinib, an orally active, small-molecule, multitargeted tyrosine kinase inhibitor." Eur J Drug Metab Pharmacokinet **42**(6): 903-914.

Husson, O., H. R. Haak, W. A. Oranje, F. Mols, P. H. Reemst, et al. (2011). "Health-related quality of life among thyroid cancer survivors: a systematic review." Clin Endocrinol (Oxf) **75**(4): 544-554.

Huster, D. (2010). "Wilson disease." Best Pract Res Clin Gastroenterol **24**(5): 531-539.

Illouz, F., C. Briet, L. Cloix, Y. Le Corre, N. Baize, T. Urban, L. Martin and P. Rodien (2017). "Endocrine toxicity of immune checkpoint inhibitors: essential crosstalk between endocrinologists and oncologists." Cancer Med **6**(8): 1923-1929.

Ito, Y., T. Kudo, M. Kihara, Y. Takamura, K. Kobayashi, et al. (2012). "Prognosis of low-risk papillary thyroid carcinoma patients: its relationship with the size of primary tumors." Endocr J **59**(2): 119-125.

Jain, S., J. Cohen, M. M. Ward, N. Kornhauser, E. Chuang, et al. (2013). "Tetrathiomolybdate-associated copper depletion decreases circulating endothelial progenitor cells in women with breast cancer at high risk of relapse." Ann Oncol **24**(6): 1491-1498.

Johnson, T. L., R. V. Lloyd, N. W. Thompson, W. H. Beierwaltes and J. C. Sisson (1988). "Prognostic implications of the tall cell variant of papillary thyroid carcinoma." Am J Surg Pathol **12**(1): 22-27.

Juarez, J. C., O. Betancourt, Jr., S. R. Pirie-Shepherd, X. Guan, M. L. Price, et al. (2006). "Copper binding by tetrathiomolybdate attenuates angiogenesis and tumor cell proliferation through the inhibition of superoxide dismutase 1." Clin Cancer Res **12**(16): 4974-4982.

Juarez, J. C., M. Manuia, M. E. Burnett, O. Betancourt, B. Boivin, et al. (2008). "Superoxide dismutase 1 (SOD1) is essential for H2O2-mediated oxidation and inactivation of phosphatases in growth factor signaling." Proc Natl Acad Sci USA **105**(20): 7147-7152.

Kakarmath, S., H. T. Heller, C. A. Alexander, E. S. Cibas, J. F. Krane, et al. (2016). "Clinical, sonographic, and pathological characteristics of ras-mutant versus braf-mutant thyroid carcinoma." J Clin Endocrinol Metab **101**(12): 4938-4944.

Kandil, E., A. Hauch, P. Friedlander, M. Sheng, K. Tsumagari, et al. (2013). "A novel mouse model of metastatic thyroid carcinoma using human adipose tissue-derived stromal/stem cells." Anticancer Res **33**(10): 4213-4217.

Karakas, B., K. E. Bachman and B. H. Park (2006). "Mutation of the PIK3CA oncogene in human cancers." Br J Cancer **94**(4): 455-459.

Karoulia, Z., E. Gavathiotis and P. I. Poulikakos (2017). "New perspectives for targeting RAF kinase in human cancer." Nat Rev Cancer **17**(11): 676-691.

Karoulia, Z., Y. Wu, T. A. Ahmed, Q. Xin, J. Bollard, (2016). "An integrated model of RAF inhibitor action predicts inhibitor activity against oncogenic BRAF signaling." Cancer Cell **30**(3): 485-498.

Karunamurthy, A., F. Panebianco, J. H. S, J. Vorhauer, M. N. Nikiforova, S. Chiosea, et al. (2016). "Prevalence and phenotypic correlations of EIF1AX mutations in thyroid nodules." Endocr Relat Cancer **23**(4): 295-301.

Kato, S., S. Iida, T. Higuchi, T. Ishikawa, Y. Takagi, et al. (2007). "PIK3CA mutation is predictive of poor survival in patients with colorectal cancer." Int J Cancer **121**(8): 1771-1778.

Keutgen, X. M., S. M. Sadowski and E. Kebebew (2015). "Management of anaplastic thyroid cancer." Gland Surg **4**(1): 44-51.

Kim, K. B., M. E. Cabanillas, A. J. Lazar, M. D. Williams, D. L. Sanders, et al. (2013). "Clinical responses to vemurafenib in patients with metastatic papillary thyroid cancer harboring BRAF(V600E) mutation." Thyroid **23**(10): 1277-1283.

Kim, Y. H. (2016). "Dual inhibition of BRAF and MEK in BRAF-mutant metastatic non-small cell lung cancer." J Thorac Dis **8**(9): 2369-2371.

Kimura, E. T., M. N. Nikiforova, Z. Zhu, J. A. Knauf, Y. E. Nikiforov, et al. (2003). "High prevalence of BRAF mutations in thyroid cancer: genetic evidence for constitutive activation of the RET/PTC-RAS-BRAF signaling pathway in papillary thyroid carcinoma." Cancer Res **63**(7): 1454-1457.

Kitahara, C. M. and J. A. Sosa (2016). "The changing incidence of thyroid cancer." Nat Rev Endocrinol **12**(11): 646-653.

Klein, M., J. M. Vignaud, V. Hennequin, B. Toussaint, L. Bresler, et al. (2001). "Increased expression of the vascular endothelial growth factor is a pejorative prognosis marker in papillary thyroid carcinoma." J Clin Endocrinol Metab **86**(2): 656-658.

Kodama, H., C. Fujisawa and W. Bhadhprasit (2012). "Inherited copper transport disorders: biochemical mechanisms, diagnosis, and treatment." Curr Drug Metab **13**(3): 237-250.

Kogai, T. and G. A. Brent (2012). "The sodium iodide symporter (NIS): regulation and approaches to targeting for cancer therapeutics." Pharmacol Ther **135**(3): 355-370.

Krenz, M., J. Gulick, H. E. Osinska, M. C. Colbert, J. D. Molkentin, et al. (2008). "Role of ERK1/2 signaling in congenital valve malformations in Noonan syndrome." Proc Natl Acad Sci USA **105**(48): 18930-18935.

Kumar, V., A. Abbas, N. Fausto and J. Aster (2010). Robbins and Cotran Pathologic Basis of Disease. W. Schmitt. Philadelphia, PA, Saunders Elsevier.

Kuo, Y. M., B. Zhou, D. Cosco and J. Gitschier (2001). "The copper transporter CTR1 provides an essential function in mammalian embryonic development." Proc Natl Acad Sci USA **98**(12): 6836-6841.

Larkin, J., P. A. Ascierto, B. Dreno, V. Atkinson, G. Liszkay, et al. (2014). "Combined vemurafenib and cobimetinib in BRAF-mutant melanoma." N Engl J Med **371**(20): 1867-1876.

Larson, S. M., J. R. Osborne, R. K. Grewal and R. M. Tuttle (2017). "Redifferentiating thyroid cancer: selumetinib-enhanced radioiodine uptake in thyroid cancer." Mol Imaging Radionucl Ther **26**(Suppl 1): 80-86.

Leckman, J. F., D. E. Grice, J. Boardman, H. Zhang, A. Vitale, et al. (1997). "Symptoms of obsessive-compulsive disorder." Am J Psychiatry **154**(7): 911-917.

Lee, J., J. R. Prohaska and D. J. Thiele (2001). "Essential role for mammalian copper transporter Ctr1 in copper homeostasis and embryonic development." Proc Natl Acad Sci USA **98**(12): 6842-6847.

Leijen, S., P. M. Soetekouw, T. R. Jeffry Evans, M. Nicolson, J. H. Schellens, et al. (2011). "A phase I, open-label, randomized crossover study to assess the effect of dosing of the MEK 1/2 inhibitor Selumetinib (AZD6244; ARRY-142866) in the presence and absence of food in patients with advanced solid tumors." Cancer Chemother Pharmacol **68**(6): 1619-1628.

Lesche, R., M. Groszer, J. Gao, Y. Wang, A. Messing, H, et al. (2002). "Cre/loxP-mediated inactivation of the murine Pten tumor suppressor gene." Genesis **32**(2): 148-149.

Li, S. Y., M. Rong, F. Grieu and B. Iacopetta (2006). "PIK3CA mutations in breast cancer are associated with poor outcome." Breast Cancer Res Treat **96**(1): 91-95.

Lim, H., S. S. Devesa, J. A. Sosa, D. Check and C. M. Kitahara (2017). "Trends in thyroid cancer incidence and mortality in the united states, 1974-2013." JAMA **317**(13): 1338-1348.

Lindblad, O., E. Cordero, A. Puissant, L. Macaulay, A. Ramos, et al. (2016). "Aberrant activation of the PI3K/mTOR pathway promotes resistance to sorafenib in AML." Oncogene **35**(39): 5119-5131.

Lito, P., N. Rosen and D. B. Solit (2013). "Tumor adaptation and resistance to RAF inhibitors." Nat Med **19**(11): 1401-1409.

Liu, D., S. Hu, P. Hou, D. Jiang, S. Condouris, et al. (2007). "Suppression of BRAF/MEK/MAP kinase pathway restores expression of iodide-metabolizing genes in thyroid cells expressing the V600E BRAF mutant." Clin Cancer Res **13**(4): 1341-1349.

Liu, R., J. Bishop, G. Zhu, T. Zhang, P. W. Ladenson, et al. (2016). "Mortality risk stratification by combining BRAF V600E and TERT promoter mutations in papillary thyroid cancer: genetic duet of BRAF and TERT promoter mutations in thyroid cancer mortality." JAMA Oncol **3**(2):202-208.

Llovet, J. M., S. Ricci, V. Mazzaferro, P. Hilgard, E. Gane, et al. (2008). "Sorafenib in advanced hepatocellular carcinoma." N Engl J Med **359**(4): 378-390.

Long, G. V., Z. Eroglu, J. Infante, S. Patel, A. Daud, et al. (2017). "Long-term outcomes in patients with braf v600-mutant metastatic melanoma who received dabrafenib combined with trametinib." J Clin Oncol **36**(7):667-673..

Long, G. V., K. T. Flaherty, D. Stroyakovskiy, H. Gogas, E. Levchenko, et al. (2017). "Dabrafenib plus trametinib versus dabrafenib monotherapy in patients with metastatic BRAF V600E/K-mutant melanoma: long-term survival and safety analysis of a phase 3 study." Ann Oncol **28**(7): 1631-1639.

Long, G. V., A. Hauschild, M. Santinami, V. Atkinson, M. Mandala, et al. (2017). "Adjuvant dabrafenib plus trametinib in Stage III BRAF-mutant melanoma." N Engl J Med **377**(19): 1813-1823.

Long, G. V., D. Stroyakovskiy, H. Gogas, E. Levchenko, F. de Braud, et al. (2014). "Combined BRAF and MEK inhibition versus BRAF inhibition alone in melanoma." N Engl J Med **371**(20): 1877-1888.

Lorusso, L., L. Pieruzzi, A. Biagini, E. Sabini, L. Valerio, et al. (2016). "Lenvatinib and other tyrosine kinase inhibitors for the treatment of radioiodine refractory, advanced, and progressive thyroid cancer." Onco Targets Ther **9**: 6467-6477.

Lubitz, C. C., C. Y. Kong, P. M. McMahon, G. H. Daniels, Y. Chen, et al. (2014). "Annual financial impact of well-differentiated thyroid cancer care in the United States." Cancer **120**(9): 1345-1352.

Lubitz, C. C. and J. A. Sosa (2016). "The changing landscape of papillary thyroid cancer: Epidemiology, management, and the implications for patients." Cancer **122**(24): 3754-3759.

Mariotto, A. B., K. R. Yabroff, Y. Shao, E. J. Feuer and M. L. Brown (2011). "Projections of the cost of cancer care in the United States: 2010-2020." J Natl Cancer Inst **103**(2): 117-128.

Matter-Walstra, K., R. Braun, C. Kolb, Z. Ademi, R. Dummer, et al. (2015). "A cost-effectiveness analysis of trametinib plus dabrafenib as first-line therapy for metastatic BRAF V600-mutant melanoma in the Swiss setting." Br J Dermatol **173**(6): 1462-1470.

McFadden, D. G., A. Vernon, P. M. Santiago, R. Martinez-McFaline, A. Bhutkar, et al. (2014). "p53 constrains progression to anaplastic thyroid carcinoma in a Braf-mutant mouse model of papillary thyroid cancer." Proc Natl Acad Sci USA **111**(16): E1600-1609.

McQuaid, A. and J. Mason (1991). "A comparison of the effects of penicillamine, trientine, and trithiomolybdate on [35s]-labeled metallothionein in vitro; implications for Wilson's Disease therapy." J Inorg Biochem **41**(2):87-92.

Melo, M., A. G. da Rocha, J. Vinagre, R. Batista, J. Peixoto, et al. (2014). "TERT promoter mutations are a major indicator of poor outcome in differentiated thyroid carcinomas." J Clin Endocrinol Metab **99**(5): E754-765.

Mills, C. F., T. T. El-Gallad and I. Bremner (1981). "Effects of molybdate, sulfide, and tetrathiomolybdate on copper metabolism in rats." J Inorg Biochem **14**(3): 189-207.

Mills, C. F., T. T. El-Gallad, I. Bremner and G. Wenham (1981). "Copper and molybdenum absorption by rats given ammonium tetrathiomolybdate." J Inorg Biochem **14**(2): 163-175.

Min, L. (2016). "Immune-related endocrine disorders in novel immune checkpoint inhibition therapy." Genes & Diseases **3**(4): 252-256.

Morrison, J. A., L. A. Pike, G. Lund, Q. Zhou, B. E. Kessler, et al. (2015). "Characterization of thyroid cancer cell lines in murine orthotopic and intracardiac metastasis models." Hormones Cancer **6**(0): 87-99.

Nakamura, T., J. Gulick, R. Pratt and J. Robbins (2009). "Noonan syndrome is associated with enhanced pERK activity, the repression of which can prevent craniofacial malformations." Proc Natl Acad Sci USA **106**(36): 15436-15441.

Nikiforov, Y. E. (2002). "RET/PTC rearrangement in thyroid tumors." Endocr Pathol **13**(1): 3-16.

Nikiforov, Y. E. and M. N. Nikiforova (2011). "Molecular genetics and diagnosis of thyroid cancer." Nat Rev Endocrinol **7**(10): 569-580.

O'Hayer, K. M. and C. M. Counter (2006). "A genetically defined normal human somatic cell system to study ras oncogenesis in vivo and in vitro." Methods Enzymol **407**: 637-647.

Oishi, K., K. Gaengel, S. Krishnamoorthy, K. Kamiya, I. K. Kim, et al. (2006). "Transgenic drosophila models of Noonan syndrome causing PTPN11 gain-of-function mutations." Hum Mol Genet **15**(4): 543-553.

Pagani, M. R., K. Oishi, B. D. Gelb and Y. Zhong (2009). "The phosphatase SHP2 regulates the spacing effect for long-term memory induction." Cell **139**(1): 186-198.

Pandit, B., A. Sarkozy, L. A. Pennacchio, C. Carta, K. Oishi, et al. (2007). "Gain-of-function RAF1 mutations cause Noonan and LEOPARD syndromes with hypertrophic cardiomyopathy." Nat Genet **39**(8): 1007-1012.

Parke, A., P. Bhattacherjee, R. M. Palmer and N. R. Lazarus (1988). "Characterization and quantification of copper sulfate-induced vascularization of the rabbit cornea." Am J Pathol **130**(1): 173-178.

Pass, H. I., G. J. Brewer, R. Dick, M. Carbone and S. Merajver (2008). "A phase II trial of tetrathiomolybdate after surgery for malignant mesothelioma: final results." Ann Thorac Surg **86**(2): 383-389.

Pratilas, C. A., B. S. Taylor, Q. Ye, A. Viale, C. Sander, et al. (2009). "(V600E)BRAF is associated with disabled feedback inhibition of RAF-MEK signaling and elevated transcriptional output of the pathway." Proc Natl Acad Sci USA **106**(11): 4519-4524.

Prescott, J. D. and M. A. Zeiger (2015). "The RET oncogene in papillary thyroid carcinoma." Cancer **121**(13): 2137-2146.

Prohaska, J. R., W. R. Bailey, A. M. Gross and J. J. Korte (1990). "Effect of dietary copper deficiency on the distribution of dopamine and norepinephrine in mice and rats." J Nutr Biochem **1**(3): 149-154.

Puzanov, I., R. K. Amaravadi, G. A. McArthur, K. T. Flaherty, P. B. Chapman, et al. (2015). "Long-term outcome in BRAF(V600E) melanoma patients treated with vemurafenib: Patterns of disease progression and clinical management of limited progression." Euro J Cancer (Oxford) **51**(11): 1435-1443.

Quiros, R. M., H. G. Ding, P. Gattuso, R. A. Prinz and X. Xu (2005). "Evidence that one subset of anaplastic thyroid carcinomas are derived from papillary carcinomas due to BRAF and p53 mutations." Cancer **103**(11): 2261-2268.

Rajakulendran, T., M. Sahmi, M. Lefrancois, F. Sicheri and M. Therrien (2009). "A dimerization-dependent mechanism drives RAF catalytic activation." Nature **461**(7263): 542-545.

Raju, K. S., G. Alessandri, M. Ziche and P. M. Gullino (1982). "Ceruloplasmin, copper ions, and angiogenesis." J Natl Cancer Inst **69**(5): 1183-1188.

Ramsey, S., D. Blough, A. Kirchhoff, K. Kreizenbeck, C. Fedorenko, et al. (2013). "Washington State cancer patients found to be at greater risk for bankruptcy than people without a cancer diagnosis." Health Aff **32**(6): 1143-1152.

Randolph, G. W., Q. Y. Duh, K. S. Heller, V. A. LiVolsi, S. J. Mandel, et al. (2012). "The prognostic significance of nodal metastases from papillary thyroid carcinoma can be stratified based on the size and number of metastatic lymph nodes, as well as the presence of extranodal extension." Thyroid **22**(11): 1144-1152.

Rasmussen, S. and J. M. JFriedman (2000). "NF1 Gene an Neurofibromatosis 1." Am J Epidemiol **151**(1): 7.

Rauen, K. A. (2013). "The RASopathies." Annu Rev Genomics Hum Genet **14**: 355-369.

Redman, B. G., P. Esper, Q. Pan, R. L. Dunn, H. K. Hussain, et al. (2003). "Phase II trial of tetrathiomolybdate in patients with advanced kidney cancer." Clin Cancer Res **9**(5): 1666-1672.

Ribas, A., R. Gonzalez, A. Pavlick, O. Hamid, T. F. Gajewski, et al. (2014). "Combination of vemurafenib and cobimetinib in patients with advanced BRAF(V600)-mutant melanoma: a phase 1b study." Lancet Oncol **15**(9): 954-965.

Robbins, R. J., Q. Wan, R. K. Grewal, R. Reibke, M. Gonen, et al. (2006). "Real-time prognosis for metastatic thyroid carcinoma based on 2-[18F]fluoro-2-deoxy-D-glucose-positron emission tomography scanning." J Clin Endocrinol Metab **91**(2): 498-505.

Robert, C., B. Karaszewska, J. Schachter, P. Rutkowski, A. Mackiewicz, et al. (2015). "Improved overall survival in melanoma with combined dabrafenib and trametinib." N Engl J Med **372**(1): 30-39.

Rodriguez-Viciana, P., O. Tetsu, W. E. Tidyman, A. L. Estep, B. A. Conger, et al. (2006). "Germline mutations in genes within the MAPK pathway cause cardio-facio-cutaneous syndrome." Science **311**(5765): 1287-1290.

Rosignolo, F., M. Sponziello, C. Durante, C. Puppin, C. Mio, et al. (2016). "Expression of PAX8 target genes in papillary thyroid carcinoma." PLoS One **11**(6): e0156658.

Rothenberg, S. M., D. G. McFadden, E. L. Palmer, G. H. Daniels and L. J. Wirth (2015). "Redifferentiation of iodine-refractory BRAF V600E-mutant metastatic papillary thyroid cancer with dabrafenib." Clin Cancer Res **21**(5): 1028-1035.

Roy, M., H. Chen and R. S. Sippel (2013). "Current understanding and management of medullary thyroid cancer." Oncologist **18**(10): 1093-1100.

Ruark, E., K. Snape, P. Humburg, C. Loveday, I. Bajrami, et al. (2013). "Mosaic PPM1D mutations are associated with predisposition to breast and ovarian cancer." Nature **493**(7432): 406-410.

Rucker, R. B., T. Kosonen, M. S. Clegg, A. E. Mitchell, B. R. Rucker, et al. (1998). "Copper, lysyl oxidase, and extracellular matrix protein cross-linking." Am J Clin Nutr **67**(5 Suppl): 996s-1002s.

Saiselet, M., S. Floor, M. Tarabichi, G. Dom, A. Hebrant, et al. (2012). "Thyroid cancer cell lines: an overview." Front Endocrinol **3**: 133.

Santarpia, L., J. N. Myers, S. I. Sherman, F. Trimarchi, G. L. Clayman, et al. (2010). "Genetic alterations in the RAS/RAF/mitogen-activated protein kinase and phosphatidylinositol 3-kinase/Akt signaling pathways in the follicular variant of papillary thyroid carcinoma." Cancer **116**(12): 2974-2983.

Scheinberg, I. H., M. E. Jaffe and I. Sternlieb (1987). "The use of trientine in preventing the effects of interrupting penicillamine therapy in Wilson's Disease." N Engl J Med **317**(4): 209-213.

Schlumberger, M., M. Tahara, L. J. Wirth, B. Robinson, M. S. Brose, et al. (2015). "Lenvatinib versus placebo in radioiodine-refractory thyroid cancer." N Engl J Med **372**(7): 621-630.

Schubbert, S., G. Bollag and K. Shannon (2007). "Deregulated Ras signaling in developmental disorders: new tricks for an old dog." Curr Opin Genet Dev **17**(1): 15-22.

Schubbert, S., K. Shannon and G. Bollag (2007). "Hyperactive Ras in developmental disorders and cancer." Nat Rev Cancer **7**(4): 295-308.

Schweppe, R. E., J. P. Klopper, C. Korch, U. Pugazhenthi, M. Benezra, et al. (2008). "Deoxyribonucleic acid profiling analysis of 40 human thyroid cancer cell lines reveals cross-contamination resulting in cell line redundancy and misidentification." J Clin Endocrinol Metab **93**(11): 4331-4341.

Sciuto, R., L. Romano, S. Rea, F. Marandino, I. Sperduti, et al. (2009). "Natural history and clinical outcome of differentiated thyroid carcinoma: a retrospective analysis of 1503 patients treated at a single institution." Ann Oncol **20**(10): 1728-1735.

Sewell, W., A. Reeb and R. Y. Lin (2013). "An orthotopic mouse model of anaplastic thyroid carcinoma." J Vis Exp **17**(74).

Shah, A. A., P. P. Jain, A. S. Dubey, G. N. Panjwani and H. A. Shah (2018). "A study of clinicopathological characteristics of thyroid carcinoma at a Tertiary Care Center." J Cancer Res Ther **14**(2): 357-360.

Sherman, S. I., D. S. Ross and J. E. Mulder (2016). "Differentiated thyroid cancer refractory to standard treatment: Chemotherapy." UpToDate Retrieved Jan 28, 2018, from https://www.uptodate.com/contents/differentiated-thyroid-cancer-refractory-to-standard-treatment-chemotherapy.

Singer, S., O. Husson, I. M. Tomaszewska, L. D. Locati, N. Kiyota, et al. (2016). "Quality of life priorities in patients with thyroid cancer: a multinational european organisation for research and treatment of cancer Phase I study." Thyroid **26**(11): 1605-1613.

Skrott, Z., M. Mistrik, K. K. Andersen, S. Friis, D. Majera, et al. (2017). "Alcohol-abuse drug disulfiram targets cancer via p97 segregase adaptor NPL4." Nature **552**(7684): 194-199.

Soares, P., V. Trovisco, A. S. Rocha, J. Lima, P. Castro, et al. (2003). "BRAF mutations and RET/PTC rearrangements are alternative events in the etiopathogenesis of PTC." Oncogene **22**(29): 4578-4580.

Sobrinho-Simões, M., C. Eloy, J. Magalhães, C. Lobo and T. Amaro (2011). "Follicular thyroid carcinoma." Mod Pathol **24**: S10-8.

Stinchcombe, T. E. and G. L. Johnson (2014). "MEK inhibition in non-small cell lung cancer." Lung Cancer **86**(2): 121-125.

Stjepanovic, N. and J. Capdevila (2014). "Multikinase inhibitors in the treatment of thyroid cancer: specific role of lenvatinib." Biologics **8**: 129-139.

Subbiah, V., R. J. Kreitman, Z. A. Wainberg, J. Y. Cho, J. H. M. Schellens, et al. (2017). "Dabrafenib and trametinib treatment in patients with locally advanced or metastatic BRAF V600-mutant anaplastic thyroid cancer." J Clin Oncol: Jco2017736785.

Tagliavacca, L., N. Moon, W. R. Dunham and R. J. Kaufman (1997). "Identification and functional requirement of Cu(I) and its ligands within coagulation factor VIII." J Biol Chem **272**(43): 27428-27434.

Tang, K. D. and M. T. Ling (2014). "Targeting drug-resistant prostate cancer with dual PI3K/mTOR inhibition." Curr Med Chem **21**(26): 3048-3056.

Tartaglia, M., L. A. Pennacchio, C. Zhao, K. K. Yadav, V. Fodale, et al. (2007). "Gain-of-function SOS1 mutations cause a distinctive form of Noonan syndrome." Nat Genet **39**(1): 75-79.

The Cancer Genome Atlas. (2014). "Integrated genomic characterization of papillary thyroid carcinoma." Cell **159**(3): 676-690.

Tomayko, M. M. and C. P. Reynolds (1989). "Determination of subcutaneous tumor size in athymic (nude) mice." Cancer Chemother Pharmacol **24**(3): 148-154.

Turski, M. L., D. C. Brady, H. J. Kim, B. E. Kim, Y. Nose, et al. (2012). "A novel role for copper in Ras/mitogen-activated protein kinase signaling." Mol Cell Biol **32**(7): 1284-1295.

Tuttle, M. R., D. S. Ross and J. E. Mulder (2018). "Differentiated thyroid cancer: Overview of management." UpToDate Retrieved Jan 15, 2018, from https://www.uptodate.com/contents/differentiated-thyroid-cancer-overview-of-management

Tuttle, R. M., H. Tala, J. Shah, R. Leboeuf, R. Ghossein, et al. (2010). "Estimating risk of recurrence in differentiated thyroid cancer after total thyroidectomy and radioactive iodine remnant ablation: using response to therapy variables to modify the initial risk estimates predicted by the new American Thyroid Association staging system." Thyroid **20**(12): 1341-1349.

Ullrich, M., M. Weber, A. M. Post, S. Popp, J. Grein, et al. (2018). "OCD-like behavior is caused by dysfunction of thalamo-amygdala circuits and upregulated TrkB/ERK-MAPK signaling as a result of SPRED2 deficiency." Mol Psychiatry **23**(2): 444-458.

Undeutsch, H., C. Lof, S. Offermanns and J. Kero (2014). "A mouse model with tamoxifen-inducible thyrocyte-specific cre recombinase activity." Genesis **52**(4): 333-340.

Vanden Borre, P., D. G. McFadden, V. Gunda, P. M. Sadow, S. Varmeh, et al. (2014). "The next generation of orthotopic thyroid cancer models: immunocompetent orthotopic mouse models of BRAF V600E-mutant papillary and anaplastic thyroid carcinoma." Thyroid **24**(4): 705-714.

Vasko, V., M. Ferrand, J. Di Cristofaro, P. Carayon, J. F. Henry, et al. (2003). "Specific pattern of RAS oncogene mutations in follicular thyroid tumors." J Clin Endocrinol Metab **88**(6): 2745-2752.

Vassilopoulou-Sellin, R., P. N. Schultz and T. P. Haynie (1996). "Clinical outcome of patients with papillary thyroid carcinoma who have recurrence after initial radioactive iodine therapy." Cancer **78**(3): 493-501.

Volpe, V. O., D. M. Klufas, U. Hegde and J. M. Grant-Kels (2017). "The new paradigm of systemic therapies for metastatic melanoma." J Am Acad Dermatol **77**(2): 356-368.

Vonk, W. I., C. Wijmenga, R. Berger, B. van de Sluis and L. W. Klomp (2010). "Cu,Zn superoxide dismutase maturation and activity are regulated by COMMD1." J Biol Chem **285**(37): 28991-29000.

Walshe, J. M. (1956). "Penicillamine, a new oral therapy for Wilson's Disease." Am J Med **21**(4): 487-495.

Walshe, J. M. (1982). "Treatment of Wilson's Disease with trientine (triethylene tetramine) dihydrochloride." Lancet **319**(8273): 643-647.

Wan, P. T., M. J. Garnett, S. M. Roe, S. Lee, D. Niculescu-Duvaz, et al. (2004). "Mechanism of activation of the RAF-ERK signaling pathway by oncogenic mutations of B-RAF." Cell **116**(6): 855-867.

Wells, S. A., Jr., S. L. Asa, H. Dralle, R. Elisei, D. B. Evans, et al. (2015). "Revised American Thyroid Association guidelines for the management of medullary thyroid carcinoma." Thyroid **25**(6): 567-610.

Wu, B., B. M. Guo, J. Kang, X. Z. Deng, Y. B. Fan, et al. (2016). "PPM1D exerts its oncogenic properties in human pancreatic cancer through multiple mechanisms." Apoptosis **21**(3): 365-378.

Wu, X., J. Simpson, J. H. Hong, K. H. Kim, N. K. Thavarajah, et al. (2011). "MEK-ERK pathway modulation ameliorates disease phenotypes in a mouse model of Noonan syndrome associated with the Raf1(L613V) mutation." J Clin Invest **121**(3): 1009-1025.

Xing, M. (2010). "Genetic alterations in the phosphatidylinositol-3 kinase/Akt pathway in thyroid cancer." Thyroid **20**(7): 697-706.

Xing, M. (2010). "Prognostic utility of BRAF mutation in papillary thyroid cancer." Mol Cell Endocrinol **321**(1): 86-93.

Xing, M. (2013). "Molecular pathogenesis and mechanisms of thyroid cancer." Nat Rev Cancer **13**(3): 184-199.

Xing, M. (2016). "Clinical utility of RAS mutations in thyroid cancer: a blurred picture now emerging clearer." BMC Med **14**:doi: 10.1186.

Xing, M., A. S. Alzahrani, K. A. Carson, D. Viola, R. Elisei, et al. (2013). "Association between BRAF V600E mutation and mortality in patients with papillary thyroid cancer." JAMA **309**(14): 1493-1501.

Xing, M., R. Liu, X. Liu, A. K. Murugan, G. Zhu, et al. (2014). "BRAF V600E and TERT promoter mutations cooperatively identify the most aggressive papillary thyroid cancer with highest recurrence." J Clin Oncol **32**(25): 2718-2726.

Yang, H., X. Y. Gao, P. Li and T. S. Jiang (2015). "PPM1D overexpression predicts poor prognosis in non-small cell lung cancer." Tumour Biol **36**(3): 2179-2184.

Yao, R., C. G. Chiu, S. S. Strugnell, S. Gill, S. M. Wiseman (2011). "Gender differences in thyroid cancer." Metab **6**(2):215-243.

Yu, X.-M., D. F. Schneider, G. Leverson, H. Chen and R. S. Sippel (2013). "Follicular variant of papillary thyroid carcinoma is a unique clinical entity: a population-based study of 10,740 cases." Thyroid **23**(10): 1263-1268.

Zafar, S. Y. (2016). "Financial toxicity of cancer care: it's time to intervene." J Natl Cancer Inst **108**(5):doi: 10.1093.

Zafar, S. Y., R. B. McNeil, C. M. Thomas, C. S. Lathan, J. Z. Ayanian, et al. (2015). "Population-based assessment of cancer survivors' financial burden and quality of life: a prospective cohort study." J Oncol Pract **11**(2): 145-150.

Zhang, L., K. Gaskins, Z. Yu, Y. Xiong, M. J. Merino, et al. (2014). "An in vivo mouse model of metastatic human thyroid cancer." Thyroid **24**(4): 695-704.

Zhang, P., Y. Yang, F. Wen, X. He, R. Tang, et al. (2015). "Cost-effectiveness of sorafenib as a first-line treatment for advanced hepatocellular carcinoma." Eur J Gastroenterol Hepatol **27**(7): 853-859.

Zhao, Y. and A. A. Adjei (2014). "The clinical development of MEK inhibitors." Nat Rev Clin Oncol **11**(7): 385-400.

Zhu, Z., M. Gandhi, M. N. Nikiforova, A. H. Fischer and Y. E. Nikiforov (2003). "Molecular profile and clinical-pathologic features of the follicular variant of papillary thyroid carcinoma. An unusually high prevalence of ras mutations." Am J Clin Pathol **120**(1): 71-77.

Biography

MengMeng Xu was born in Wuhan, China. Her family moved to Cleveland, Ohio in 1997 where she first learned English before moving to Indiana. Her family made a final move to Maryland in 2004, where MengMeng attended high school, then college at the University of Maryland- College Park, where she received a B.S. in Biochemistry and B.A. in Economics in 2011. MengMeng matriculated into the Medical Scientist Training Program at Duke University in 2011 and joined the lab of Dr. Christopher Counter in 2014. MengMeng received a 2015 Gertrude B. Elion Mentored Medical Research Award while working towards her PhD degree.

Publications:

Xu M, Casio M, Range DE, Sosa JA, and Counter CM. *Copper chelation as targeted therapy in a mouse model of oncogenic BRAF-driven papillary thyroid cancer*. Clin Caner Res, in press.

Anderson GR, Winter PS, Lin KH, Nussbaum DP, Cakir M, Stein EM, Soderquist RS, Crawford L, Leeds JC, Newcomb R, Stepp P, Yip C, Wardell SE, Tingley JP, Ali M, Xu M, Ryan M, McCall SJ, McRee AJ, Counter CM, Der CJ, and Wood KC. *A Landscape of Therapeutic Cooperativity in KRAS Mutant Cancers Reveals Principles for Controlling Tumor Evolution*. Cell Rep, 20(4):999-1015, 2017.

Weyandt JD, Carney JM, Pavlisko EN, Xu M, Counter CM. *Isoform-Specific Effects of Wild-Type Ras Genes on Carcinogen-Induced Lung Tumorigenesis in Mice.* PLoS One, 11(12): e0167205, 2016.

Pershing NL, Yang CJ, Xu M, Counter CM. *Treatment with the nitric oxide synthase inhibitor L-NAME provides a survival advantage in a mouse model of Kras mutation-mutant, non-small cell lung cancer.* Oncotarget, 9874:1949-2443, 2016.